UNIVERSIDADE FEDERAL DE CIÊNCIAS DA SAÚDE DE PORTO ALEGRE – UFCSPA
PROGRAMA DE PÓS-GRADUAÇÃO EM BIOCIÊNCIAS

Luiza Steffens Reinhardt

Desenvolvimento e avaliação do potencial terapêutico de sistemas de entrega de drogas antitumorais para o tratamento de gliomas

Porto Alegre
2019

Luiza Steffens Reinhardt

Desenvolvimento e avaliação do potencial terapêutico de sistemas de entrega de drogas antitumorais para o tratamento de gliomas

Dissertação submetida ao Programa de Pós-Graduação em Biociências da Fundação Universidade Federal de Ciências da Saúde de Porto Alegre como requisito para a obtenção do grau de Mestre

Orientadora: Prof. Dra. Dinara Jaqueline Moura

Porto Alegre

2019

INSTITUIÇÕES E FONTES FINANCIADORAS

Este trabalho foi desenvolvido na Universidade Federal de Ciências da Saúde de Porto Alegre e no Instituto de Tecnologia de Athlone. Este trabalho contou com recursos financeiros da CAPES, FAPERGS e *Government of Ireland Scholarship* (GOI).

AGRADECIMENTOS

À minha orientadora, Profª Dra. Dinara Jaqueline Moura, a quem tive a oportunidade de conhecer durante a graduação e quem me orienta desde a iniciação científica. Dinja, tenho uma admiração enorme por ti que cresce a cada dia! Obrigada pela confiança no meu trabalho, pelos conhecimentos compartilhados, e pela amizade!

À Profª Dra. Jenifer Saffi, por ter me recebido no Lab GENTOX. Obrigada pela oportunidade de fazer parte desse grupo de pesquisa incrível o qual tenho muito orgulho!

Aos demais colegas do Lab GENTOX, que apesar de eu ter realizado grande parte do projeto fora fazem parte de todo meu crescimento científico! Obrigada pelas festas, discussões de artigos e amizade. Senti falta de vocês!

Aos colegas e professores do AIT pelo auxílio no desenvolvimento deste trabalho e por todo o conhecimento repassado.

Aos meus colegas Ana Moira e Jeferson, pela ajuda e paciência (sei que não sou fácil às vezes haha). Obrigada pela amizade de vocês! Podem contar comigo sempre.

Às minhas amigas/colegas/veteranas/irmãs Ana, Marina e Nathalia por serem esses “serumaninhos” que eu amo muito. Vocês são muito especiais na minha vida!

À minha família de Athlone. Vocês me acolheram e nós nos acolhemos, e nessa mistura de nacionalidades percebi que família a gente escolhe sim! É rir, conversar, discutir, beber, dar adeus, e mesmo assim jamais esquecer a importância que cada um teve.

Aos familiares e amigos, que mesmo de longe sempre me apoiaram e acreditaram em mim. Por fim, e de maneira imensurável, agradeço aos meus pais, Karla e José Roberto, e minha irmã, Roberta, pelo apoio incondicional nos meus estudos, acreditando no meu esforço, sendo para mim um exemplo em tudo. Amo vocês!

“I do not know what I may appear to the world, but to myself I seem to have been only like a boy playing on the seashore, and diverting myself in now and then finding a smoother pebble or a prettier shell than ordinary, whilst the great ocean of truth lay all undiscovered before me.”

Isaac Newton

SUMÁRIO

LISTA DE ABREVIATURAS

5-FU: 5-fluorouracil

AF: ácido fólico

AuNP: nanopartícula de ouro

Bax: proteína X associada a BCL-2

BCNU: 1,3-bis (2-cloroetil)-1-nitrosoureia

BHE: barreira hematoencefálica

c-Met: proteína tirosina cinase Met

Ca: cálcio

CDX: candoxina

COX-2: ciclo-oxigenase-2

CS: chitosan

CTX: clorotoxina

Cur: curcumina

DDS: sistema de administração de fármacos *(drug delivery system)*

DOX: doxorrubicina

DTIC: dacarbazina

EGFR: receptor do fator de crescimento epidérmico *(epidermal growth fator receptor)*

EPR: efeito de permeabilidade e retenção

FDA: *Food and Drug Administration*

FTA: ácido farnesil tiosalicílico

FuS: ultrassom focalizado

GB: glioblastoma

GNR: nanorods de ouro *(gold nanorods)*

GFP: proteína fluorescente verde (*green fluorescent protein)*

GT: glutationa

INCA: Instituto Nacional de Câncer

LF: lactoferrina

Mdm-2: *Mouse double minute 2 homolog*

MGMT: O^6-metilguanina DNA metiltransferase

MMP-2/9: metaloproteinase da matriz-2/9

MNP: nanopartícula magnética

MPEG: metoxi-polietilenoglicol

MTIC: 5-(3-metiltriazeno-1-il)imidazol-4-carboxamida

NF: nanofibra

NP: nanopartícula

Nrk: *Nima-related kinases*

p53: *tumor protein 53*

P-80: polissorbato-80

PACA: poli (alquil-cianoacrilato)

PAMAM: poliamidoamina

PBCA: poli (n-butil-2-cianoacrilato)

PC: policarbonato

PCEC: PCL-PEG-PCL

PCL: policaprolactona

PD-1: receptor de morte programada 1 de célula T

PD-L1: ligante do receptor de morte programada 1 de célula T

PEG: poli (etileno glicol)

PEI: polietilenimina

PEO: poli (óxido de etileno)

PIHC: cerâmica híbrida infiltrada de polímero

PLA: ácido poliláctico

PLGA: ácido poliláctico-co-glicólico

PLLA: ácido polilático

PMM: poli (metileno malonato)

PMMA: poli (metacrilato de metila)

PNP: nanopartículas poliméricas

PPC: polipropileno copolímero

PS: poliestireno

PTEN: *phosphatase and tensin homolog*

PTMC: poli (carbonato de trimetileno)

PTX: paclitaxel

PU: poliuretano

PVA: álcool polivinílico

PVP: polivinilpirrolidona

QT: quimioterapia

RT: radioterapia

RVG: glicoproteína do vírus da raiva

SLN: nanopartícula lipídica sólida

SNC: sistema nervoso central

SPION: nanopartícula de óxido de ferro superparamagnética

SS-PEI: polietilenimina dissulfureto

TF: transferrina

THM: terapia de hipertermia magnética

TMZ: temozolomida

VEGF: anti-fator de crescimento endotelial vascular

LISTA DE FIGURAS E TABELAS

RESUMO

Os tumores cerebrais, principalmente os glioblastomas (GBs), representam um desafio para a ciência médica atual, tendo em vista a ineficácia e as limitações das terapias convencionais, bem como o diagnóstico tardio. A fisiologia do cérebro apresenta características distintas e, para superá-las, várias estratégias utilizando sistemas de distribuição estão sendo desenvolvidas, incluindo nanoprodutos poliméricos como nanopartículas e nanofibras. Questões relacionadas à quimioterapia atual, como toxicidade sistêmica, resistência a drogas e biodistribuição não específica, podem ser resolvidas utilizando o adequado sistema de entrega de drogas. Além disso, esses sistemas normalmente são estáveis em fluidos biológicos, tornando-os uma abordagem promissora para fornecer liberação controlada de drogas, reduzindo assim a toxicidade após a administração sistêmica. Nanoprodutos precisamente desenvolvidos e biofuncionalizados são promissores para o uso no transporte direcionado e eficiente, acarretando melhores resultados clínicos. Alterações moleculares são extremamente importantes para entender os GBs e, potencialmente, poderiam ser usadas para uma terapia direcionada. Recentemente foi descrito que a proteína Nek1 está superexpressa em diferentes linhagens de gliomas e o nível de expressão está diretamente relacionado com o grau de severidade do tumor, a taxa de proliferação e a resistência à temozolomida. Neste trabalho, objetivou-se produzir nanoprodutos poliméricos, nanopartículas (NP) e nanofibras (NF), utilizando o álcool polivinílico e drogas quimioterápicas, dacarbazina e temozolomida, e inibidor da proteína Nek1 para o tratamento de glioblastomas. Os nanoprodutos foram caracterizados em relação a suas morfologias, a suas propriedades mecânicas (viscoelasticidade), químicas (interações químicas) e físicas (transições de estado físico), a suas taxas de liberação das drogas, a suas eficácias e ao seu impacto na terapia do câncer cerebral *in vitro* utilizando a linhagem U87MG. As NP e as NF apresentaram maior eficiência no tratamento antitumoral em comparação com as drogas quando testadas isoladamente. Foi possível concluir que os nanoprodutos produzidos podem trazer melhorias na eficiência dos medicamentos quimioterápicos tradicionais e apresentam um grande potencial de translação clínica.

Palavras-chave: Nanoprodutos. Nanopartículas. Nanofibras. Nanotecnologia. Sistemas de entrega de drogas. Glioblastoma. Nek1.

ABSTRACT

Brain tumors, particularly glioblastomas (GBs), are an unresolved clinical problem and a challenge for current medical science given the limitations of conventional therapies and late diagnosis. The physiology of the brain has distinct characteristics, and to overcome it, several strategies using distribution systems are being developed, including polymer nanoproducts such as nanoparticles and nanofibers. Issues related to current chemotherapy such as systemic toxicity, drug resistance and non-specific biodistribution can be resolved using the appropriate drug delivery system. In addition, such systems are usually stable in biological fluids and are a promising approach to provide controlled drug release, thereby reducing toxicity following systemic administration. Precisely developed and biofunctionalized nanoproducts are promising for use in targeted and efficient transport resulting in better clinical outcomes. Molecular changes are extremely important to understand GBs and could potentially be used for targeted therapy. It has recently been reported that Nek1 protein is overexpressed in different glioma lines and the level of expression is directly related to the degree of tumor severity, proliferation rate and resistance to temozolomide. In this work, the objective was to produce polymeric nanoproducts, nanoparticles (NP) and nanofibres (NF), using polyvinyl alcohol and chemotherapeutic drugs, dacarbazine and temozolomide and Nek1 protein inhibitor for the treatment of glioblastomas. Nanoproducts were characterized in terms of their morphology, their mechanical (viscoelasticity), chemical properties (chemical interactions) and physical properties (state transitions), their drug release rates, their efficacy and their impact on *in vitro* brain cancer therapy by using U87MG cell line. NP and NF showed greater efficiency in antitumor treatment compared to drugs when tested singly. It was possible to conclude that the nanoproducts produced can bring improvements in the efficiency of the traditional chemotherapeutic drugs and present a great clinical potential.

Keywords: Nanoproducts. Nanoparticles. Nanofibers. Nanotechnology. Drug delivery systems. Glioblastoma. Nek1.

1. INTRODUÇÃO

O câncer é uma doença complexa e uma das principais razões de morbidade e mortalidade humana. A projeção de novos casos do GLOBOCAN 2012 no mundo foi de 14,1 milhões por ano, com estimativa de aumento para 19,3 milhões até 2025 (Ferlay et al., 2012). Cirurgia, radioterapia (RT), quimioterapia (QT) e imunoterapia são as principais abordagens utilizadas para terapia do câncer (Masood, 2016). Para erradicar cânceres localizados, cirurgia e RT funcionam relativamente, porém, quando há metástase associada, a QT e a imunoterapia são os principais tratamentos funcionais (Aftab et al., 2018). Porém, a alta toxicidade, a quantidade insuficiente de agentes terapêuticos liberados, a insolubilidade em água de algumas drogas, a circulação errática, a biodistribuição inespecífica e a liberação do fármaco tanto para as células cancerígenas quanto para as não tumorais são as principais limitações da QT (Cho et al., 2008; Masood, 2016). Consequentemente, abordagens inteligentes e eficientes são necessárias para diminuir essas estatísticas de mortalidade (Ferlay et al., 2012).

1.1 VISÃO GERAL DO GLIOBLASTOMA

Os tumores cerebrais desenvolvem-se a partir de vários tipos diferentes de células. Os gliomas, por exemplo, são tumores cerebrais semelhantes às células gliais típicas, como astrócitos, oligodendrócitos e células ependimárias (Glaser et al., 2017). Em geral, esses tumores são incuráveis e altamente resistentes à QT e RT. Os gliomas podem infiltrar-se através das regiões cerebrais e são essencialmente categorizados de acordo com a sua semelhança morfológica com as correspondentes naturezas celulares gliais, citoestrutura e imuno-histologia (Glaser et al., 2017). O sistema de classificação do glioma, segundo a Organização Mundial de Saúde (OMS), diferencia os astrocitomas em quatro graus (I, II, III e IV) e oligodendrogliomas, em dois graus (II e III). O astrocitoma grau IV, conhecido como glioblastoma (GB) é o glioma mais prevalente e com pior prognóstico (Glaser et al., 2017).

O Instituto Nacional de Câncer (INCA) estima que para cada ano do biênio 2018/2019, sejam diagnosticados 11.320 novos casos de tumores cerebrais/sistema nervoso central (SNC), 5.810 em homens e 5.510 em mulheres, no Brasil (INCA, 2017). Esses números correspondem a um risco estimado de 5,62 novos casos a cada 100 mil homens e 5,17 para cada 100 mil mulheres. O GB é um dos tipos mais frequentes e agressivos de câncer do SNC em adultos (Brandes et al., 2008), compreendendo 16% dos tumores cerebrais primários. Além disso, por ser um câncer cerebral maligno primário majoritariamente recorrente, é responsável por 77% de todos os cânceres cerebrais malignos (Ching et al., 2015; Thakkar & Misra, 2014).

Características clínicas e malignidade são utilizadas para categorizar os gliomas, tendo o GB uma histopatologia que compreende pleomorfismo celular, alta taxa mitótica e celularidade com núcleos incomuns. Além disso, o GB pode ser distinguido pela heterogeneidade das células, resistência das células cancerosas ao tratamento com quimioterápicos, desenvolvimento de necrose e angiogênese (Ostrom et al., 2015). Embora os GBs se desenvolvam essencialmente apenas no cérebro, eles podem ocorrer em alguns casos na medula espinhal, no cerebelo e no tronco encefálico (Associação Americana de Enfermeiras de Neurociência - AANN, 2014). Inicialmente, acreditava-se que o GB resultava exclusivamente de células gliais, porém estudos mais recentes propõem que os GBs podem se desenvolver a partir de várias células com características tronco neural (Davis, 2016).

GBs se desenvolvem primordialmente em pacientes com uma idade média de 64 anos (Thakkar & Misra, 2014). A sobrevida média em pacientes com GB é inferior a 50 semanas, mesmo com o manejo exaustivo o qual inclui ressecção cirúrgica, CT e RT (Stupp et al., 2005). O protocolo clínico atual para GB é um procedimento combinatório de doses de RT e entrega sistemática de drogas anticâncer (Kim et al., 2014). A recomendação do *BC Cancer Agency Management Guidelines* (protocolo: CNAJ12TZRT) para o tratamento de GB inclui tratamento concomitante de TMZ e RT por cinco dias, com folga de dois dias de RT, totalizando 7 dias de exposição. Este ciclo, no protocolo clínico de pacientes é repetido por seis semanas (BC Cancer Agency Management Guidelines, 2018). Embora o tratamento combinatório seja mais eficaz, o mesmo acarreta em efeitos colaterais frustrantes. Dadas as características complexas

das células de GB e a presença de barreiras fisiológicas, particularmente a barreira hematoencefálica (BHE), a cura desse câncer permanece um desafio (Pourgholi et al., 2016; Lapointe et al., 2018).

1.1.1 ASPECTOS MOLECULARES DO GLIOBLASTOMA

Os GBs apresentam um perfil genético complexo. O projeto Atlas do Genoma do Câncer analisou o perfil genômico do GB de duzentas espécimes tumorais e aproximadamente 600 genes estavam superexpressos (Chen, McKay & Parada, 2012). Com base nesta análise, estabeleceu-se três principais vias de sinalização proteica: (a) a proteína *tumor protein 53* (p53), (b) o receptor tirosina quinase/Ras/fosfoinositídeo 3-quinase e (c) as vias relacionadas com retinoblastoma (Parsons et al., 2008). Devido a modificações nessas vias proteicas, tumores primários e secundários, predominantemente, têm proliferação celular descontrolada. Isso permite que as células malignas evitem os pontos de verificação do ciclo celular e os processos de morte celular, como senescência e apoptose (Chen, McKay & Parada, 2012).

Os GBs primários e secundários exibem padrões complexos de expressão gênica: a superexpressão do receptor do fator de crescimento epidérmico (EGFR), as mutações na *phosphatase and tensin homolog* (PTEN) e a perda do braço longo do cromossomo 10 são exemplos de alterações genéticas e moleculares características do GB primário. Por outro lado, mutações na isocitrato desidrogenase 1 (IDH1) e p53, bem como e perda do braço longo do cromossomo 19 são comumente observadas no GB secundário (Young et al., 2015; Wilson et al., 2014; Alifieris & Trafalis, 2015).

Nek1 é uma proteína que está associada com resistência tumoral em gliomas (Zhu et al., 2016). Essa proteína pertence à família das *Nima related kinases* (Nrk). Esta família abrange proteínas ortólogas à *Never in Mitosis A* (NIMA), uma serina treonina cinase identificada em *Aspergilus nidulans* que possui um papel central na mitose, uma vez que sua deleção impede a entrada nessa fase. Em humanos existem 11 Nrks, conhecidas como Nek1 a Nek11, e elas são ortólogas à NIMA, pois o domínio catalítico dessas proteínas cinases é bastante conservado. No entanto, a região C-terminal é bem variada, em tamanho e

sequência (O'Connell, 2003). A necessidade de 11 proteínas em humanos para desempenhar o papel de apenas uma em fungos sugere possíveis papéis adicionais. Já foram descritas, por exemplo, funções na mitose, resposta aos danos de DNA e associação com vias de reparo de DNA (Melo-Hanchul et al., 2017). Os papéis fisiológicos destas proteínas ainda estão sendo esclarecidos, mas estudos recentes indicam que Neks podem ter um papel importante na progressão e resistência ao processo apoptótico do tumor (Zhu et al., 2016).

Recentemente foi descrito que Nek1 está superexpressa em diferentes linhagens de gliomas e, interessantemente, o nível de expressão está diretamente relacionado com o grau de severidade do tumor, a taxa de proliferação e a resistência à temozolomida. Além disso, analisando amostras de pacientes, observou-se a associação com prognóstico de sobrevida ($p = 0.03$) (Zhu et al., 2016). Um segundo estudo, avaliando Nek1 em células de tumor renal, concluiu que o aumento da expressão de Nek1 está vinculado a uma falha no processo de degradação. Esse estudo também descreveu a relação de Nek1 com apoptose pela interação com VDAC1, uma proteína de membrana mitocondrial, e mostrou que o *knockdown* de Nek1 impede a célula de progredir no ciclo celular e diminui o recrutamento de Ku80 à cromatina (Chen, 2014). Nek1 também está listado entre os genes relevantes na base genética do adenocarcinoma pancreático (Smith et al., 2016). O papel de Nek1 com reparo de DNA foi explorado por Spies, et al. (2013), em que um envolvimento com a recombinação homóloga foi proposto. Neste trabalho, demonstrou-se que, em G2, Nek1 fosforila Rad54 na S572, promovendo o desacoplamento de Rad51 do DNA. Além disso, Nek1 parece ter um papel na sinalização de dano, pois promove a ativação de ATR, possibilitando a interação ATRIP/ATR (Lio, 2013). Inibidores da atividade cinase desta proteína já foram testados (Moras et al., 2015; Melo-Hanchul et al., 2017) visando inibir a resposta de danos no DNA sinalizados por Nek1 (figura 1). Apesar dos resultados indicarem que Nek1 está de alguma forma relacionada ao processo tumoral, ainda faltam muitas informações necessárias para identificar seu real papel na resistência tumoral.

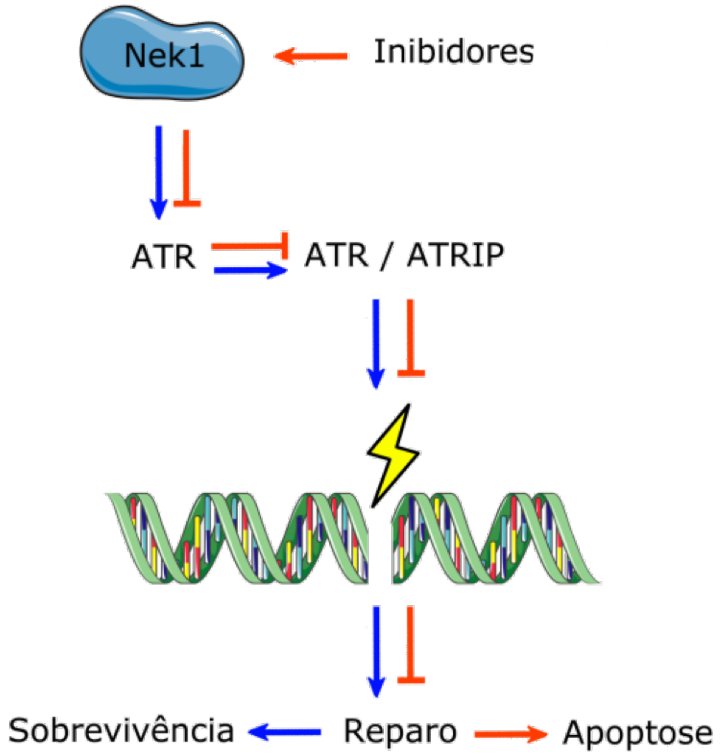

Figura 1 - Atuação de Nek1 no reparo de lesões no DNA. Inibidores da proteína diminuem a eficiência de reparo e aumentam a morte celular. Imagem cedida por Pablo Arantes.

Tendo em vista todas as complexas alterações nas vias de sinalização destas células tumorais, os GBs se tornaram um grande obstáculo na oncologia com diversos desfechos de progressão e sobrevida. Essas alterações moleculares são extremamente importantes para entender os GBs e, potencialmente, poderiam ser usadas para uma terapia direcionada (Wang et al., 2015, Verhaak et al., 2010 e Brennan, 2013).

1.2 O DESAFIO IMPOSTO PELA BARREIRA HEMATOENCEFÁLICA (BHE)

A BHE é uma barreira cerebral que apresenta desafios em termos de permeabilidade, uma vez que nas células endoteliais que revestem o lúmen dos capilares do cérebro há uma ausência de processos de pinocitose e fenestrações

devido à existência de complexos de junções estreitas (Papademetriou & Porter, 2015).

Dadas as características da BHE, a entrega de medicamentos através dela é quase impossível. As quatro principais razões são:

(a) a vasculatura cerebral da composição de células da BHE é formada por linhas endoteliais estreitas. Essas células endoteliais podem desenvolver uma forte conexão entre células vizinhas. Portanto, o transporte paracelular do cérebro é restringido por esse limite físico (Yang, 2010);

(b) a presença de enzimas específicas que degradam alguns fármacos, impedindo que eles atinjam o local específico no cérebro;

(c) os transportadores ativos de efluxo, que enviam os medicamentos de volta ao sangue, acarretando na sua metabolização e consequente incapacidade de chegarem ao destino (Papademetriou & Porter, 2015).

(d) os prolongamentos dos astrócitos formam uma rede de lamelas próxima e aderida na superfície externa do endotélio da BHE (Cardoso et al., 2010).

As junções estreitas entre as células na BHE são essencialmente compostas de ocludinas e claudinas (Haseloff et al., 2015). O último grupo é crítico para a restrição de pequenas moléculas. Por exemplo, a claudina 5 restringe moléculas menores que 800 daltons. Além disso, o prejuízo no funcionamento de algumas claudinas, como a claudina 3, está associado à maior penetrabilidade da BHE na vasculatura do câncer (Wolburg et al., 2003). No entanto, nos gliomas infiltrantes e micro-metastáticos, a barreira permanece intacta. Esse aspecto importante indica que a modulação da permeabilidade nesses locais é fundamental e pode ser usada para aumentar a eficácia do tratamento.

As duas principais formas de transporte através da BHE são o transporte mediado por transportadores e o transporte mediado por receptores. Além disso, o transporte molecular através da BHE é especificamente limitado a partículas maiores que 12 nm (Papademetriou & Porter, 2015). Calcula-se que quase a totalidade das moléculas pequenas e grandes não conseguem atravessar a barreira; esta é a razão pela qual vários fármacos promissores não chegam ao local do tumor em concentrações suficientes (Pardridge, 2005).

Devido a isso, a BHE impede a rota de inúmeras drogas antitumorais para os locais do cérebro, fazendo da QT em GB um dos maiores desafios entre os

atuais tratamentos contra o câncer. Com o objetivo de melhorar o transporte de medicamentos ou evitar a BHE, muitos grupos de pesquisa vêm desenvolvendo novas nanotecnologias para superar esses obstáculos. Uma opção para transportar fármacos para o cérebro, controlando as limitações citadas, é a utilização de nanocarreadores (Patel et al., 2012). Alterações bioquímicas em fármacos e nanocarreadores têm sido propostas por pesquisadores, permitindo a liberação local de fármacos em concentrações suficientes, evitando a exposição ao sistema e superando as limitações da BHE (Aftab et al., 2018).

1.3 ESTRATÉGIAS ATUAIS NO TRATAMENTO DE GB

O tratamento de GB recentemente detectado envolve uma abordagem multidisciplinar. Atualmente, a terapia padrão para o tratamento de GBs utiliza ressecção cirúrgica, seguida por RT e QT simultâneas com temozolomida (TMZ), conhecida como Temodal®, e QT adjuvante com TMZ (National Comprehensive Cancer Network - NCCN, 2015). Os GBs são normalmente tumores invasivos e localizam-se regularmente em locais importantes do cérebro, como as áreas responsáveis pelo controle dos sentidos, função motora e fala, portanto, a ressecção cirúrgica é arriscada. Além disso, esses tumores são altamente invasivos; portanto a ressecção completa da massa tumoral não é viável. As células malignas remanescentes e infiltrantes persistem consistentemente no interior do cérebro, levando à progressão tumoral avançada e até recidiva da doença (Wilson et al., 2014). Existem várias complicações relacionadas com o manejo do GB, incluindo a entrega insuficiente de medicamentos, lesão de tecidos saudáveis e resistência à QT. Entre as abordagens existentes, a QT, a imunoterapia e a RT podem, até certo ponto, auxiliar os pacientes com GB; no entanto essas estratégias apresentam características desfavoráveis (Piroth et al., 2007).

1.3.1 IMUNOTERAPIA

Na última década, aumentou-se o interesse no desenvolvimento de abordagens imunoterapêuticas para responder à malignidade do tumor. Entre os vários métodos imunoterapêuticos, linfócitos estimulados, medicamentos virais, vacinas baseadas em peptídeos, citocinas e tratamento de células dendríticas parecem ser abordagens prósperas para uso na terapia de GB (Polyzoidis et al., 2015). Um amplo número de estudos concentra-se na administração de bevacizumabe, um anticorpo monoclonal humanizado anti-fator de crescimento endotelial vascular (anti-VEGF), que age sobre a angiogênese. Quando combinado com TMZ em pacientes recém diagnosticados, não foi capaz de aumentar a sobrevida total dos pacientes (Gilbert et al., 2014).

Outra estratégia de tratamento é o uso de uma vacina anti-EGFRvIII. Esta abordagem, denominada Rindopepimute, foi demonstrada satisfatória no estudo de fase II combinada à TMZ com uma sobrevida de 21,8 meses (Choi et al., 2009), porém o estudo de fase III foi descontinuado em 2016 após a segunda análise parcial demonstrar falha em aumento da sobrevida comparado ao padrão (20,1 vs 20 meses) (Elsamadicy et al., 2017). Outro tratamento imunológico para terapia é a utilização de um anticorpo que inibe o receptor de morte programada 1 de célula T (PD-1) ou o seu ligante (PD-L1) (Xue et al., 2017). O inibidor de PD-1 (pembrolizumabe) já acarretou respostas satisfatórias em pacientes com melanoma avançado, câncer de pulmão de não pequenas células e carcinoma renal (Polivka et al., 2017). Em gliomas, um estudo clínico foi iniciado em 2014, com data de término estimada para 2018, mas ainda não apresenta resultados parciais (NCT02017717).

Embora as imunoterapias sejam opções interessantes para o tratamento, existem algumas complicações, como a seleção do paciente para desenvolver ensaios clínicos, o monitoramento da resposta corporal e a avaliação dos efeitos colaterais e consequências clínicas (Polyzoidis et al., 2015). Além disso, existem questões que precisam ser avaliadas: primeiro, os resultados pré-clínicos eficazes devem ser cuidadosamente analisados, pois é crucial levar em consideração as variações interespecíficas; em segundo lugar, a determinação da dosagem máxima aceitável não é alcançável na maioria dos casos e, finalmente, as respostas imunes durante o monitoramento *in vivo* são muito complexas.

1.3.2 RADIOTERAPIA

A opção de tratamento inicial mais usual para pacientes com GB é a RT. No entanto, existem inúmeras desvantagens relativas ao uso desta abordagem. Um aspecto importante é que a reação do tumor à RT é influenciada pelo seu tamanho. Dada a biologia do tumor multifacetado, tumores grandes quase não respondem à RT, em contraste com amostras menores, e além disso, quanto mais cedo o tratamento começar, melhor será o resultado, tendo em vista que a RT é mais eficaz nos primeiros cinco anos após a ressecção (Stupp et al., 2005). Os efeitos colaterais da RT incluem efeitos agudos e crônicos. Os efeitos colaterais agudos incluem esterilidade, abscessos gastrintestinais e danos nas superfícies epiteliais da boca e da garganta. Os efeitos tardios incluem doenças cardíacas, perda de cabelo, fibrose e linfedema (Piroth et al., 2007).

1.3.3 QUIMIOTERAPIA

A TMZ é o fármaco de escolha central para o tratamento do GB (Verma et al., 2014), consistindo de uma imitatrazazina imitativa de segunda geração, e seu efeito tóxico é devido à metilação do DNA (Baumann et al., 2004). A TMZ é um pró-fármaco, o que significa que ela é espontaneamente hidrolisada em pH fisiológico e se converte no medicamento ativo, o 5-(3-metiltriazeno-1-il)imidazol-4-carboxamida (MTIC) (Baumann et al., 2004).

A TMZ é administrada por via oral usada regularmente nos estágios iniciais do tratamento com GB. Mesmo que a TMZ tenha benefícios na terapia com GB, existem inúmeras complicações, como por exemplo a existência da BHE, que limita a entrega de fármacos a locais específicos, assim como a O^6-metilguanina DNA metiltransferase (MGMT), que pode gerar um reparo inadequado do DNA. A última consequência pode modificar o fenótipo celular e, consequentemente, aumentar a resistência celular à TMZ (Hegi et al., 2008). Esses fenótipos podem alterar a expressão de proteínas-chave, como p53, PTEN, EGFR, *Mouse double minute 2 homolog* (Mdm-2) e galectina-1. Para superar essas complicações, novas drogas que podem direcionar essas proteínas são necessárias. Por exemplo, para inibir MGMT é possível usar O^6-benzilguanina também, alguns

inibidores de tirosina quinase podem suprimir EGFR e finalmente, nutlin-3 pode atuar como um inibidor de Mdm2 (Bischoff et al., 2009; Sok et al., 2006).

A dacarbazina (DTIC) é outro agente antitumoral que apesar de demonstrar uma absorção errática e pouca solubilidade (Di Bei & Bi-Botti, 2009), vem sendo estudada em GBs recorrentes, mostrando-se eficaz (Fazeny-Dorner et al., 2003). Apesar disso, DTIC causa toxicidade severa em tecidos saudáveis (Di Bei & Bi-Botti, 2009), por isso, novas formulações são necessárias para diminuir a toxicidade sistêmica.

A QT tem inúmeros efeitos nocivos, como náuseas e vômitos, erupção cutânea, diarreia, perda de cabelo, insônia, infertilidade e danos nos nervos. Atualmente, alguns relatos inferem que a QT em associação com diferentes abordagens, principalmente RT, oferece a estratégia de tratamento de GB mais eficiente (Charnley et al., 2009; Wong et al., 2007).

Imunoterapia, RT e QT apresentam resultados benéficos e prejudiciais. Acredita-se que a associação desses tratamentos pode melhorar os efeitos. Van Linde e colaboradores (2015) aplicaram abordagem de manejo neo-adjuvante para o GB recentemente identificado, que compreende um anticorpo monoclonal quimérico, bevacizumab, seguido por RT juntamente com TMZ. Seus resultados revelaram que este tratamento combinatório era seguro, no entanto, os pacientes apresentaram uma baixa taxa de resposta (Messaoudi et al., 2015).

1.3.4 HIPERTERMIA

A hipertermia é uma abordagem alternativa ao manejo do GB (Gong et al., 2011) e baseia-se na eliminação de células malignas dependente da produção de calor no local do tumor. Esse tratamento, portanto, induz alterações funcionais nas células e isso pode levar à morte celular (Yang et al., 2008). A hipertermia ocorre a uma temperatura de aproximadamente 45ºC e estimula vários mecanismos intra e extracelulares que incluem degradação celular, agregação de organelas celulares e desdobramento de proteínas, mecanismos esses que podem levar à apoptose (Hildebrandt et al., 2002).

Os parâmetros de tratamento, como a temperatura no local do tumor e a duração da exposição, alteram expressivamente a eficiência desse tratamento

(Baronzio et al., 2009). Entre as metodologias convencionais de indução de hipertermia, as mais comuns são irradiação infravermelha, micro-ondas e ultrassom (Mornet et al., 2004). No entanto, todos esses métodos apresentam limitações, como a baixa difusão de calor para as metástases tumorais. Particularmente em tumores que são bem vascularizados, o calor pode ser dissipado pelo sangue e isso pode ser um problema porque os tecidos saudáveis podem ser afetados. Com o objetivo de solucionar esses problemas, em 1957, partículas magnéticas passaram a ser utilizadas para hipertermia (Gilchrist et al., 1957) tornando-a conhecida como terapia de hipertermia magnética (THM). As limitações que vêm com o uso desta abordagem são a preparação dos materiais e o custo dos mesmos (Gilchrist et al., 1957). Ainda, ao longo dos anos, muitas pesquisas foram feitas para provar que a hipertermia é a única abordagem que falta para o sucesso da terapia GB. No entanto, muito poucos estudos combinatórios foram relatados. Alguns dos estudos clínicos realizados até o momento descreveram que a hipertermia poderia ser aplicada com segurança e com efeitos colaterais mínimos (Grupta & Sharma, 2019).

Para desenvolver técnicas-alvo com baixa toxicidade para tecidos saudáveis, várias abordagens diferentes estão sendo investigadas, como radioimunoterapia, radiocirurgia estereotáxica, hiperfracionamento e braquiterapia com iodo-125. No entanto, esses métodos não têm aumentado significativamente a sobrevida dos pacientes (Barani & Larson, 2015). Devido a algumas deficiências, como baixo acúmulo de drogas no tecido, baixa especificidade e toxicidade, os manejos convencionais do GB restringiram seu uso em pacientes. Consequentemente, o uso de novas nanotecnologias é uma abordagem promissora, uma vez que apresentam resultados promissores no tratamento de GB.

1.4 ABORDAGENS NANOTECNOLÓGICAS

A categoria de tecnologia que se dedica ao emprego, produção e análise de materiais no tamanho nanométrico é conhecida como nanotecnologia. Esta categoria utiliza nanomateriais para fins de praticamente todos os aspectos de uso (Ganguly et al., 2014; Sohail et al., 2016; Peer et al., 2007; Wilhelm et al.,

2016; Lamprecht et al., 2015; Vert et al., 2012; Aminabhavi & Deshmukh, 2016, Jain et al., 2013, Xia et al., 2014, Aminabhavi et al., 2017). Os sistemas de administração de fármacos, do inglês *drug delivery systems* (DDS), baseados na nanotecnologia apresentam características farmacocinéticas melhoradas. Entre eles é possível citar elevada taxa de depuração, distribuição de grande volume de fármacos e elevada biodisponibilidade de fármacos no tumor, devido ao maior efeito de permeabilidade e retenção (EPR). Além disso, métodos baseados na nanomedicina podem transportar drogas através de barreiras biológicas (Cheng et al., 2011).

As formulações de nanocarreadores mais pesquisadas são emulsões, dendrímeros, micelas, lipossomas e polímeros. Os nanoprodutos poliméricos podem ser divididos em diferentes sistemas, incluindo nanoesferas, nanocápsulas, nanopartículas (NP) e nanofibras (NF) (Letchford & Burt, 2007). O primeiro grupo é composto por partículas coloidais sólidas nas quais drogas podem ser dispersas ou adsorvidas em uma matriz feita de polímeros. O tamanho das nanoesferas varia de 100 a 200 nm (Reis et al., 2006). As nanocápsulas, por outro lado, são sistemas vesiculares. Neste tipo de sistemas, a droga é encapsulada por uma cápsula de polímero. As nanocápsulas são um sistema comum a ser utilizado no aprisionamento de substâncias hidrofóbicas e, consequentemente, alguns homopolímeros que podem impedir a opsonização desses sistemas podem ser utilizados na formulação, como o ácido poliláctico (PLA) (Pourgholi et al., 2016). Finalmente, as NP e NF são nanoprodutos sólidos (tamanho entre 1 e 1000 nm) nos quais é possível encapsular ou dissolver drogas (Teixeira et al., 2005).

As NP e NF apresentam qualidades interessantes, uma vez que é possível utilizar esses carreadores para vários objetivos, como diagnóstico e imagem, entrega de genes e liberação de medicamentos. Devido à incorporação do fármaco no material, os efeitos secundários comuns dos fármacos podem ser diminuídos e, assim como, a rápida degradação enzimática do fármaco. Além disso, esses produtos biofuncionalizados podem atingir os tecidos-alvo em maior concentração, sendo uma boa escolha na entrega de substâncias biológicas como proteínas, peptídeos, ácidos nucléicos e antibióticos (Misra et al., 2003). A figura 2 mostra uma representação esquemática das NP e sua biofuncionalização. Ainda, dependendo da composição desenvolvida, esses

produtos, principalmente as NP, podem ser administradas por diversas vias, incluindo intravascular, oral, nasal, transdérmica e intraocular (Tzeng & Green, 2013). Portanto, os DDS baseados em nanotecnologia podem ser abordagens úteis em terapias relacionadas a doenças do SNC.

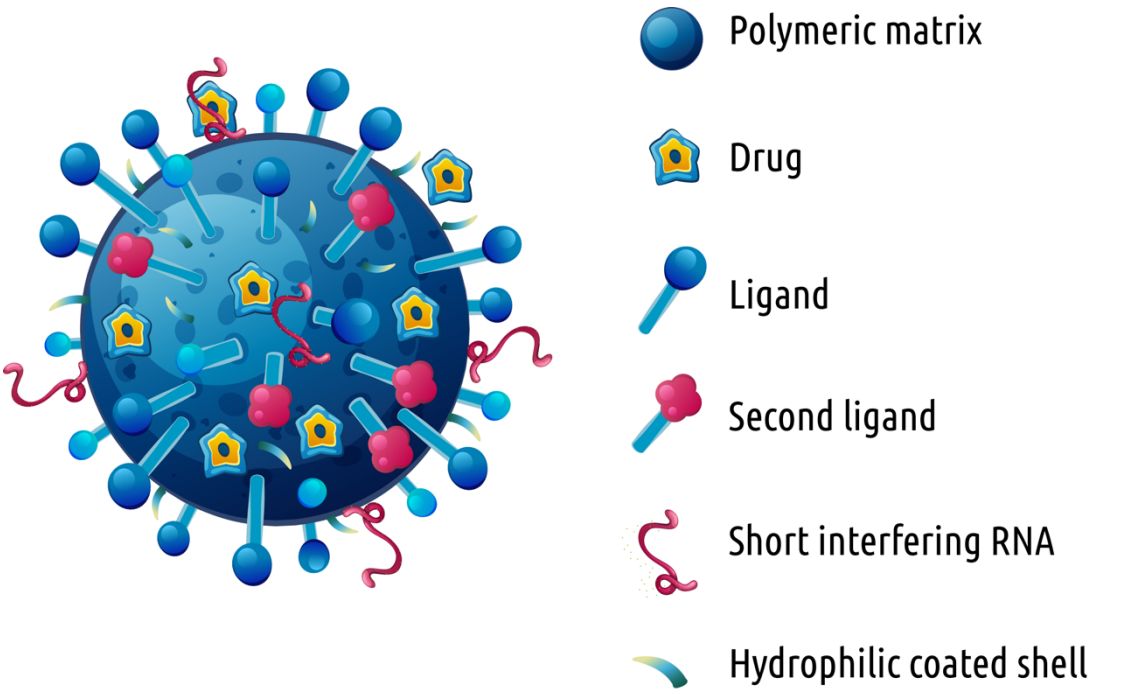

Figura 2: Representação esquemática de nanopartículas poliméricas e opções de biofuncionalização, tais como: ligantes na superfície, RNA de interferência e revestimento com substâncias hidrofílicas. Figura elaborada pelo autor.

1.4.1 SISTEMAS DE ENTREGA DE DROGAS (*Drug delivery systems* - DDS)

Numerosos obstáculos na terapia do câncer cerebral estão sendo abordados neste trabalho, tais como a baixa absorção, biodisponibilidade e baixa biodistribuição de drogas uma vez que resultados clínicos apropriados não são encontrados usando DDS convencionais (Xia et al., 2014). Para superar esses problemas, o desenvolvimento de novos DDS capazes de melhorar as propriedades farmacológicas das drogas é uma necessidade urgente. Nessa questão, a nanotecnologia associada ao DDS poderia ser a melhor abordagem na qual os sistemas devem prevenir os efeitos colaterais em células saudáveis (Zhu et al., 2013), uma vez que DDS aprimorados são capazes de melhorar a

adesão ao tratamento do paciente, além disso, podem aumentar a vida útil do fármaco e, consequentemente, diminuir os custos associados à assistência médica (Aminabhavi et al., 2017). Posteriormente, o desenvolvimento de DDS que apresentem propriedades controladas está demonstrando grande potencial e várias formulações nano-DDS estão sendo oferecidas para tratamento do câncer (Sun et al., 2016; Oh et al., 2010; Pan, 2013; She et al., 2013; Xi et al., 2014, Man et al., 2014, Sun et al., 2014).

Para desenvolver um DDS eficiente, algumas características são essenciais, tais como:

(a) um alvo específico;

(b) um transportador de fármaco útil;

(c) uma via de administração adequada.

As características físico-químicas do sistema DDS e do fármaco devem ser claramente entendidas, dado que o objetivo é atingir as células cancerígenas e evitar as células normais. Neste tópico, outro aspecto importante é a concentração do fármaco, pois os nano-DDS podem conter quantidades menores de fármacos, diminuindo a toxicidade, e consequentemente, os efeitos colaterais (Aftab et al., 2018).

Conforme descrito por Wen & Reardon (2011), apesar de todos os esforços para tratar GBs, nenhuma nova abordagem modificou o prognóstico da doença, justificando a necessidade de estudos sobre abordagens promissoras usando nanocarreadores.

1.4.2 ELETROFIAÇÃO

Existem diversas metodologias associadas ao desenvolvimento de DDS. Como exemplo, a eletrofiação (ou *electrospinning*) onde há a remoção do passo da emulsão que pode fazer com que os fármacos sensíveis percam a sua atividade, o que difere de outros métodos para produzir nanocarreadores (Cao et al., 2017). A eletrofiação é uma técnica utilizada para criar filamentos sintéticos em tamanho nanométrico utilizando forças eletrostáticas (Greiner e Wendorff, 2007).

Essa técnica permite a produção de NP e NF poliméricas com diâmetros variando de 3 nm a 5 µm (Subbiah et al., 2005). Tais nanoprodutos têm várias aplicações em nanocatálise, engenharia de tecidos, roupas protetoras e membranas filtrantes (Frenot e Chronakis, 2003; Subbiah et al., 2005).

A eletrofiação é uma técnica interessante tendo em vista a robustez do equipamento, o qual consiste em um suporte com a solução polimérica, uma seringa conectada a uma agulha, uma bomba de pressão cuja finalidade é controlar o fluxo da solução, uma fonte elétrica de alta voltagem e um suporte coletor produzido de material condutor (Ghorani & Tucker, 2015). O desenvolvimento do nanoproduto dá-se quando a solução é bombeada pelo sistema e um campo elétrico de alta voltagem é aplicado de forma a induzir a repulsão entre as cargas na solução polimérica. Devido à voltagem aplicada, ocorre uma deformação na gota formada na extremidade da agulha, alterando a sua forma para uma estrutura semelhante à de um cone, chamado de Taylor Cone (Taylor, 1964). Quando a força eletrostática supera a tensão superficial do polímero na extremidade da agulha, um jato (*spray* ou *spin*) é formado em direção à placa coletora enquanto que o solvente evapora permitindo a solidificação do material (Pham et al., 2006). Um esquema de um aparelho de *electrospinning* pode ser visto na figura 3.

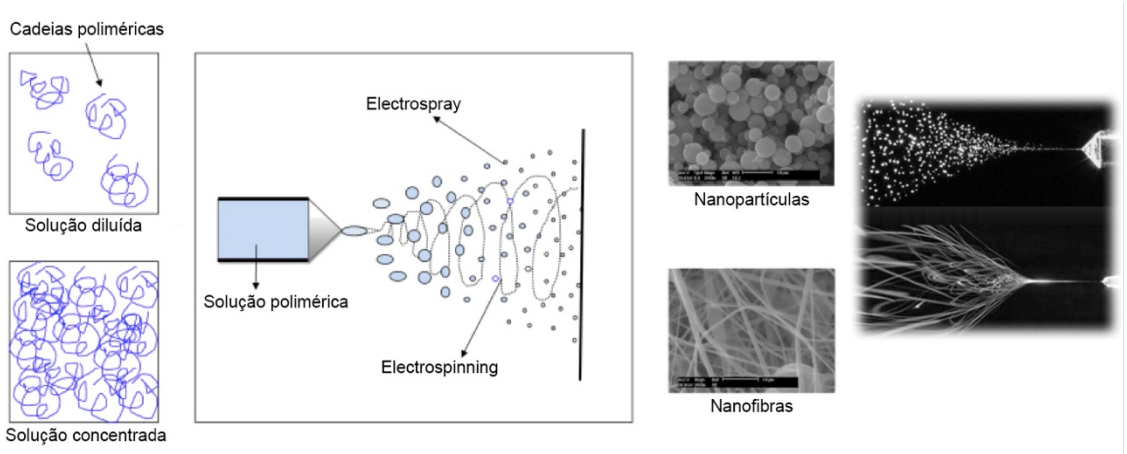

Figura 3: Esquema experimental da metodologia de eletrofiação. Adaptado de Ghorani & Tucker, 2015.

As características finais das fibras e partículas produzidas, tais como seu diâmetro, morfologia, grau de alinhamento e resistência mecânica podem sofrer interferência de vários parâmetros ajustáveis na técnica. Para esclarecer esses

efeitos, vários estudos têm sido realizados elucidando a correlação entre os parâmetros utilizados e a fibra resultante. Pham e colaboradores (2006) em sua revisão indicaram as variações de morfologia e diâmetro das fibras em função das mudanças nos parâmetros da eletrofiação (Pham et al., 2006). Lee e colaboradores (2004) estudaram a influência do peso molecular sobre a estrutura e propriedades de nanofibras de álcool polivinílico (PVA), e demonstraram as condições ótimas para a obtenção de fibras uniformes (Lee et al., 2004). Entre os parâmetros que afetam o processo estão: o polímero utilizado e a conformação da sua cadeia, o solvente, a viscosidade e a concentração da solução, elasticidade, condutividade, polaridade e tensão superficial do solvente, campo elétrico aplicado, distância entre o capilar e o coletor, velocidade de fluxo da solução polimérica pelo sistema, temperatura e umidade relativa do ar (Frenot e Chronakis, 2003; Huang et al., 2003).

Além disso, a estrutura resultante do nanoproduto, NF ou NP, normalmente é ditada pela concentração de polímero da solução. Partículas esféricas são produzidas em concentrações mais baixas de solução. Para encontrar a solução ideal, é importante ajustar sua viscosidade. Se a concentração da solução for excessivamente baixa, não há enredamentos de cadeias adequados dentro de uma gota para estabilizar o desenvolvimento do NP durante o *electrospray*, no entanto, se a concentração é alta há uma quantidade aumentada de emaranhados de cadeia que serve para estabilizar o jato, criando redes poliméricas e produção de fibras (Felice et al., 2015).

1.4.3 NANOCARREADORES POLIMÉRICOS

As propriedades do polímero, tais como cristalinidade, solubilidade, composição, peso molecular, polidispersividade e hidrofobicidade são características importantes para desenvolver um DDS (Masood, 2016).

Considerando os numerosos benefícios das NP poliméricas (PNP), tais como a administração direcionada da droga, biodisponibilidade melhorada, diminuição dos efeitos colaterais dos medicamentos, proteção da droga contra degradação, melhoria da solubilidade da droga e liberação sustentada do fármaco, seu uso no diagnóstico e tratamento de doenças do SNC é vantajoso (Zhang et al., 2013).

O DDS direcionado pode ser descrito como um material capaz de liberar um medicamento em um local preciso com dose apropriada. Essa abordagem pode ser separada em passiva e ativa (Gullotti & Yeo, 2009). No primeiro sistema, a liberação depende das diferenças entre tecidos saudáveis e não saudáveis. Sabe-se que os tecidos lesados apresentam diversas alterações em uma condição fisiológica através do efeito EPR (Guo et al., 2011). No entanto, os locais de tumor normalmente apresentam altas concentrações de drogas quando comparados aos locais normais (Kumari et al., 2010). O segundo sistema, usando técnicas de nanotecnologia, pode ser realizado adicionando ligantes específicos na superfície dos PNP (Bazak et al., 2015). Conjugação de ácidos nucléicos específicos, peptídeos e anticorpos revestindo PNP levam ao direcionamento específico. Além disso, isso pode modificar as vias de sinalização das células tumorais (Kim et al., 2014). A capacidade de modificar facilmente a superfície é uma propriedade excepcional adicional dos PNP (Sohai et al., 2016; Greineder et al., 2016). No entanto, para realizar a entrega desejada da droga, é importante compreender a natureza das PNP e as propriedades da droga. Conhecendo esses aspectos, é possível predizer a biocompatibilidade e a liberação (Aftab et al., 2018; Wang et al., 2008).

Polímeros tais como PLGA, poli (metacrilato de metila) (PMMA), poli (etilenoiminas) (PEI), poliésteres, poli (metileno malonatos) (PMM) e poli (alquil cianoacrilatos) (PACA) foram usados como transportadores de liberação de drogas (Kulkarni et al., 2010). A escolha correta do polímero dependerá do objetivo do tratamento. Por exemplo, o PEG é um polímero biocompatível, inerte e hidrofílico, tendo sido amplamente utilizado para projetar PNP, aumentando sua estabilidade (Cole et al., 2011). No entanto, o dano oxidativo evita seus usos a longo prazo (Jokerst et al., 2011). O PLA e o PLGA são os polímeros mais eficazes utilizados até o momento, uma vez que seus metabólitos são eliminados pelo ciclo de Krebs, sendo, portanto, não são tóxicos (Danhier et al., 2012). O PVA, um polímero hidrofílico não-tóxico aprovado pela FDA (*Food and Drug Administration)*, é uma opção interessante para projetar nanoprodutos, uma vez que este polímero apresenta baixa citotoxicidade e é biodegradável. O PVA também tem um excelente histórico em aplicações biomédicas como hidrogels principalmente (Chen et al., 2015; De Lima et al., 2015; Canillas et al., 2016).

1.4.3.1 NANOPARTÍCULAS POLIMÉRICAS

As NP poderiam ser eficientes no tratamento GB em função de suas várias propriedades, entre as quais, biocompatibilidade, tamanho pequeno e à produção simples, rápida e de baixo custo (Pourgholi et al., 2016). Adicionalmente, as NP podem melhorar vários aspectos da droga, incluindo estabilidade e liberação (Dikpati et al., 2012). Existem inúmeras diversidades de construções de NP e diferentes estratégias de design. A necessidade de desenvolver DDS efetivos, tanto sistemas seguros quanto biodegradáveis, fez das PNP uma das abordagens mais encorajadoras, alcançando reconhecimento abrangente no campo de DDS, particularmente em terapias contra o câncer (Tzeng & Green, 2013; Wilhelm et al., 2016).

As PNP são partículas coloidais de tamanho submicrônico que podem encapsular ou adsorver drogas, substâncias de imagem e agentes biológicos dentro ou sobre sua superfície. Considerando que as estruturas da matriz PNP permitem a adição de drogas, as superfícies facilitam a distribuição do corpo. Além disso, as PNP podem resolver limitações da QT, incluindo a resistência aos medicamentos usuais e efeitos indesejáveis (Pourgholi et al., 2016).

As PNP podem ser sintetizadas a partir de polímeros sintéticos tais como PVA, (poli (etilenoglicol) - PEG, poli (acrilamida) - PAM, ε-poli (caprolactona) - PCL e poli (acrilato) - PA) ou compostos naturais, como quitosana, gelatina, polissacarídeo e albumina (Wilczewska et al., 2012). PNP sintéticos, como PLA, PLGA e PGA são biocompatíveis e degradam-se hidroliticamente (Couvreur et al., 2002). Entre os PNP biocompatíveis, a FDA aprovou PVA, PLGA e PCL. Para entregar agentes a tumores cerebrais, principalmente polímeros catiônicos têm sido utilizados, especialmente para transporte de ácidos nucléicos, pois, possuem cargas positivas que lhes permitem interagir com DNA e RNA (He et al., 2011; Tzeng & Green, 2013).

As PNP podem ser alocadas em PNP biodegradáveis ou não biodegradáveis. Dada à baixa imunogenicidade, alta biodisponibilidade e estabilidade, baixa citotoxicidade e liberação administrável do medicamento, PNP biodegradáveis são geralmente usadas para DDS e são a opção apropriada para o encapsulamento de drogas hidrofóbicas (Pourgholi et al., 2016). Além disso, essas PNP mostram melhor estabilidade em fluidos biológicos (Lee, 2017), e

suas versões biodegradáveis são frequentemente empregadas com a finalidade de melhorar a solubilidade e a biodisponibilidade de substâncias bioativas (Kumari et al., 2010).

Embora as PNP sejam extensivamente estudadas para a entrega de medicamentos GB, a BHE permanece um desafio (Ma et al., 2015). Resultados significativos foram obtidos quando uma entrega intravenosa de NP de poli (n-butil-2-cianoacrilato) (PBCA) foi testada (Lin et al., 2012). Além disso, diferentes polímeros, como o PGA e o PLA, foram similarmente investigados como transportadores aumentando a eficiência de entrega de fármacos (Mundargi et al., 2008). Usando uma via não convencional, a administração intranasal que é capaz de contornar a BHE, Sekerdag e colaboradores (2017) analisaram as NP híbridas carregadas de ácido farnesil tiosalicílico (FTA) lipídicas-PEG-PLGA em ratos e estas PNP atingiram uma redução substancial da área do tumor.

Recentemente, Baghirov e colaboradores (2017) produziram uma nova plataforma com microbolhas de ultrassom focalizado (FuS) e NP de poli (cianoacrilato de 2-etil-butilo) que poderiam espaçar a BHE e acumular-se no parênquima cerebral. Nesta área, Mead e colaboradores (2016) estudaram em ratos um método combinado com entrega de material genético com liberação contínua. Notavelmente, este sistema alcançou resultados importantes sem indução de toxicidade ou ativação de astrócitos.

1.4.3.1.1 PNP NO TRATAMENTO DO GLIOBLASTOMA

A primeira PNP usado para entrega de drogas ao SNC foi a PNP de PBCA (Kreuter et al., 1995). Subsequentemente, o projeto de NP baseou-se na capacidade das PNP de atingir a BHE e de distribuir drogas no local do tumor usando endocitose mediada por receptores. Esse mecanismo faz com que materiais endógenos passem pela BHE. Além disso, mudanças na superfície das PNP (figura 4), como cobertura de surfactantes ou ligação de ligantes aumentam significativamente a captação celular, principalmente quando o ligante está associado a proteínas relacionadas ao receptor, que melhoram a ligação dos receptores às células do SNC (Aftab et al., 2018).

As modificações de superfície com surfactantes são uma abordagem muito comum. Em 2010, Gelperina e colaboradores demonstraram que NP de PLGA com uma superfície modificada com poloxâmero-188 apresentam resultados mais substanciais do que PNP sem a modificação. Em outro estudo que utilizou glioblastomas de ratos 101/18, Wohlfart e colaboradores (2011) mostraram que NP de PLGA com poloxâmero-188 e com doxorrubicina (DOX) foram capazes de atingir o cérebro e atravessar a BHE. Em outro estudo, poli (isohexil cianoacrilato) (PIHC) modificado com polissorbato-80 (P-80) foi testado *in vitro* contra células de GB, apresentando um uso promissor como um tratamento não invasivo de GB. Uma alternativa ao revestimento de NP são as PNP revestidos com glutationa. Geldenhuys e colaboradores (2011) apresentaram NP de PLGA com paclitaxel (PTX) e revestidos com glutationa que aumentaram a capacidade de atingir a passagem através da BHE.

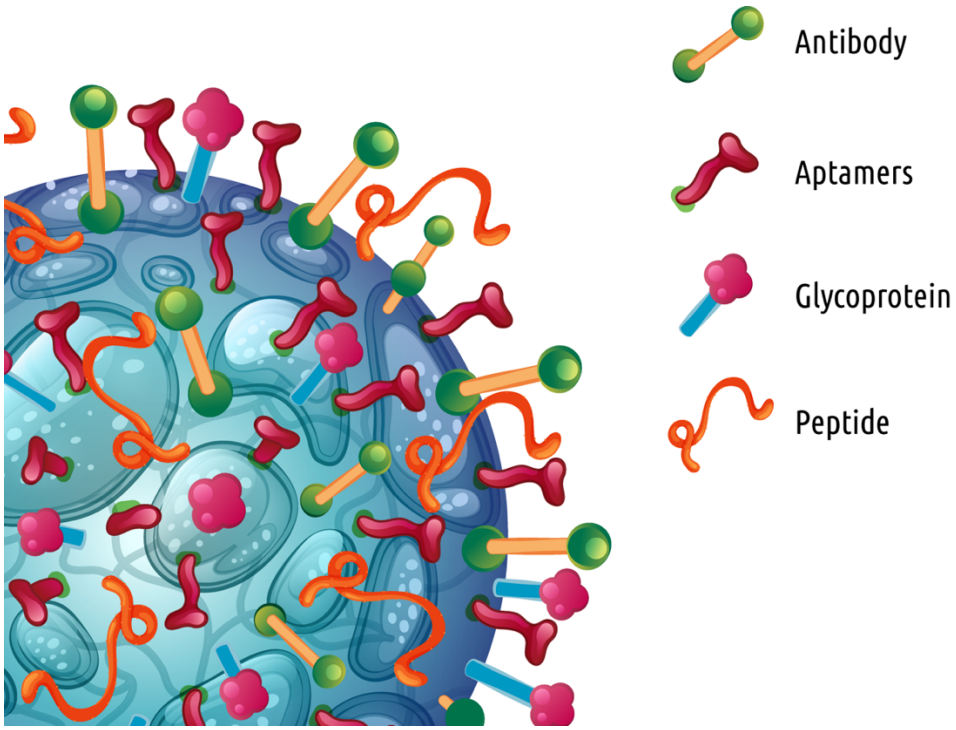

Figura 4: Nanopartículas poliméricas com modificações na superfície. Figura elaborada pelo autor.

Modificações adicionais, como a ligação de proteínas, podem levar a melhores resultados. A transferrina (TF), um ligante da glicoproteína dirigida ao cérebro que apresenta um receptor nas células endoteliais foi utilizada por Ren e colaboradores (2010) na funcionalização de PEG-PLA NP com resultados

demonstrando que a formulação atinge células C6 e atravessa a BHE de camundongos. A glicoproteína lactoferrina (LF) usada em NP de PEG-PLGA, também se mostrou eficaz para alcançar o cérebro dos camundongos (Hu et al., 2011). Son e colaboradores, em 2011, estudaram NP de PEI reticulados por dissulfeto modificados com a glicoproteína do vírus da raiva (RVG) (SS-PEI) que foram usados para fornecer microRNA ao GB.

Uma NP revestida por membrana de glóbulos vermelhos com a neurotoxina candoxina (CDX), um peptídeo que apresenta alta afinidade com receptores expressos nas células endoteliais do SNC, tais como os receptores nicotínicos de acetilcolina, também se mostraram eficientes (Chai et al., 2017). Devido a estas NP serem muito flexíveis, este sistema de metodologia poderia ser usado para vários tipos de membranas, atendendo diferentes propósitos médicos.

Fang e colaboradores (2016) usaram a clorotoxina (CTX), uma neurotoxina que se liga a membranas celulares, na superfície de uma PNP que continha um núcleo de quitosana funcionalizado com biotina e PEG e foi covalentemente conjugado com TMZ. As TMZ-CTX-PNP apresentaram maior captação pelas células de GB e foram mais eficientes no tratamento do que PNP sem CTX. Elas também foram capazes de atravessar a BHE e transportar a droga para o local do tumor, demonstrando-se uma opção promissora para transportar a TMZ em concentrações significativas e evitar a toxicidade em células saudáveis (Fang et al., 2016).

Ainda, Liu e colaboradores (2017) construíram um lipossoma contendo TF (TF-CPP-SSL) no núcleo via PEG. Estas TF-CPP-SSL PNP exibiram uma penetração pela BHE eficiente, aumentaram a circulação do fármaco *in vivo* e foram capazes de atingir o tumor. Além disso, mostraram alta captação celular e conseguiram evitar a degradação lisossômica.

Um aspecto importante para analisar o prognóstico em pacientes com GB é a ressecção necessária. No entanto, é difícil estabelecer um nível seguro de ressecção devido à malignidade do GB. Em um estudo recente, os autores desenvolveram uma cirurgia guiada por fluorescência, permitindo uma ressecção segura do GB. Tang e colaboradores conjugaram um aptâmero 32 a uma NP peguilada produzindo uma sonda de aptâmero capaz de se ligar especificamente às células cancerígenas (Tang et al., 2017).

A descoberta de alvos moleculares promissores para tratar GB é um desafio de pesquisa, no entanto, estimulou o desenvolvimento de abordagens de tratamento genético (Tabela 1). O baixo sucesso das terapias disponíveis está relacionado com a incapacidade dos vetores de chegar ao cérebro (Aftab et al., 2018).

Tabela 1: Nanopartículas poliméricas no tratamento de glioblastomas.

NP	Revestimento da superfície	Ligante	Droga	Resultados	Referências
MPEG	PLA	Folato	PTX	Ácido fólico induziu aumento na absorção celular.	Wang et al. (2010)
PLGA	PEG	AS1411, um aptâmero de DNA	PTX	Circulação da droga prolongada e acúmulo de PTX no tecido tumoral. Aumento na inibição do crescimento de gliomas em ratos e aumento da sobrevida do animal.	Guo et al. (2011)
PLGA	PEG	F3 e tLyp-1 peptideos	PTX	Acúmulo da droga no tecido tumoral, aumento na penetração no tecido e aumento da sobrevida do modelo animal.	Hu et al. (2013b)
PEG-co-PCL	MMP-2/9		PTX	Aumento da eficácia de PTX. Aumento da sobrevida animal.	Gu et al. (2013)
PLGA	Poloxamero 188/ Polisorbato 80		DOX/ lopeamida	Aumento da eficácia do tratamento devido a parâmetros da formulação como: surfactantes, droga e estabilizante.	Gelperina et al. (2010)
PLA	PEG	transferina		As NP funcionalizadas conseguiram penetrar no tecido tumoral.	Ren et al. (2010)
PLGA	PEG	lactoferrina		Testes de viabilidade demonstraram baixa toxicidade sistêmica.	Hu et al. (2011)
GNRs	PEG	Arg-Gly-Asp		Devido a ligação ao avβ3 houve um aumento da citotoxidade.	Verna et al. (2014)
PEG-PCL			PTX	Aumento da toxicidade via estabilização dos microtúbulos.	Xin et al. (2012)
PLGA			celecoxib	Inibição da ciclo-oxygenase-(COX).	Yoo et al. (2014)
PEG-SLN			c-Met siRNA	Inibição o c-Met e diminuição da proliferação celular.	Jin et al. (2011)

PEG lipossomal			DOX	Aumento da difusão de DOX pela BHE.	Steinigh et al. (2005)
PLGA	Poloxamero 188		DOX	Acúmulo de DOX no glioma.	Agarwal et al. (2011)
PAMAM dendrímero			mir-21 5-FU	Aumento da eficácia de 5-FU e da apoptose em GB.	Ren et al. (2010)
PLGA	Poloxamero 188		DOX	Entrega eficaz de DOX pela BHE.	Wohlfart et al. (2011)
PLGA	Glutationa		PTX	Aumento da habilidade de transporte pela BHE.	Geldenhuys et al. (2011)
SS-PEI		RVG	micro-RNA	Aumento da habilidade de transporte pela BHE.	Jon et al. (2011)
PIHC	Polisorbato 80		DOX	Potente vetor para o uso em terapias não invasivas.	Wohlfart et al. (2011)
MNP	PEG	CTX		Aumento da eficácia da droga.	Sun et al. (2008)
SPION	PEG	CTX		Aumento da absorção celular e diminuição da invasão tumoral.	Veiseh et al. (2009)
MNP	PEG e chitosan	CTX	siRNA	Sistema ideal para entrega de material genético na presença de um campo magnético.	Veiseh et al. (2010)
PLGA			celecoxib	Aumento da atividade antitumoral.	Suzuki et al. (2013)
PEG-co-PTMC	2-deoxy-d-glucose			Aumento da absorção celular.	Jiang et al. (2014)
MNP	PEG, chitosan e PEI	CTX	GFP	Aumento da absorção celular e da expressão de GFP.	Kievit et al. (2010)
MNP	PEG	Arg-Gly-Asp		Alvo-específico de células GB.	Cabada et al. (2012)
MNP	PEG		DOX	Liberação da droga promovida por luz infravermelha.	Agarwal et al. (2011)

AuNP	PEG		Aumento do dano no DNA de células GB após RT.	John et al. (2013)
AuNP	PEG	DOX	Aumento da absorção celular e da meia vida da droga.	Ruan et al. (2015)
PEG-PCL		PTX Angiopep	Aumento da habilidade de transporte pela BHE.	Dilnawez et al. (2012)

NP: nanopartículas; MPEG: metoxi-polietilenoglicol; PLA: ácido poliláctico; PTX: paclitaxel; PLGA: ácido poliláctico-co-glicólico; PEG: poli (etileno glicol); PCL: policaprolactona; MMP-2/9: metaloproteinase da matriz-2/9; DOX: doxorrubicina; GNRs: nanorods de ouro *(gold nanorods);* SLN: nanopartícula lipídica sólida; c-Met: proteína tirosina cinase Met; BHE: barreira hematoencefálica; 5-FU: 5-fluorouracil; GB: glioblastoma; PAMAM: poliamidoamina; SS-PEI: polietilenimina dissulfureto; RVG: glicoproteína do vírus da raiva; PIHC: cerâmica híbrida infiltrada de polímero; MNP: nanopartícula magnética; SPION: nanopartícula de óxido de ferro superparamagnética; CTX: clorotoxina; PTMC: poli (carbonato de trimetileno); GFP: *green fluorescent protein*; Au: ouro.

O PTX é usado para prevenir a mitose porque promove a congregação e a estabilização dos microtúbulos. No entanto, PTX é uma substância altamente hidrofóbica e não é capaz de atravessar a BHE. Para resolver este problema, o PTX pode ser absorvido em uma PNP (Hu et al., 2013c). O angiopep (ANG1005) é um peptídeo com 19 aminoácidos que é conjugado com o taxano, um inibidor mitótico. As PEG-PCL-NP conjugadas com angiopep e com PTX foram testados na terapia de glioma, reduzindo a proliferação de células do GB e aumentando a apoptose celular (Xin et al., 2012). Ainda, usando PLA NP, Wang e colaboradores (2010) produziram um alvo de folato modificado com monometoxi-PEG-PLA-PTX-NP que aumentaram a citotoxicidade contra as linhagens celulares HeLa e C6.

Em um estudo usando o AS1411 (Ap), um aptâmero de DNA, os autores produziram uma NP para a entrega de siRNA que diminuíram significativamente a proliferação celular devido à liberação prolongada do fármaco e apresentaram uma melhor biodistribuição do fármaco no local do tumor em comparação com o fármaco (Taxol®) (Guo et al., 2011). Em um estudo diferente com PEG-PLA-NP, o peptídeo F3, que similarmente ao Ap, se liga à nucleolina, foi usado para atingir as células tumorais promovendo um aumento na captação celular. Estas PNP exibiram maior acumulação, infiltração no local do tumor e sobrevida do modelo animal (Hu et al., 2013b).

Gu e colaboradores (2013) conjugaram a protamina de baixo peso molecular ativada MMP-2/9 com PEG-co-PCL-NP, estas NP melhoraram a captação em células, enquanto os resultados *in vivo* mostraram a acumulação de NP no local do tumor. Além disso, camundongos com implante de C6 e tratados com a formulação apresentaram maior tempo de sobrevida quando comparados aos grupos controle.

Um inibidor da ciclo-oxigenase (COX-2), o celecoxibe, apresenta sua ação promovendo a morte celular e diminuindo a proliferação celular (Suzuki et al., 2013). De um modo dose-dependente, as PLGA-NP com celecoxib apresentaram atividade contra linhagens celulares U87MG e C6. Esses resultados revelam essas NP como uma escolha eficiente para a entrega de medicamentos no GB (Kim et al., 2011).

Outra estratégia promissora são os dendrímeros de poli amidoamina (PAMAM) utilizados como transportadores de 5-fluorouracil (5-FU) e

oligonucleotidio anti-sentido miR-21 (as-miR-21) para locais específicos no GB (Yan et al., 2012). Quando testadas em células U251, a co-entrega de 5-FU e as-miR-21 aumentou expressivamente a citotoxicidade e a morte celular. Consequentemente, a co-administração de drogas e vetores moleculares, principalmente se o tumor apresentar uma superexpressão gênica conhecida, é uma abordagem interessante e eficaz no tratamento do GB (Ren et al., 2010).

Uma abordagem interessante é regulação negativa da proteína tirosina cinase Met (c-Met) que é um receptor de tirosina quinase que pode interagir com o fator de crescimento de hepatócitos e essa interação leva a um aumento na proliferação celular, corroborando com a invasividade e a resistência do GB à QT. Portanto, usando siRNA é possível suprimir c-Met e isso pode melhorar a terapia. A formulação PEG/c-Met-siRNA inibiu significativamente a resistência tumoral a fármacos e proliferação celular (Jin et al., 2011).

Liu e colaboradores (2017) apresentaram uma PNP que transporta e protege com sucesso siRNAs. As PNP formuladas envolveram AuNP PEGuiladas revestidas com PEI e quitosana. O siRNA para Ape1 foi adicionado à formulação e as NP foram testadas em células de câncer cerebral mostrando que a redução da expressão do Ape1 está relacionada a uma intensificação do dano ao DNA após a exposição à radiação.

Recentemente, Wadajkar e colaboradores (2017) formularam nanocarreadores particulados utilizando PLGA e PEG ligando o receptor Fn14, geralmente superexpresso em GB invasivo, na superfície. O aumento da eficácia observado sugere que essas PNP otimizaram o fornecimento de medicamentos para tratar GBs invasivos. Em outro estudo, os pesquisadores desenvolveram uma PNP usando poliestireno (PS) com uma superfície funcionalizada com um anticorpo que se liga ao Fn14. Os resultados mostraram que esta PNP foi capaz de penetrar no tecido tumoral visando seletivamente as células de GB (Schneider et al., 2015). Apesar desses estudos com PNP parecerem promissores, os métodos usuais de preparação são por vezes inconsistentes e complexos, o que prejudica a produção em série. Por outro lado, a eletrofiação é um método interessante para produzir NP sem o emprego de surfactantes e em grande escala.

1.4.3.2 NANOFIBRAS POLIMÉRICAS

Eventualmente, praticamente todo tumor recorre (Stupp et al., 2009). Os GB recorrentes são menos responsivos à QT do que o tumor original e são extremamente invasivos. Tendo em vista que o GB pode recorrer e invadir áreas funcionais do cérebro, a segunda ressecção cirúrgica é arriscada. Apesar da aplicação de todas as estratégias dos tratamentos, GB continua sendo uma doença incurável e a sobrevida global dos pacientes é entre 12 e 15 meses do diagnóstico inicial (Weller et al., 2013). Estudos de autópsia sugerem que GB recorrentes são principalmente locais e aparecem dentro de 2 centímetros do local inicial do tumor (Campos et al., 2016). Portanto, QT localizada que pode ser administrada durante a cirurgia e diretamente no local do tumor fornece um DDS alternativo para o tratamento do GB reduzindo significativamente os efeitos colaterais sistêmicos, podendo prevenir a recorrência do tumor.

1.4.3.2.1 NANOFIBRAS POLIMÉRICAS NO TRATAMENTO DO GLIOBLASTOMA

Apesar desta opção de tratamento ser extremamente promissora, poucos estudos foram realizados utilizando NF no tratamento de GB (Tabela 2). Como citado anteriormente, o PTX apresenta uma série de dificuldades em sua aplicação (Hu et al., 2013a), por isso, uma aplicação local da droga é uma escolha interessante para melhorar sua eficácia. Em um estudo, PLGA e PTX foram utilizados para fabricar submicro e microfibras. Ambas as formulações mostraram liberação prolongada de PTX *in vitro* ao longo de 80 dias, em que submicrofibras apresentaram maior taxa de liberação em comparação microfibras devido à maior área superficial e maior taxa de degradação do polímero. A superioridade das NF sobre a administração sistêmica de Taxol® em termos de apoptose também foram relatados. Além disso, a inibição tumoral em camundongos revelou que os animais tratados com fibra tinham tumores menores no dia 24 (até 44%) e no dia 32 (até 61%) pós inoculação do tumor comparada com animais tratados com Taxol®, indicando vantagens significativas da liberação prolongada de PTX (Ranganath & Wang, 2008). Em um estudo

similar, NF de PLGA carregadas com PTX com uma liberação de alta concentração de drogas apresentaram uma penetração de drogas no cérebro de ratos a 5 mm do local do implante, mesmo após 42 dias pós implante. Ainda, as NF demonstraram inibição tumoral e um baixo índice de proliferação tumoral após 41 dias de tratamento em modelos animais em comparação com o placebo (Ranganath et al., 2010).

Recentemente, Ramachandran e colaboradores (2017) desenvolveram NF de PLGA-PLA-PCL contendo TMZ, implantadas em modelo ortotópico de GB, que demonstraram uma liberação constante de droga (116,6 mg/dia), com um pequeno extravasamento para o sangue periférico (< 100 ng), indicando 1000 vezes maior concentração do fármaco no local do tumor em comparação com sangue periférico.

BCNU [1,3-bis (2-cloroetil) -1-nitrosoureia] (carmustina) é um dos agentes antineoplásicos mais comuns utilizados para terapia de GB que pode penetrar na BHE (Mehta et al., 2015). Seu mecanismo de ação é baseado na formação de *crosslinks* no DNA e RNA levando a inibição da síntese de DNA, produção de RNA, e tradução de RNA (Xu et al., 2006). No entanto, a perfusão intravenosa de BCNU está frequentemente associada a efeitos adversos, incluindo supressão medular, disfunção hepática e fibrose pulmonar. Além disso, sua curta meia vida plasmática (aproximadamente 20 min *in vitro* e menos de 15 min *in vivo*) limita a eficácia da aplicação sistêmica do BCNU (Xu et al., 2006). Gliadel® é um *wafer* biodegradável de poli (carboxifenoxi-propano/ácido sebácico) que libera BCNU; pode ser implantado na cavidade do tumor após a ressecção cirúrgica (Bregy et al., 2013). O medicamento foi aprovado pelo FDA para uso clínico e tem mostrado algumas melhorias na sobrevivência de pacientes de até dois meses a mais do que aqueles que não receberam o tratamento (Bregy et al., 2013). No entanto, a liberação rápida da maior parte da droga e a rigidez do *wafer* são importantes desvantagens. Tendo em vista isso, Tseng e colaboradores (2013) desenvolveram NF de PLGA que liberam altas concentrações de BCNU por mais de seis semanas no cérebro de ratos. Além disso, nenhuma reação inflamatória foi observada no tecido cerebral.

Em um estudo, a MMP-2 foi selecionada como um alvo terapêutico. Um plasmídeo de RNA suprimindo a expressão de MMP-2 em células tumorais foi desenvolvida e complexada com PEI. O gene e PTX foram encapsulados em NF

de PLGA para alcançar a prolongada liberação de ambos, demonstrando inibição tumoral significativa em modelos de tumor intracraniano comparados com NF carregadas com PTX e tratamento comercial de PTX, indicando efeitos terapêuticos sinérgicos do gene e do PTX (Lei et al., 2013).

Em outro estudo, três agentes quimioterápicos (bis-cloroetilnitrosoureia, irinotecan e cisplatina) e um agente antiangiogênico (combretastatina) foram carregados em NF de PLGA. Os agentes quimioterápicos foram rapidamente liberados das NF, enquanto a combretastatina mostrou um perfil de liberação de 2 semanas. Esta formulação foi considerada eficaz diminuindo o crescimento do tumor e prolongando a sobrevivência em ratos com GB em comparação com NF sem o agente antiangiogênico (Tseng et al., 2016).

Embora tenha se observado um aumento no interesse de pesquisadores em desenvolver fibras que podem fornecer uma liberação mais gradual de drogas durante um longo período de tempo para melhorar os efeitos das mesmas, as concentrações utilizadas nas formulações são muitas vezes tóxicas. Além disso, o procedimento experimental testado nos animais não reflete o que de fato acontece na clínica, tendo em vista que não são realizadas ressecções cirúrgicas.

Tabela 2: Nanofibras poliméricas no tratamento de glioblastoma.

NF	Droga	Resultados	Referências
PLGA	PTX	Liberação prolongada de PTX até 80 dias no qual submicrofibras demonstraram liberação mais rápida do que microfibras.	Ranganath & Wang (2008)
PLGA	PTX	Aumento da penetração da droga (5 mm) observada após 42 dias após implante.	Ranganath et al. (2010)
PPC-Ca-alginato MPs	PTX, TMZ	Efeito sinérgico das drogas.	Ni et al. (2014)
PCL-Diol-b-PU	TMZ	Liberação prolongada de TMZ até 30 dias.	Irani et al. (2018)
PCL	TMZ	NF upregularam p53 e Bax mais do que apenas TMZ.	Tavakoli et al. (2018)
PLGA, PLA, PCL	TMZ	Animais tratados com as NF com liberação prolongada demonstraram maior sobrevida (> 4 meses) do que àqueles tratados com NF de liberação curta (74 dias).	Ramachandran et al. (2017)
PCL	TMZ	Inibiu o crescimento tumoral e favoreceu a diferenciação de neurônios para reconstrução tecidual.	Huang et al. (2016)
PCL-Diol-b-PU-CS NP	TMZ e Au NP	Aumento da atividade antitumoral.	Irani et al. (2017)
PCL-Diol-b-PU	TMZ e Au NP	Aumento da atividade antitumoral.	Irani et al. (2017)

PEG-PLLA	BCNU	BCNU apresentou toxicidade apenas após 72 horas devido à liberação controlada.	Xu et al. (2006)
PLGA	BCNU	NF apresentaram liberação de BCNU por mais de 6 semanas em cérebros de ratos.	Tseng et al. (2013)
PEO, PLA	Rapamicina	Diminuição da viabilidade celular após tratamento.	Wang et al. (2016)
PC, PVP	Ácido micofenólico	Fibras preparadas com electrospinning coaxial demonstraram liberação gradual da droga.	Han et al. (2017)
PCL	Daunorubicina	Liberação controlada e prolongada da droga.	Lian & Meng et al. (2017)
PLGA	Bis-cloroetilnitrosurea, irinotecan, cisplatina, combretastatina	Diminuição da malignidade tumoral, do crescimento tumoral e aumento da sobrevida do modelo animal.	Tseng et al. (2016)
PCL-GT	SN-38	Aumento da citotoxidade após 72 horas.	Zhu et al. (2015)
PLGA,PEI	MMP-2 mRNA e PTX	Significante regressão do crescimento tumoral no tratamento com fibras com droga e gene.	Lei et al. (2013)
PLA	TRAIL	NF liberaram a proteína TRAIL acarretando redução do volume tumoral em camundongos.	Bagó et al. (2016)
PCEC	Curcumina	Bloqueio de vias de sinalização de proliferação celular.	Guo et al. (2011)

NF: nanofibras; PLGA: ácido poliláctico-co-glicólico; PTX: paclitaxel; PPC: polipropileno copolímero; Ca: cálcio; MPs: nanopartículas magnéticas; TMZ: temozolomida; PCL: policaprolactona; PU: poliuretano; p53: *tumor protein 53;* Bax: proteína X associada a BCL-2; PLA: ácido poliláctico; CS: chitosan; NPs:

nanopartículas; PEG: poli (etileno glicol); PLLA: ácido polilático; Au: ouro; BCNU: 1,3-bis (2-cloroetil)-1-nitrosoureia; PEO: poli (óxido de etileno); PC: policarbonato ; PVP: polivinilpirrolidona; GT: gluotationa; PEI: polietilenimina; PCEC: PCL-PEG-PCL.

1.4.3.3 EFEITOS ADVERSOS DOS NANOCARREADORES

Normalmente, a maioria dos estudos que desenvolvem nanoprodutos utilizam materiais biocompatíveis e biodegradáveis. Por isso, os efeitos nocivos dos nanocarreadores devem ser mínimos. No entanto, existem alguns efeitos adversos descritos que podem estar relacionados com a área de superfície do produto, porque, esta superfície pode resultar na formação de espécies reativas de oxigênio (EROs), como o ânion superóxido e o peróxido de hidrogênio (Nel et al., 2006). Devido à existência de sítios de receptores de elétrons e doadores na superfície de transporte que podem reagir com as moléculas de oxigênio, isso pode levar à oxidação de compostos químicos mais próximos ou mesmo de organelas (Nel et al., 2006). Portanto, um fator essencial para analisar ao avaliar os efeitos colaterais dos nanoprodutos é sua área de superfície.

Além disso, um efeito colateral frequente são as reações de hipersensibilidade que alguns pacientes descrevem após a injeção intravenosa. Esse efeito adverso é comum não apenas para as formulações de NP, mas também para várias outras drogas e pode ser evitado com a administração de outra medicação aos pacientes ou diminuindo a taxa de infusão (Allen & Cullis, 2004). Geralmente, as reações de hipersensibilidade são maiores na administração de medicamentos livres quando comparadas às formulações de DDS. Um exemplo interessante é a administração da DOX. Sabe-se que este fármaco induz um efeito de cardiotoxicidade que pode ser diminuído quando se aplica uma formulação DDS. Além disso, é importante avaliar a possível toxicidade relacionada à substância transportadora remanescente. Por causa disso, polímeros biodegradáveis com uma expectativa de vida conhecida são essenciais para produzir formulações seguras (Senter & Springer, 2001; Aftab et al., 2018).

2. OBJETIVOS

2.1 Objetivo Geral

Desenvolver e caracterizar nanofibras e nanopartículas, contendo drogas antitumorais (dacarbazina e temozolomida) associadas a inibidor proteico de Nek1 produzidas utilizando a técnica de eletrofiação, e avaliar o potencial terapêutico *in vitro*.

2.2 Objetivos Específicos

Produção de nanopartículas utilizando álcool polivinílico e dacarbazina pela técnica de electrospray.

Produção de nanofibras utilizando álcool polivinílico, dacarbazina, temozolomida e inibidor da proteína Nek1 pela técnica de electrospinning.

Caracterização de nanoprodutos em relação a suas morfologias.

Caracterização química os nanoprodutos e seus contentes.

Anaálise da liberação dos fármacos pelos nanoprodutos.

Avaliação da viabilidade de células normais frente aos nanoprodutos.

Investigação do potencial antitumoral dos nanoprodutos em células de glioblastomas.

CAPÍTULO 1: Freeze-thaw electrospun PVA-Dacarbazine nanoparticles: preparation, characterization and anticancer evaluation

Artigo aceito no periódico International Journal of Polymeric Materials and Polymeric Biomaterials

The International Journal of Polymeric Materials and Polymeric Biomaterials - Decision on Manuscript ID GPOM-2019-4894

International Journal of Polymeric Materials and Polymeric Biomaterials <onbehalfof@manuscriptcentral.com>
Dom, 07/04/2019 08:19
luizasteffens@live.com

07-Apr-2019

Dear Dr. Reinhardt:

Ref: Freeze-thaw electrospun PVA-Dacarbazine nanoparticles: preparation, characterization and anticancer evaluation

Our referees have now considered your paper and have recommended publication in The International Journal of Polymeric Materials and Polymeric Biomaterials. We are pleased to accept your paper in its current form which will now be forwarded to the publisher for copy editing and typesetting. The reviewer comments are included at the bottom of this letter.

Once copy editing and typesetting is completed for your manuscript, you will receive proofs for checking from the publisher. You will receive these proofs for checking, and instructions for transfer of copyright in due course. The publisher requests that, once you receive these proofs, they are checked and returned within 48 hours of receipt.

Thank you for your contribution to The International Journal of Polymeric Materials and Polymeric Biomaterials and we look forward to receiving further submissions from you.

Sincerely,
Dr Munmaya Mishra
Editor in Chief, The International Journal of Polymeric Materials and Polymeric Biomaterials
munmaya@gmail.com

Freeze-thaw electrospun PVA-Dacarbazine nanoparticles: preparation, characterization and anticancer evaluation

Luiza Steffens[ab], Bor Shin Chee[a], Zhi Cao[a], Dinara Jaqueline Moura[b], Michael Nugent[a*]

a. Athlone Institute of Technology, Materials Research Institute, Athlone, Co. Westmeath, Ireland
b. Laboratory of Genetic Toxicology, Federal University of Health Sciences of Porto Alegre – UFCSPA, Sarmento Leite Street, n° 245, Lab.714, Porto Alegre City, Rio Grande do Sul State, Brazil

* Corresponding author. Address: Athlone Institute of Technology, Dublin road Athlone, Co. Westmeath, Ireland
E-mail address: MNugent@ait.ie (Michael Nugent)

E-mail addresses: luizasteffens@live.com (L. Steffens), b.schee@research.ait.ie (B.S Chee), zcao@research.ait.ie (Zhi Cao), dinaram@ufcspa.edu.br (D.J. Moura), MNugent@ait.ie (M. Nugent).

GRAPHICAL ABSTRACT

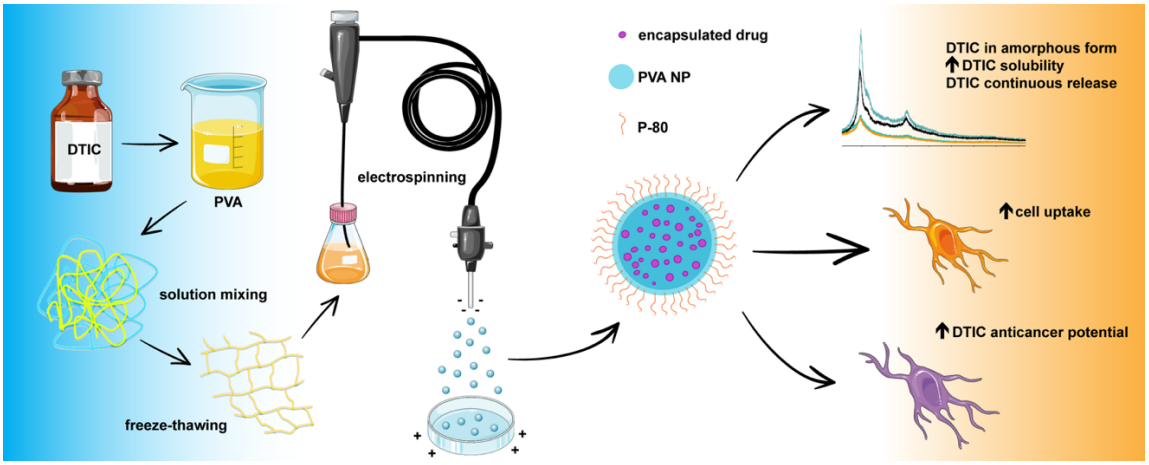

ABSTRACT

Dacarbazine (DTIC) is an antitumor agent that has limited clinical applications due to its insolubility, instability and toxicity to normal cells. One possibility to achieve controlled release is PVA-based NPs. This work presents electrospun NPs that combines PVA and DTIC. The results showed that DTIC NPs had mean particle sizes of 458.2±113.6 nm, suggested the presence of DTIC in an amorphous state and showed a burst *in vitro* drug release followed by constant release. The cytotoxicity evaluation showed that DTIC NPs were effective against glioblastoma cells. This study indicates that the formulated NPs improved DTIC solubility and efficacy.

Key-words: Electrospinning; Dacarbazine; Nanoparticles; Polyvinyl alcohol; Anticancer activity; Freeze-thaw.

Abbreviations: ANOVA: one-way analysis of variance, ATR-FTIR: attenuated total reflectance Fourier transform infrared spectroscopy, DMEM: dulbeco's modified eagle medium, DMSO: dimethyl sulfoxide, DSC: differential scanning calorimeter, DTIC: dacarbazine, EE%: percentage encapsulation efficiency, FBS: fetal bovine serum, F/T: freeze/thaw, MTIC: methyldiazonium, MTT: 3-(4,5-dimethylthiazol-2-yl)-2,5-diphenyltetrazolium bromide, MW: molecular weight, NP: nanoparticles, OD: optical density, PBS: phosphate-buffered saline, PNPs: polymeric NPs, P-80: polysorbate-80, PVA: polyvinyl-alcohol, Rho-B: rhodamine-B, SEM: scanning electron microscope, Tm: melting point, Tg: glass transition, UV: ultraviolet, XRD: x-ray diffraction.

1. INTRODUCTION

Dacarbazine (DTIC) is an antitumor drug analog of AICA ribonucleotide (5-aminoimidazole-4-carboxamide), which is an intermediate in the formation of inosine monophosphate in the purine biosynthesis [1]. By reason of that, DTIC was designed as an antimetabolite originally [1]. Though, given the action of its

metabolite, methyldiazonium (MTIC), which methylates DNA, DTIC has a significant cytotoxic activity [1].

Currently, DTIC is used as a chemotherapy drug against metastatic malignant melanoma [2,3]. Furthermore, it is used in combination with different drugs in the treatment of Hodgkin's disease, soft tissue sarcoma and can be used to treat recurrent glioblastoma, neuroblastoma and Kaposi's sarcoma, as an alternative treatment [4,5]. However, DTIC has some serious issues. Normally the administration route is intravenous, which results in low patient compliance, due to its associated pain. Moreover, the DTIC absorption in the body is generally inconsistent, slow and partial. Additionally, the drug has poor solubility, instability, photosensitivity and severe toxicity to non-cancerous cells, meaning that its medical applications are limited [6].

To encapsulate this drug using nanocarriers or nanoparticles (NPs) systems intended for controlled drug delivery is a promising approach to overcome these issues. NPs are nanosized materials that can bypass normal cells while delivering continuous doses of therapeutic substances into tumor cells. Moreover, NPs can improve the chemotherapy addressing issues, such as drug resistance, non-specific biodistribution and undesirable side effects [7]. Interesting NPs studies have been developed focus on the admission of NP-based treatments into clinical trials during the past decade [8].

Due to the capacity for targeting tumors, polymeric NPs (PNPs) are one of the most encouraging approaches to use in cancer therapy [9]. PNPs are also biocompatible; they normally present small sizes and the production is relatively simple and with low cost when compared to other drug delivery approaches [9]. PNPs can be separated into biodegradable and non-biodegradable. Biodegradable PNPs are usually used for drug delivery systems owing to several characteristics, such as low immunogenicity and significant encapsulation. In addition, they can improve some drug characteristics, for example, they can increase the stability, bioavailability and release rate of the drug [9]. Given the low systemic toxicity of the PNPs as drug delivery systems, they are an appropriate option in the delivery of hydrophobic medicines as DTIC. In this context polyvinyl alcohol (PVA) is a viable choice, since this polymer is very biocompatible, non-toxic and has an outstanding history when

used as bioproducts [10,11,12]. Owing their appropriate mechanical and swelling features, freeze/thaw (F/T) hydrogels can be produced with significant potential for using as delivery systems. These F/T hydrogels are produced by exposing PVA/water solutions to cycles of freezing and thawing; this process results in the formation of stable gels by the presence of crystalline regions [13,14].

Among the diverse categories of nanotechnologies to produce NPs, electrospinning has proved its effectiveness in producing nanoproducts in a one-step straightforward manner [15]. Even though the electrospinning method has an easy implementation, this method also has potential for generating NPs with multifaceted structures in an industrialized scale [16]. In addition, electrospinning can produce PNPs with different sizes, porosity, drug loading and release rate, leading to an opportunity of adapting the drug release rate for each usage [17].

The present study presents the first production and characterization of F/T electrospun PVA NPs for the encapsulation and controlled release of DTIC that could eventually be used to improve drug stability, efficacy, and safety in cancer treatment.

2. MATERIALS AND METHODS

2.1 Materials

PVA (MW 13000-23000, 90% hydrolyzed), Dacarbazine (DTIC), Rhodamine B (Rho-B), Ethanol, Acetic Acid, Methanol, Dimethyl sulfoxide (DMSO), Polysorbate-80 (P-80) and 3-(4,5-dimethylthiazol-2-yl)-2,5-diphenyltetrazolium bromide (MTT) were purchased from Sigma e Aldrich (Arklow, Ireland). Trypan blue, phosphate buffered saline (PBS), Dulbecco's modified eagle medium (DMEM), fetal bovine serum (FBS), L-glutamine, trypsin-EDTA and penicillin/streptomycin and were purchased from Gibco-BRL (Dublin, Ireland).

2.2 PVA nanoparticles preparation

PVA solutions were prepared by dissolving PVA (molecular weight of 13,000-23,000) at 10% concentration (wt/vol) in distilled water, at 90°C with continuous stirring until the complete solubilization of PVA was accomplished. Then, for samples containing drugs the temperature was decreased to 50°C and dacarbazine (10 mg) or rhodamine (10 mg) were mixed. After the solutions cooled down, ethanol

(10%) and polysorbate-80 (1%) were added. Then, the solutions were frozen (-80°C) for 1 h (Innova U535 freezer, New Brunswick Scientific, Edison, NJ). The samples were then thawed to room temperature. The solutions were electrospun using a blunt-end 20-gauge needle and a flow rate of 0.5 ml/h. 12 kV was applied to the tip of the needle and the needle tip to collector distance was 5 cm. For comparison proposes, two PVA solutions in the same concentration were prepared. One solution, PVA hydrogel, was submitted to the FT process and let dry at room temperature, the other solution, PVA film, was let it dry at room temperature without the FT process.

2.3 Determination of viscosity

The viscosity of the hydrogel solutions was measured by using a Discovery HR-2 rheometer (TA instruments, DE, USA). As the heating component, a Peltier plate was used at a temperature ramp and a 60 mm steel plate was used as the top geometry. The solutions were transferred into the plate of rheometer and viscosity of the samples was analyzed as a function of the temperature ramp (10-40°C).

2.4 Analysis of particle size and morphology

The NPs shape was studied using a scanning electron microscope (Tescan mira XMU SEM, TESCAN, Brno, CZ) in back scattered electron mode. The magnifications used ranged from 10kX to 80kX. The samples were sputtered with gold for 110 s at 0.1 mBar vacuum before testing. After the images recording, ImageJ software was used (ImageJ Version 1.48v) to determine the NP mean diameter. More than 200 DTIC NPs were evaluated.

2.5 Determination of loaded amount and encapsulation efficiency of DTIC

To evaluate the percentage encapsulation efficiency (EE%) of the loaded DTIC in the NPs, DTIC-NPs were completely dissolved in dH_2O to ensure that only free drug was quantified and the solutions were filtered. The amount of released DTIC was measured by ultraviolet (UV) light on Shimadzu UV 1280 spectrometer at 323 nm. The EE% of the DTIC was determined using a calibration curve of DTIC and the equation below:

$$EE(\%) = \frac{actual\ amount\ of\ loaded\ DTIC\ in\ NPs}{theoretical\ amount\ of\ loaded\ DTIC\ in\ NPs} X100$$

In this equation the actual amount of released DTIC in NPs was measured and the theoretical amount was calculated according to the concentration of DTIC added in the PVA solution.

2.6 Fourier transform infrared spectral study

Aiming to investigate the possible chemical interactions between DTIC and PVA after electrospray, attenuated total reflectance Fourier transform infrared spectroscopy (ATR-FTIR) was used. The analysis was accomplished using a Perkin Elmer Spectrum One fitted with a universal ATR sampling accessory (Perkin Elmer, Dublin, Ireland). The data were analyzed in the range of 4000-650 cm^{-1} using 4 scans per sample. Following investigation was performed using Spekwin32 software.

2.7 Differential scanning calorimetry

The physical state of DTIC after encapsulation in PVA NPs was examined using differential scanning calorimeter (DSC). The results were acquired by using a DSC TAQ2000 (TA instruments, DE, USA). The samples weights were measured and then, they were fitted in sealed aluminum pans, with weights between 5 and 10 mg. A temperature ramped from 20°C to 270°C was tested at a rate of 10°C per min with an empty pan as a reference. The results were plotted as a function of heat flow (W/g) against temperature (°C).

2.8 X-Ray Diffraction analysis

The molecular structure of the samples was examined by X-ray diffraction (XRD) analysis. The X-ray diffractograms were obtained in an X'Pert MPD PRO diffractometer (PANalytical, Netherlands) with Cu Kα radiation (λ = 1.54060 Å) in the 2θ range of 10–60◦. The intensity and voltage applied were 40 mA and 40 kV, respectively.

2.9 *In vitro* drug release studies

Drug dissolution profiles were achieved using a Distek Model 2500 Dissolution System (Distek, Inc., USA). A phosphate buffer solution (pH 7.4 at 37°C) was used to test the samples. The stir rate was set to 50 rpm with 900 ml of buffer used per sample vessel. Samples were taken at set periods and evaluated by UV light on

Shimadzu UV 1280 spectrometer at 323 nm. In this experiment sink conditions were used aiming to allow the complete dissolution of DTIC since sufficient media was used to ensure un-impaired dissolution, therefore, after each period of sample collection, the same amount of media was added in the vessel.

2.10 Cell uptake

The glioblastoma cells (U87) were kindly provided by Dr. Brona Murphy (Department of Physiology and Medical Physics, Royal College of Surgeons in Ireland). Cells were cultured in 10% FBS DMEM with antibiotics at 37°C in a humidified atmosphere containing 5% CO_2. The cellular uptake of NPs was studied in a time-dependent way. Frist, Rhodamine-B, a fluorescent probe, was loaded in the NPs. Then, glioblastoma cells were treated with Rho-B-NPs (1mg/mL) and incubated for different time points. After treatment, cells were washed with PBS and completely dissolved in Acetic Acid:Ethanol:dH2O (1:49:50, respectively). The NPs uptake was acquired using a plate reader (BioTek Synergy HT, Swindon, UK) at 543 nm. The quantity of NPs into the cells was calculated using the subsequent formula:

$$\%\ cellular\ uptake = \frac{amount\ of\ Rho-B\ taken\ up\ by\ cells}{total\ amount\ of\ Rho-B\ added}\ X\ 100$$

Furthermore, the cells were seeded in six-well culture plates and then, incubated with Rho-B-NPs or Rho-B for 2, 6 and 24 hours. After treatment, cells were washed with PBS and fixed in methanol. Fluorescence images were acquired using the Leica DM 2000 confocal microscope with an x40 oil lens (Leica Microsystems, Ireland). Image acquisition was performed by LAS V3.8 software (Leica).

2.11 Cell viability evaluation

The NPs cytotoxicity was analyzed by using MTT colorimetric assay. U87 cells (1×10^4 per well) were seeded in 96-well culture plates and incubated at standard conditions. Cells were exposed to different concentrations of blank NPs and DTIC-loaded NPs for 24 hours or 5 days. Cells were then treated with MTT reagent for 3 hours at 37°C. To dissolve the formazan crystals, DMSO was added to each well. The absorbance was recorded at 540 nm in a plate reader (BioTek Synergy HT,

Swindon, UK), and percentage of cell viability was calculated. The cytotoxicity of blank NPs was evaluated using 3T3 cells (as a control cell line).

2.12 Statistical analysis

The results were expressed as mean value ± SD. The statistical analysis was executed using one-way analysis of variance (ANOVA) following by Tukey posttest or two-way ANOVA following by Bonferroni posttest using GraphPad Prism 5 software (La Jolla, CA, USA). P-value (<0.05) were considered to be statistically significant.

3. RESULTS AND DISCUSSION

3.1 Fabrication and characterization of electrospun nanoparticles

To establish a controllable drug delivery system, DTIC-encapsulated NPs were fabricated using the electrospray method. Electrospray removes the emulsion step that can cause sensitive drugs to lose their activity, what differs from other methods to produce NPs [18]. Electrospinning equipment can produce NPs and nanofibers, the resulting structure of the nanoproduct is dictated by polymer concentration of the solution. Spherical particles were produced at lower solution concentrations. When higher concentrations were used, nanofibers with beads started to be visible on the support material (data not shown). To find the optimal solution, it is important to adjust its viscosity. Felice et al. built a solution screening using two PVAs with different molecular weights (MW) (low and high) and several concentrations. They suggested that the morphology transitions of the nanoproduct occur due to changes of MW or polymer concentration and that the leading underlying mechanism that effects the variation is the number of chains entanglements which accordingly causes modifications in solution viscosity. For electrospraying, it is essential to prepare solutions that have concentrations varying from the critical chain overlap concentration to entanglement concentration. If the concentration is excessively low there are not adequate chain entanglements inside a drop to stabilize the NP development and it loses its structure, however, if the concentration is high there is an augmented quantity of chain entanglements which serves to stabilize the jet, creating polymeric networks and producing fibers [39].

PVA, an FDA-approved non-toxic hydrophilic polymer, was used to produce the

NPs. Given that decreasing PVA MW, the solubility, flexibility and water sensitivity increase, PVA 13-23 kDa was selected. Moreover, low MW PVA solution presents low viscosity and facilitate the production of a spray [18, 39]. The NPs were coated with polysorbate-80 (P-80) to improve the cell absorption, given that there have been numerous reports of NPs coated with P-80 and these NPs presented a significant improvement in the anticancer drugs delivery to the brain [19,20,21]. DTIC was chosen as a model drug to be combined in the PVA NPs since DTIC is an unstable antineoplastic drug however, it has several anticancer applications.

The characteristics of PNPs should be analyzed under their assembly, mechanical properties and functionalization in generating a worthy drug delivery system. By utilizing PVA and electrospinning, it is possible to produce PNPs with customizable composition, size, drug loading and controlled release rate [17]. However, thermosensitive compounds that are not stable in temperatures around 50°C are not indicated to be used with our preparation method. Additionally, for comparison proposes, two PVA solutions in the same concentration were prepared (PVA hydrogel that was submitted to F/T process and PVA film). It is important to compare control PVA samples with electrospun samples and evaluated its chemical and behavior modifications, because it is the first time that a NP was produced using electrospray from an F/T solution, and our results suggested that the F/T gave the adequate viscosity to produce NP and, even that the F/T process increases crystallinity of polymers, our NPs showed greatly improved solubility.

To investigate the outcome of PVA concentration different PVA solutions were tested (data not shown) and the F/T 10wt% hydrogel was chosen because had the optimal viscosity to use in the electrospray equipment, since solutions with low viscosity do not have sufficient chain entanglements inside a drop in the Taylor cone to stabilize the NP formation, losing its shape when arriving in the collector plate; while high viscosity, there is an enlarged amount of chain entanglements which stabilizing the spray throughout the process given the increased surface tension. Moreover, particle size presents an important dependency on solution viscosity where higher viscosities involve more chain entanglements. Thus, using solutions with high viscosity is possible to obtain larger NPs. Previous studies with PVA NP production showed that low MW PVA is more suitable than high MW PVA for the

preparation of electrosprayed NP [39]. Additionally, taking into considerations that sustained release profile is desired over a slower one, the concentration of 10wt% provided stable NPs with controlled release.

Figure 1A shows the viscosity of a PVA hydrogel that was submitted to F/T method in comparison with a control PVA hydrogel, the higher viscosity of F/T hydrogel permitted a stable jet flow during the electrospray process (figure 1B). It is well known that PVA hydrogels prepared by F/T methods show improved mechanical strength when compared with most hydrogels given the presence of crystalline regions [13]. These regions function as physical crosslinks [13,14]. Moreover, water solutions are not suitable for electrospraying due to the high surface tension of the solvent, thus ethanol was added, mainly because of its safety.

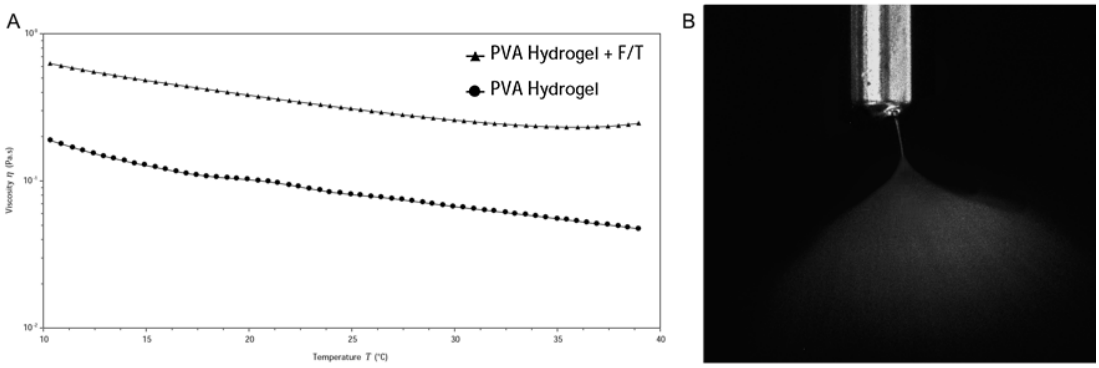

Figure 1: Viscosity analysis of the hydrogel solutions **(A)** Rheometer analysis of hydrogels viscosity **(B)** Taylor cone and resulting spray emanating from the needle tip at 12 kV (image taken with FlyCapture2 2.8.3.1 Software by Point Grey Research, Inc.).

Morphology and particle size play a substantial role in the evaluation of NPs designs [22]. Particle size has an important influence on the release of the drug, given that, smaller the size of the NP, larger the surface area, and consequently faster is the drug delivery [23]. The morphology of the NPs was observed by using SEM (figure 2A and B). The SEM images revealed that the particles were spherical and the average size was 458.2±113.6 nm (figure 2C).

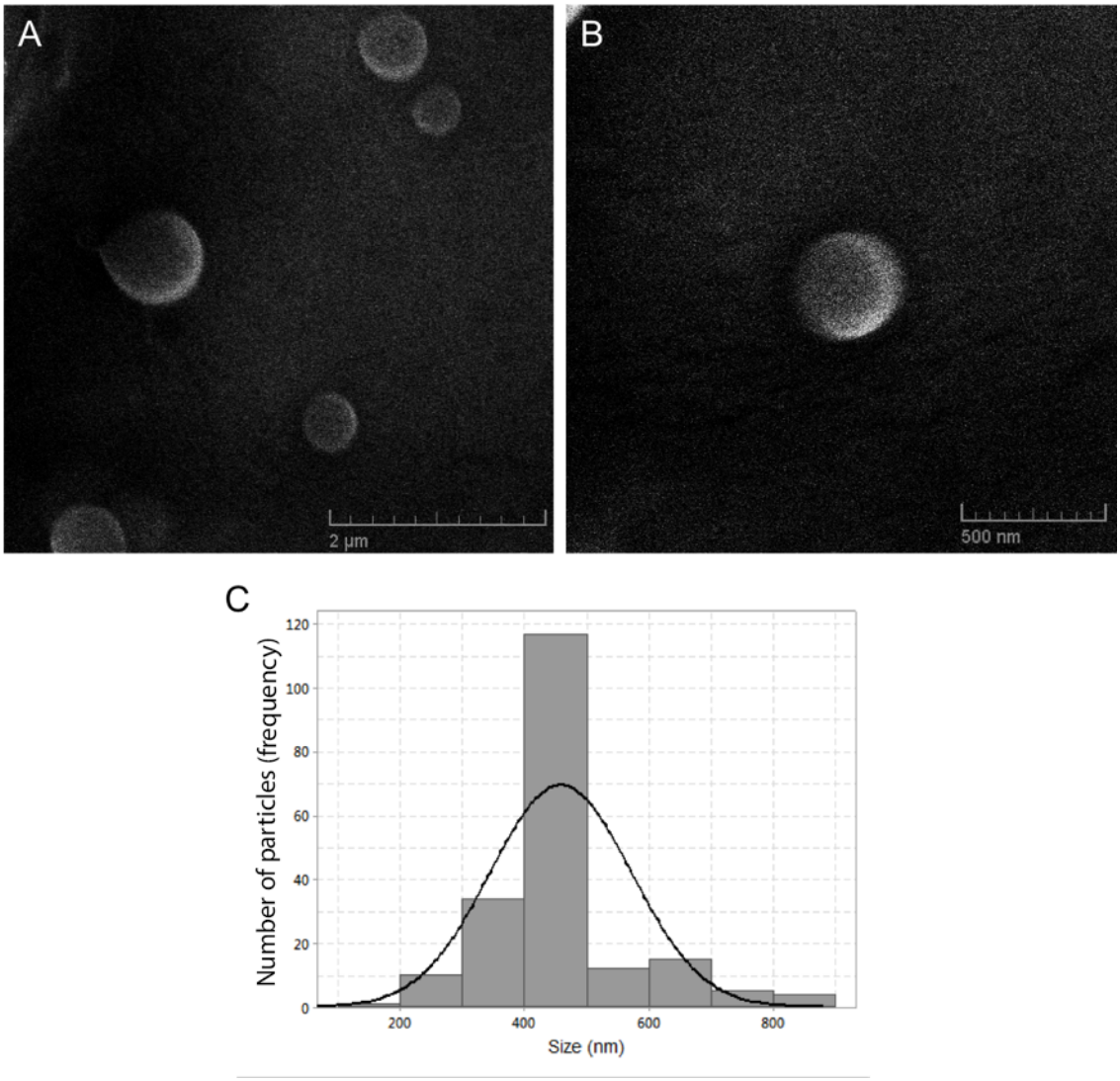

Figure 2: Characterization of the NPs **(A)** SEM images of NPs with 30kx of magnification **(B)** SEM images of NPs with 80kx of magnification **(C)** Particle size distribution of NPs.

FTIR was used to examine the characteristic chemical band of PVA electrospun NPs. FTIR fingerprints of PVA and DTIC have been reported in the literature [24,25,26]. It is possible to observe in all samples the characteristic bands of PVA. These peaks normally correspond to alcohol and carboxylic acid groups (figure 3). The large peak between 3500 and 3200 cm^{-1} was owing to the stretching O-H. The electrospun process resulted in more defined peaks and increase the 3302 cm^{-1} band which indicates the presence of more hydrogen bonding as compared to hydrogel sample, also 2948, 2850 cm^{-1} peaks are sharper. No significant shift alterations in the major peaks corresponding to PVA can be observed for DTIC NPs

when compared to Blank NPs, indicating that there are no chemical interactions between DTIC and PVA. If a band shift is detected this phenomenon is interpreted as the manifestation of changes in the FTIR associated with a specific chemical bond under the influence of molecular interactions [27, 41].

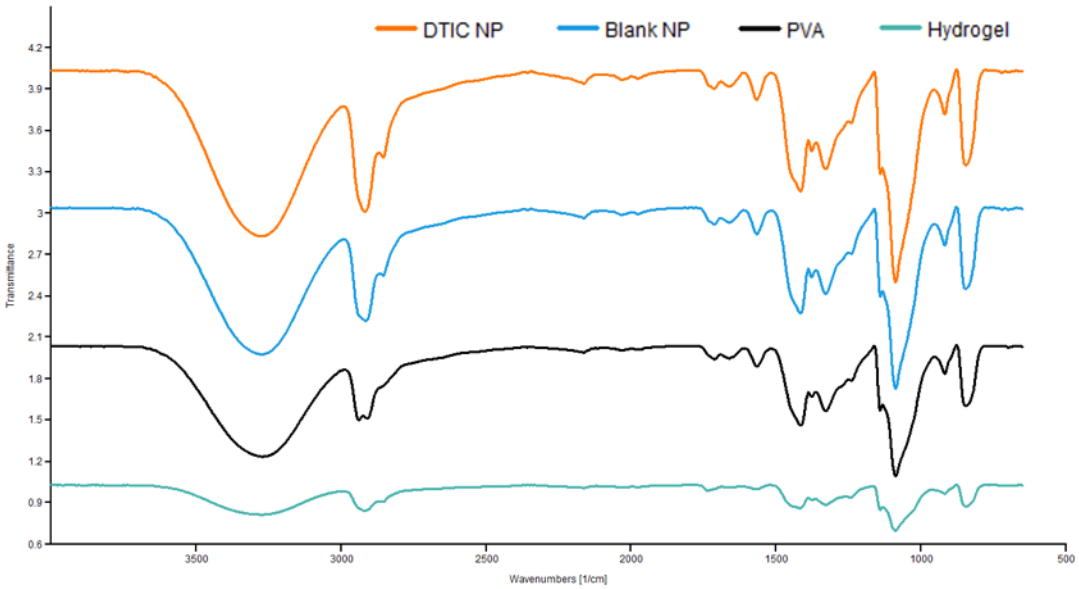

Figure 3: FTIR spectra of the PVA film (black line), PVA Hydrogel (green line), Blank NPs (blue line), DTIC NPs (orange line).

The thermal behavior of NPs loaded with DTIC in comparison with thermogram of DTIC powder is demonstrated in figure 4. It is crucial to evaluate the amorphous and crystalline properties of the samples, since the aim of the NP is to increase the solubility of the drug, therefore the comparison between different approaches (NP, hydrogel, film) with different complexity is important to understand which sample presents the best delivery properties. Additionally, it is interesting to study how the thermal transition of PVA varies after electrospinning process to evaluate if the sample preparation changed the thermal transitions of the polymer. Furthermore, one key aspect is the determination of whether the resulting blend samples results are miscible or not is the evaluation of thermal behavior of the NP with DTIC [42].
A thermogram of pure PVA film, PVA hydrogel and PVA NPs is shown in figure 4A. The sharp peak at 220°C represents the melting point (Tm) of the PVA. The α-

relaxation which characterizes the glass transition (Tg) of PVA is exemplified by the step change at around 40°C to PVA film and PVA NPs and 59°C to PVA hydrogel. These values are substantially different than the value described in previous studies [28], nevertheless, according to Hirankumar [29] this is due to the incidence of water and its plasticizing consequence on the polymer and for PVA crosslinked hydrogels it was found a Tg in the region of 55°C to 70°C [30]. The β-relaxation that characterizes secondary crystalline relaxation can be observed at 89, 113, 118°C to PVA NPs, PVA hydrogel and PVA film, respectively. These different transitions are probably due to microcrystallites or the evaporation of water [13].

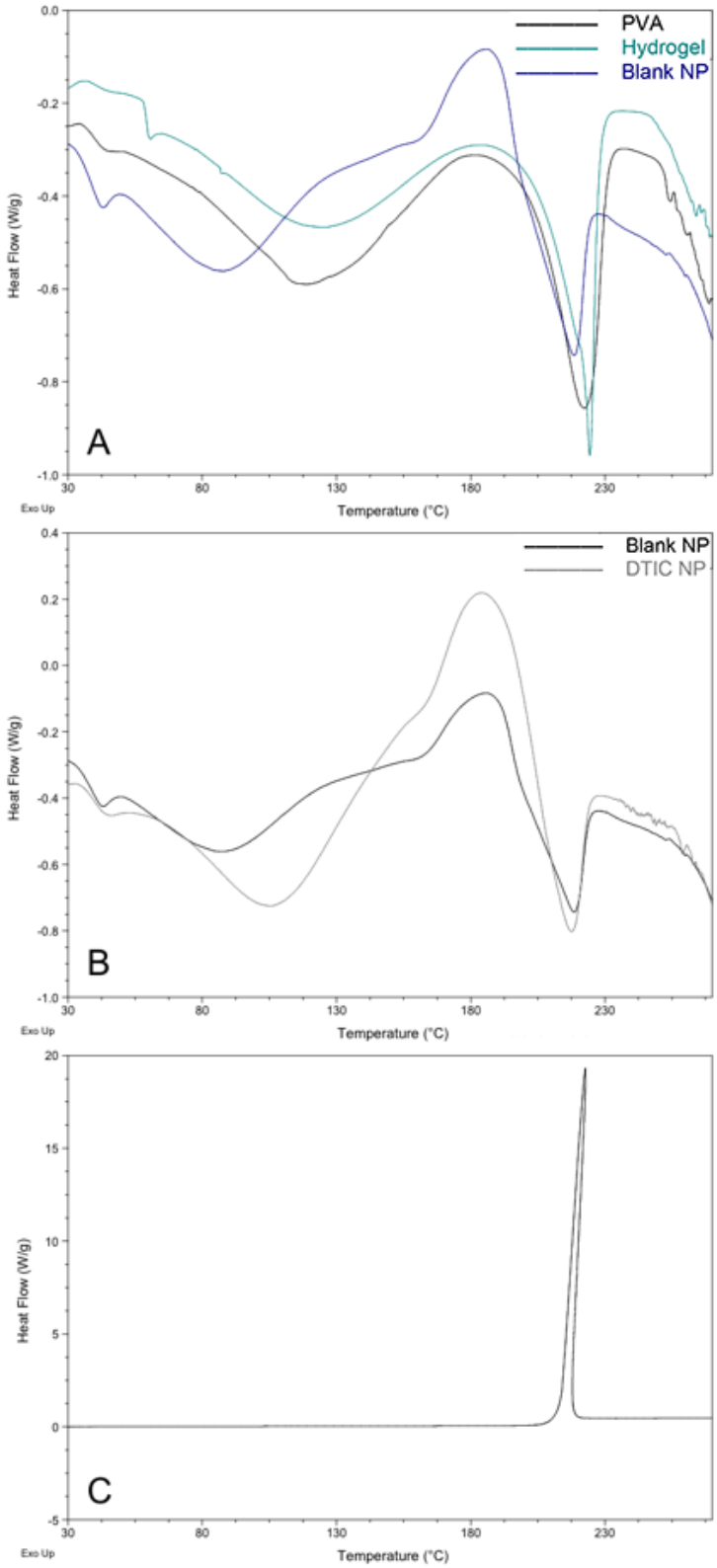

Figure 4: DCS curve obtained from (**A**) PVA film (black line), PVA Hydrogel (green line) and Blank NP (blue line) (**B**) Blank NPs (black line) and DTIC NPs (gray line) (**C**) DTIC in

powder form.

The NPs (figure 4B) also presented an exothermic peak around 180°C probably due to the elimination of adsorbed ethanol and/or water. Another hypothesis is due to the decomposition of residual organic matter and the hydroxide groups given the chemical rearrangement after the electrospinning process [31] since they lost 15.8%±3.9% (DTIC NPs) and 14.8%±5.1% (Blank NPs) of weight after the DSC process, while the PVA film and the PVA hydrogel lost 4.5%±2.1% and 5.3%±3.4%, respectively. The thermogram of DTIC powder (figure 4C) reveals a sharp exothermic peak at 213°C equivalent to its melting point. This indicates its crystalline state [6]. DTIC NPs shows an endothermic melting peak at 216°C, similar to the blank NPs. This result indicates that, probably, DTIC is incorporated in semi-crystalline state in the PVA NP construction. It is well known that modifying the physical state of a drug can change its energy state. In this case, an amorphous state of DTIC can lead to a high energy state and consequently in a high disorder and this can result in an enhanced solubility of DTIC [27,32]. This result is in agreement with the drug release analysis (figure 6).

It is possible to alter, in most polymers, the mechanical characteristics. For instance, given the constant arrangement of the polymer chains, a crystalline polymer probably will degrade and solubilize slower than an amorphous polymer. Nevertheless, amorphous polymers retain reduced mechanical robustness and in another hand, crystalline polymers are usually less suited for use in delivery systems [27]. Given that, the combination of both crystalline and amorphous polymer forms are more suitable to use as drug delivery systems [27].

It is recognized that the PVA polymer shows a semi-crystalline configuration with peaks at the 2 Â angles of 20 and 40◦ [33]. Figure 5 shows a large crystal peak at 2 Â of 20◦ in the PVA film. Given the physical crosslinked F/T process in the PVA hydrogel, where the crystalline domains of PVA act as knots of the gel network increasing the crystallinity [33] the peaks intensity augmented. It is possible to notice a greatly reduced of PVA crystal peaks intensity in the NPs diffractograms. This implies that submitted the hydrogel solution to electrospinning significantly increased the polymer amorphous region domain. This assumption is in agreement

with the DSC results (figure 4).

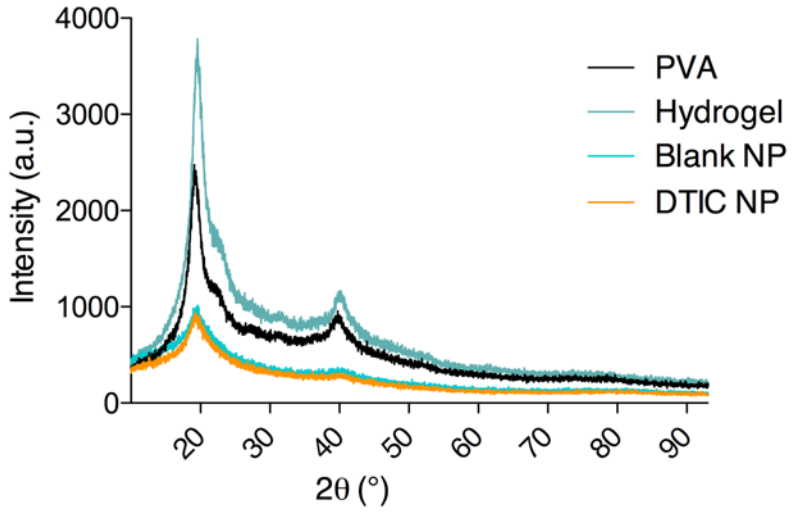

Figure 5: X-Ray diffraction of PVA film, PVA hydrogel, Blank NPs and DTIC loaded NPs.

It is possible to observe an effective DTIC encapsulation given the absence of crystallinity characteristic peaks of DTIC [6]. Additionally, during electrospinning, there is fast solvent evaporation consequently, the PVA NP sample solidified very quickly, leading to a decrease in the flexibility of DTIC molecules; this is in agreement with prior studies where the authors suggested that some drugs could lose or change the crystalline structure after the electrospun process. Depending on the drug content, these drugs can exist in amorphous from or semi-crystalline [32,34,35,36].

3.2 Drug release and encapsulation efficiency

The resulting drug release from the polymer environment strongly depends on the polymer selected for the matrix composition. In this study, PVA NPs presented a continuous release profile for DTIC during an interval of time. The hydrophobic domain of PVA mainly interacts with the hydrophobic domains of DTIC, and consequently presents a constant release, while the PVA hydrophilic domains enhanced the diffusion, permeability and degradation on the NPs. DTIC EE(%) was recorded as 59.7%±2.2%, which inferred that greater amount of DTIC was

encapsulated into PVA NPs. The sustainability of DTIC in the NPs was studied by using *in vitro* drug release method in physiological pH (7.4) at different intervals (figure 6).

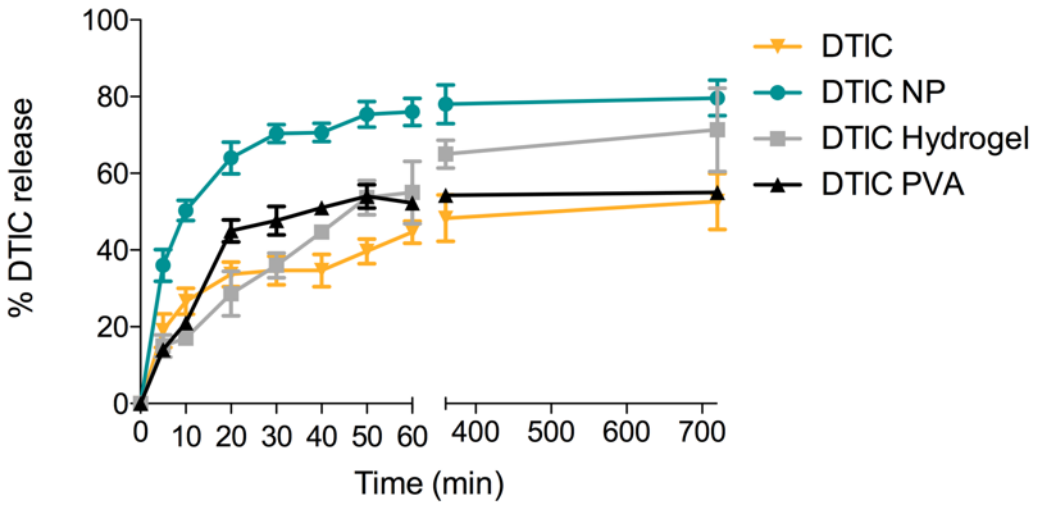

Figure 6: DTIC loaded formulations and DTIC in powder form *in vitro* drug release studies. Results of release studies are expressed as mean percentage ± standard error median of three independent experiments.

Drug dissolution procedure entails the release of individual drug molecules from the solid state into an aqueous environment. The essential factors related to this release are the chemical reactivity, solubility of the drug, system diffusion and kinetics behavior [40]. The principle behind Distek drug dissolution is to evaluate the rate of release of a substance from the dosage form. Due to NPs are usually used to enhance the bioavailability of these substances improving the dissolution rate of drugs, the DTIC by itself was also evaluated for comparison proposes. The release measurements of DTIC, DTIC NPs, DTIC/hydrogel and DTIC/film were recorded as 44.7%, 76.0%, 55.0% and 52.3% at 1 h, respectively. The release profile of the DTIC NPs exhibited an initial burst release (> 50% after 20 min) followed by a constant DTIC release during the following interval. This characteristic could be explained due to the dispersion of DTIC that is incorporated into the NPs but also adsorbed at the NPs surfaces and furthermore due to the resulted nanopores in the NP shell consequence of the electrospray process during the solvent evaporation [18,34,35].

To achieve an appropriate antitumor treatment, it is necessary to have an initial burst in the drug release following by a continuous release aiming to treat the resistant glioblastoma cells that persist in the primary contact with the drug [36]. Given that, DTIC NPs is appropriate for cancer management and can be used to achieve a continuous release for antitumor treatment. Hence, in spite of the capacity of the DTIC NPs to offer a hydrophilic dissolving environment that improves DTIC dissolution frequency, the distributed state and the solubility of incorporated DTIC, expressively influence the drug release rate [34]. Regarding a poorly water-soluble drug, such as DTIC, the release may be a function of DTIC diffusion and erosion of the PVA in the NP matrix [34].

Aiming to analyze the *in vitro* drug release kinetics, the release profiles of the samples were analyzed using various kinetic models. Given the hypothesis that DTIC was homogeneously dispersed in the NPs, hydrogels and films, the samples were modeled as systems where the drug is assumed to be loaded into PNP by a packing of the drug and polymer [34]. The drug release data were fitted into Higuchi's and Korsmeyer-Peppas models [37] to evaluate which mechanisms were related in DTIC releasing from the samples. As shown in table 1, the curves made by using both kinetic models are in accordance with the release of DTIC from PVA samples (R^2 > 0.9027). The exponential factor "n" values were recognized to be between 0.4617 and 0.6324, demonstrating an anomalous drug transport, also known as non-Fickian diffusion-controlled drug release. In this kinetic model, both diffusion and erosion mechanisms are influencing the release [37], while DTIC, the drug by itself, presented an "n" value lower (0.2370), it shows that Fickian diffusion is the main mechanism of DTIC release.

These mathematical models of drug delivery systems have a substantial potential to assist understanding complex bioproducts evaluation, nevertheless, it is improbable to use a unique mathematical model to all types of drug delivery systems [38]. Although the release mechanisms of the PVA matrices need to be more clarified, this study demonstrated that DTIC is released from the electrospun PVA NPs in an initial burst followed by continuous release.

Table 1: Release behavior of DTIC loaded formulations and DTIC in powder form.

Sample		Model		
		Korsmeyer-Peppas		Higuchi
DTIC	n	0.2370	K	33.6480
	R^2	0.7357	R^2	0.8722
DTIC NP	n	0.5543	K	10.3000
	R^2	0.9628	R^2	0.9766
DTIC	n	0.6324	K	48.8800
Hydrogel	R^2	0.9840	R^2	0.9299
DTIC PVA	n	0.4617	K	17.6220
	R^2	0.9043	R^2	0.9027

Where, R^2 = regression coefficient, n = release exponent, K = Higuchi rate constant.

3.3 Cell uptake profile

To explore the cellular uptake potential of the NPs, DTIC was replaced with Rho-B. Rho-B is commonly used to analyze the NP behavior in cell culture, given that fluorescence probes enable researches to evaluate cell uptake of substances and particles [43,44]. However, its evaluation provides only an estimation of the behavior of drug delivery systems. As seen from figure 7A, Rho-NPs showed significant uptake mostly after 1 hour of treatment and a continuous uptake until 24 h after.

By using fluorescent microscopy, the cellular uptake was additional confirmed. Nuclei were stained with SYBR Green and a rhodamine-B solution was used as control (figure 7B and C). It is possible to observe that the cells exhibited a shiny fluorescence after 2 hours of treatment and, although it is not statistically significant, given the controlled release of the PVA NPs, after 6 and 24 hours, the fluorescence intensity was higher in the Rho-NP treated cell when compared with the cell treated with a Rho solution.

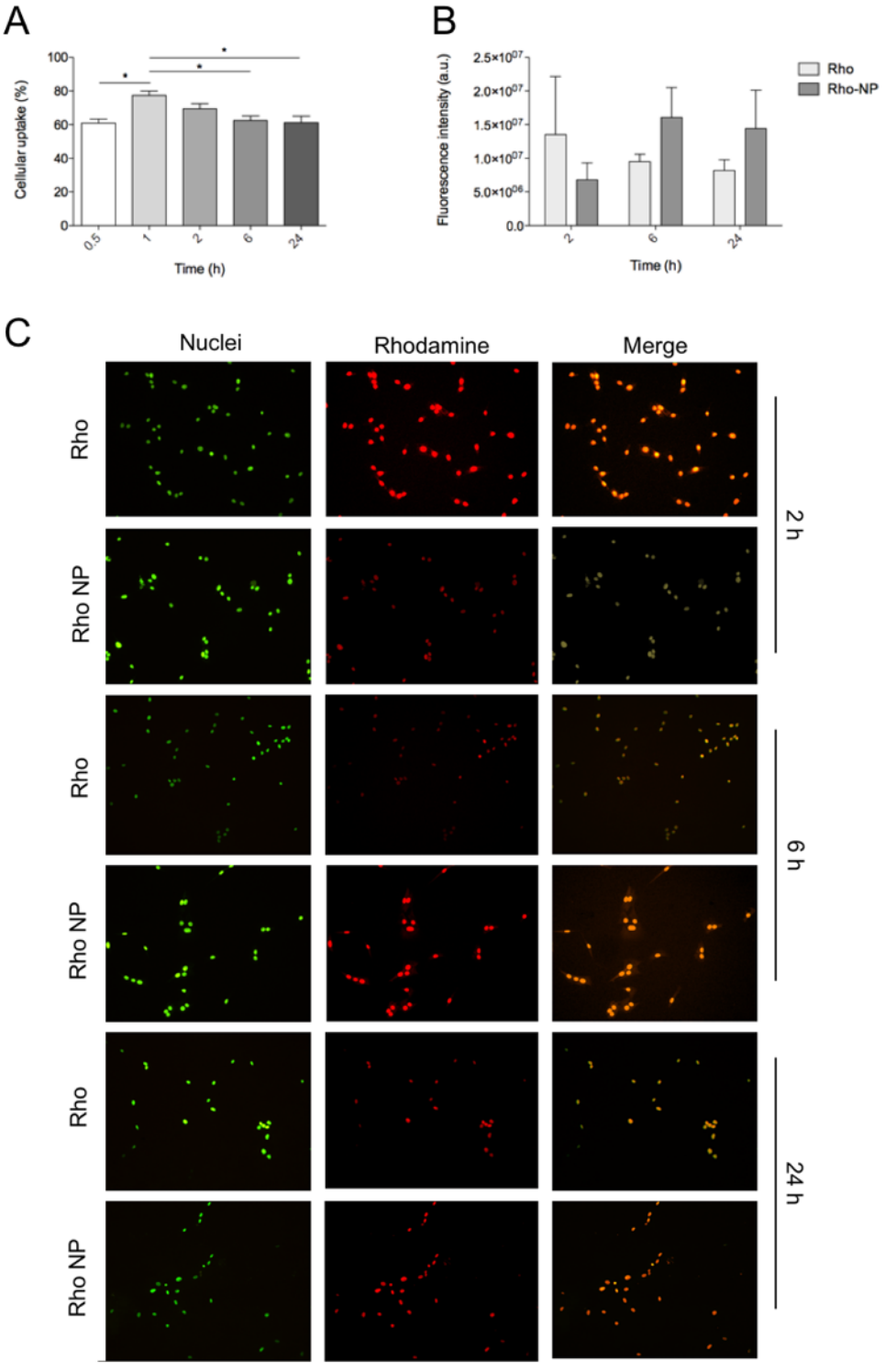

Figure 7: Cell Uptake evaluation **(A)** Cellular uptake of Rho-NP measured by spectrophotometry at 543 nm **(B, C)** Fluorescence intensity of Rho-NP and Rho solution. Results are shown as mean percentage in Rho-NP treated cells compared to Rho treated

cells ± standard error median of three independent experiments.

3.4 Cytotoxicity assay

Aiming to evaluate if the Blank NP could induce toxicity to normal cells (non-tumoral), 3T3 murine cell line was used to ensure that PVA NP is harmless and it could be used without cause side effects. The cells were treated with NPs at four different concentrations and incubated during 24 hours or 5 days. Figure 8A shows that blank NPs did not induce substantial toxicity when compared to the negative control (NC), given that the cell viability endured around 80% in all concentrations. This result indicates that the blank NPs are biocompatible and are appropriate for systemic administration in the cancer therapy.

The cytotoxic effect of DTIC NPs was estimated in U87 glioblastoma cancer cells by using MTT assay (figure 8B and C). The cytotoxic effect of DTIC NPs was estimated in U87 glioblastoma cancer cells by using MTT assay (figure 8B and C). The results showed a concentration (dose) dependent *in vitro* where the cytotoxic effect was obtained by the specific increase in the amount of tested substances. It was observed that after 24 hours, DTIC treatments were statistical more effective than DTIC NP in the concentrations of 0.2 and 0.6 mg/mL, however after 5 days of treatment DTIC NP treatments were more cytotoxic being statically significant in the concentration of 0.8 mg/mL. The concentration of 0.8 mg/mL was selected to test the Blank NPs. Moreover, after the 5-day treatment, the IC50 value of DTIC NP was 0.23 mg/mL and the IC50 of DTIC was 0.32 mg/mL, indicating that the NPs improved the efficacy of DTIC after prolonged exposure. It was possible to observe that after 5 days of treatment cells were detaching from the bottom of the plate (figure 8C). Moreover, the DTIC treatment of 0.2 mg/mL image suggest a formation of cell agglomerates, this is a typical protection mechanism of cancer cells related to stem-like properties. The same is not possible to perceive with the NP treatment, this may indicate that the NPs treatment can modify cell morphology. However, more experiments are needed to prove this hypothesis. These results indicate that cells are able to repair the damage induced by DTIC after its treatment, however, probably given the slower release of the NPs, cells are continuing to be treated for a prolonged period and are not able to perform a proper repair.

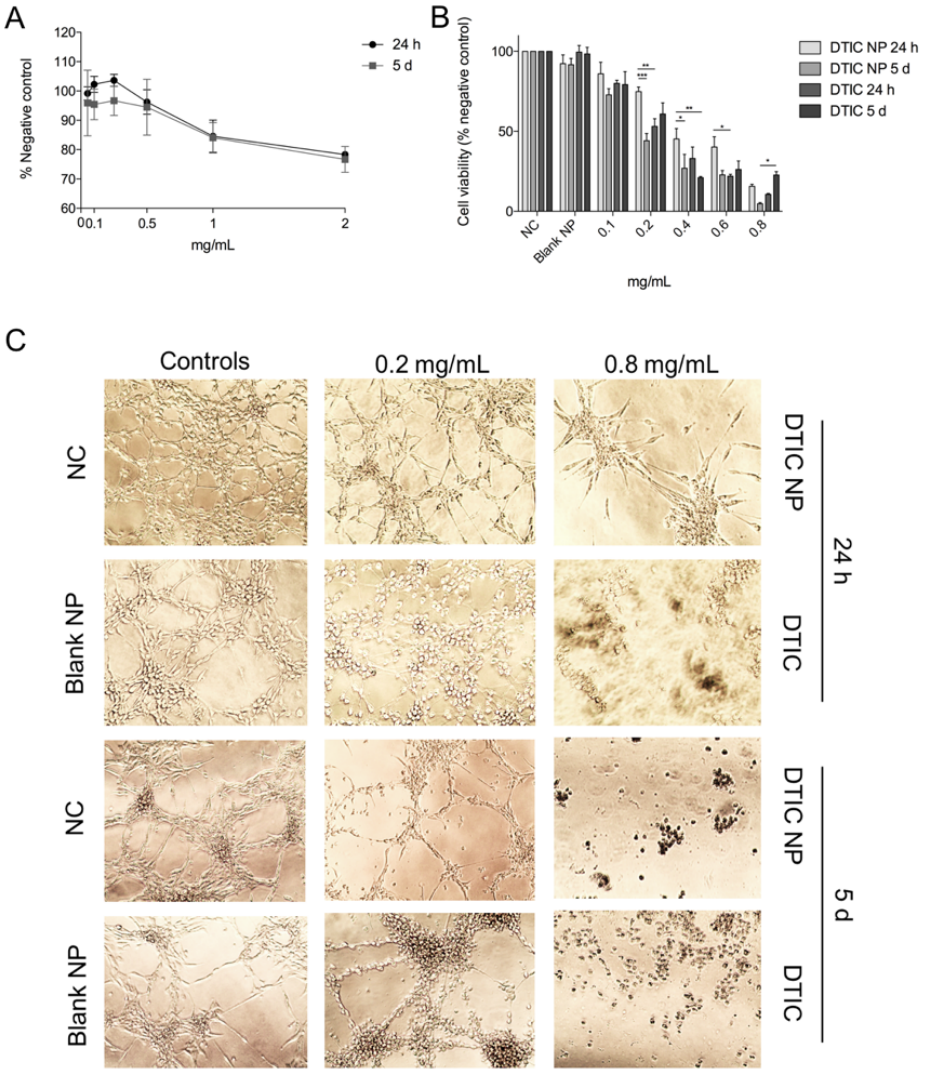

Figure 8: Cytotoxic effects of Blank NP, DTIC NP and DTIC in 3T3 and U87 cells after 24 h and 5 days exposure by MTT assay (**A**) Cytotoxic evaluation of Blank NPs in 3T3 cells (**B**) DTIC and DTIC NPs in U87 cells (**C**) U87 cells images over exposition to Blank NP, DTIC NP, DTIC and without treatment. The results are represented as mean percentage in blank NP, DTIC NP, DTIC treated cells compared to non-treated cells (negative control - NC) ± standard error median of three independent experiments.

Despite the extensive research to design efficient drug delivery treatments, drug efficacy in treating tumor cells, especially glioblastomas, remains restricted by the relatively trivial quantity of drug distribution and release in existing systems. Given that, these results suggest that the DTIC NPs have a considerably anticancer potential against glioblastoma cells.

4. CONCLUSION

DTIC was effectively entrapped in PVA NPs by using electrospinning method. The NPs particle size distribution indicated an average size of 458.2±113.6 nm, and the NPs were spherical. It could be established from characterization analysis that DTIC NPs were in an amorphous state. The cytotoxicity evaluation showed that DTIC NPs were more effective against glioblastoma cells than DTIC solution. It can be concluded that F/T electrospun PVA NPs show the potential drug release system of hydrophobic DTIC by improving its solubility and its cytotoxicity in glioblastoma cells. The future studies will incorporate *in vivo* evaluation and further refinement of the process.

Acknowledgments

This study was supported in parts by grants from the Athlone Institute of Technology research and development funding, GOI-IES (Government of Ireland International Education Scholarship) and CAPES (Coordenação de Aperfeiçoamento de Pessoal de Nível Superior, Brazil). We thank Dr. Wynette Redington (Bernal Institute, University of Limerick) for assistance with XRD analysis.

Conflict of Interest

The authors declare that there are no conflict of interest.

Statement of authors' contributions to manuscript

L.S, B.S.C and Z.C. conducted the experiments; L.S., D.J.M. and M.N. wrote the paper. All authors read and approved the final manuscript.

References

[1] Shealy, F. Y. Syntheses and biological activity of 5-aminoimidazoles and 5-triazenoimidazoles. *J. Pharm. Sci.* **1970**, 59(11), 1533-1538.

[2] Spieth, K.; Kaufmann, R.; Dummer, R.; Garbe, C.; Becker, J. C.; Hauschild, A.; Tilgen, W.; Ugurel, S.; Beyeler, M.; Bröcker, E. B.; et al. Temozolomide plus pegylated interferon alfa- 2b as first-line treatment for stage IV melanoma: a multicenter phase II trial of the Dermatologic Cooperative Oncology Group (DeCOG). *Ann Oncol*. **2008**, 19(4), 801–806.

[3] Schadendorf, D.; Ugurel, S.; Schuler-Thurner, B.; Nestle, F. O.; Enk, A.; Bröcker, E. B.; Grabbe, S.; Rittgen, W.; Edler, L.; Sucker, A.; et al. Dacarbazine (DTIC) versus vaccination with autologous peptide-pulsed dendritic cells (DC) in first-line treatment of patients with metastatic melanoma: a randomized phase III trial of the DC study group of the DeCOG. *Ann Oncol*. **2006**, 17(4), 563–570.
[4] Al-Badr, A. A. & Alodhaib, M. M. Chapter Four – Dacarbazine. *Profiles Drug Subst. Excip. Relat. Methodol*. **2016**, 41, 323-377.
[5] Fazeny-Dörner, B.; Veitl, M.; Wenzel, C.; Rössler, K.; Ungersböck, K.; Dieckmann, K.; Piribauer, M.; Hainfellner, J.; Marosi1, C. Survival with dacarbazine and fotemustine in newly diagnosed glioblastoma multiforme. *British J. of Cancer*. **2003**, 88, 496-501.
[6] Di Bei, J.M. & Bi-Botti, C. Y. Formulation of Dacarbazine-Loaded Cubosomes—Part I: Influence of Formulation Variables. *AAPS PharmSciTech*. **2009**, 10(3), 1032-1039.
[7] Bahrami, B.; Hojjat-Farsangi, M.; Mohammadi, H.; Anvari, E.; Ghalamfarsa, G.; Yousefi, M.; Jadidi-Niaragh, F. Nanoparticles and targeted drug delivery in cancer therapy. *Immun Letters*. **2017**, 190, 64-83.
[8] Bombelli, F. B.; Webster, C. A.; Moncrieff, M.; Sherwood, V. The scope of nanoparticle therapies for future metastatic melanoma treatment. *Lancet Oncol.* **2014**, 15(1), 22-32.
[9] Pourgholi, F.; Hajivalili, M.; Farhad, J. N.; Kafil, H. S.; Yousefi, M. Nanoparticles: Novel vehicles in treatment of Glioblastoma. *Biomedic&Pharmacot*. **2016**, 77, 98-107.
[10] Chen, W.; Achazi, K.; Schade, B.; Haag, R. Charge-conversional and reduction-sensitive poly(vinyl alcohol) nanogels for enhanced cell uptake and efficient intracellular doxorubicin release. *J. Controlled Release*. **2015**, 205, 15-24.
[11] De Lima, G. G.; Campos, L.; Junqueira, A.;. Devine, D. M.; Nugent, M. J. D. A novel pH-sensitive ceramic-hydrogel for biomedical applications. *Polym Advan Tech*. **2015**, 26, 1439-46.
[12] Canillas, M.; De Lima, G. G.; Rodrıguez, M. A.; Nugent, M. J. D. Bioactive Composites Fabricated by Freezing-Thawing Method for Bone Regeneration Applications. *Polym Phys*. **2016**, 54, 761-73.
[13] Nugent, M. J. D.; Hanley, A.; Tomkins, P. T.; Higginbotham, C. Investigations of a novel freeze-thaw process for the production of drug delivery hydrogels. *J. of Mat. Sci.: Mat. In Med*. **2005**, 16, 1149-1158.
[14] Mc Gann M. J.; Higginbotham, C. L.; Geever, L.M.; Nugent, M. J. The systhesis of novel pH-sensitive poly(vinyl alcohol) composite hydrogels using a freeze/thaw process for biomedical applications. *Inter. J. of Pharm*. **2009**, 372, 154-161.
[15] Liu, Y.; Hou, C.; Jiao, T.; Song, J.; Zhang, X.; Xing, R.; Zhou, J.; Zhang, L.; Peng, Q. Self-assembled AgNP-containing nanocomposites constructued by electrospinning as efficient dye photocatalyst materials for wastewater treatment. *Nanomaterials*. **2018**, 8, 35.
[16] Liu, X.; Shao, W.; Luo, M.; Bian, J.; Yu, D-G. Electrospun Blank Nanocoating for Improved Sustained Release Profiles from Medicated Gliadin Nanofibers. *Nanomaterials*. **2018**, 8(4):184.

[17] Zhang, J.; Wang, X.; Liu, T.; Liu, S.; Jing, X. Antitumor activity of electrospun polylactide nanofibers loaded with 5-fluorouracil and oxaliplatin against colorectal cancer. *Drug Delivery*. **2016**, 23(3), 784-790.
[18] Cao, Y.; Liu, F.; Chen, Y.; Yu, T.; Lou, D.; Guo, Y.; Li, P.; Wang, Z.; Ran, H. Drug release from core-shell PVA/silk fibroin nanoparticles fabricated by one-step electrospraying. *Sci. Rep*. **2017**, 7, 11913.
[19] Bagad, M. & Khan, Z. A. Poly(n-butylcyanoacrylate) nanoparticles for oral delivery of quercetin: preparation, characterization, and pharmacokinetics and biodistribution studies in Wistar rats. *Inter. J. of Nanomedicine*. **2015**, 10, 3921-3935.
[20] Wilson, B.; Samanta, M. K.; Santhi, K.; Kumar, K. P.; Paramakrishnan, N.; Suresh, B. Poly(n-butylcyanoacrylate) nanoparticles coated with polysorbate 80 for the targeted delivery of Rivastigmine into the brain to treat Alzheimer's disease. *Brain Res.* **2008**, 1200, 159-168.
[21] Gulyaev, A. E.; Gelperina, S. E.; Skidan, I. N.; Antropov, A. S.; Kivman, G. Y.; Kreuter, J. Significant transport of doxorubicin into the brain with polysorbate 80-coated nanoparticles. *Pharm Res*. **1999**, 16(10), 1564-1569.
[22] Zeng, Z.; Yu, D.; He, Z.; Liu, J.; Xiao, F. X.; Zhang, Y.; Wang, R.; Bhattacharyya, D.; Tan, T. T. Graphene Oxide Quantum Dots Covalently Functionalized PVDF Membrane with Significantly-Enhanced Bactericidal and Antibiofouling Performances. *Sci. Rep*. **2016**, 6, 20142.
[23] Hafeez, A. & Kazmi, I. Dacarbazine nanoparticle topical delivery system for the treatment of melanoma. *Sci. Rep*. **2017**, 7, 16517.
[24] Mansur, H.S.; Sadahira, C.M.; Souza, A.N.; Mansur, A.A.P. FTIR spectroscopy characterization of poly(vinyl alcohol) hydrogel with different hydrolysis degree and chemically crosslinked with formaldehyde. *Mater. Sci. Eng. C*. **2008**, 28, 539-548.
[25] Hassan, C. M. & Peppas, N. A. Structure and Applications of Poly(Vinyl Alcohol) Hydrogels Produced by Conventional Crosslinking or by Freezing/Thawing Methods. *Adv. in Pol. Sci*. **2000**, 153, 37-65.
[26] Gunasekaran, S.; Kumaresan, S.; Arunbalaji, R.; Anand, G.; Srinivasan, S. Density functional theory study of vibrational spectra, and assignment of fundamental modes of dacarbazine. *J. Chem. Sci*. **2008**, 120, 315-324.
[27] El-Feky, G. S.; El-Rafie M. H.; El-Sheikh, M. A.; El-Naggar, M. E.; Hebeish, A. Utilization of crosslinked starch nanoparticles as a carrier for indomethacin and acyclovir drugs. *J. Nanomed. Nanotechnol*. **2015**, 6, 254.
[28] Maurer, J.; Eustace, D.; Ratcliffe, C. Thermal characterization of poly(acrylic acid). *Macrom*. **1987**, 20, 196-202.
[29] Hirankumar, G.; Selvasekarapandian, S.; Kuwata, N.; Kawamura, J.; Hattori, T. Thermal, electrical and optical studies on the poly(vinyl alcohol) based polymer electrolytes. *J. Power Sources*. **2005**, 144, 262-267.
[30] Hatakeyema, T.; Uno, J.; Yamada, C.; Kishi, A.; Hatakeyama, H. Gel–sol transition of poly(vinyl alcohol) hydrogels formed by freezing and thawing. *Thermochimica Acta*. **2005**, 431(1-2):144-148.
[31] Dejene, F. B.; Ali, A. G.; Swart, H. C. Reinhardt, B.; Roro, K.; Coetsee, L.; Duvenhage, M-M. Optical properties of ZnO nanoparticles synthesized by varying the sodium hydroxide to zinc acetate molar ratios using a sol-Gel process. *Cent. Eur. J. Phys*. **2011**, 9(5), 1321-1326.

[32] Lopez, F. L.; Shearman, G. C.; Gaisford, S.; Williams, G. R. Amorphous Formulations of Indomethacin and Griseofulvin Prepared by Electrospinning. *Mol. Pharmaceutics*. **2004**, 11(12), 4327-4338.
[33] Ricciardi, R.; Auriemma, F.; De Rosa, C.; Lauprêtre, F. X-ray diffraction analysis of poly(vinyl alcohol) hydrogels, obtained by freezing and thawing techniques. *Macromolecules*. **2004,** 37(5), 1921-1927.
[34] Li, X.; Kanjwal, M. A.; Lin, L.; Chronakis, I. S. Electrospun polyvinyl-alcohol nanofibers as oral fast-dissolving delivery system of caffeine and riboflavin. *Col. and Surf. B: Biointer*. **2013**, 103, 182-188.
[35] Chen, P.; Wu, Q-S.; Ding, Y-P.; Chu, M.; Huang, Z-M.; Hu, W. A controlled release system of titanocene dichloride by electrospun fiber and its antitumor activity in vitro. *Eur. J. Pharm. Biopharm*. **2010**, 76, 413-420.
[36] Vashisth, P.; Singh, R. P.; Pruthi, V. A controlled release system for quercetin from biodegradable poly(lactide-co-glycolide)-polycaprolactone nanofibers and is in vitro antitumor activity. *Bio. and Comp. Pol*. **2015**, 1-13.
[37] Budiasih, S.; Jiyauddin, K.; Logavinod, N.; Kaleemullah, M.; Jawad, A.; Samer, A. D.; Fadli, A.; Eddy, Y. Optimization of polymer concentration for designing of oral matrix controlled release dosage form. *UK J. of Pharm. and Biosci*. **2014**, 5, 54-61.
[38] Siepmann, J. & Siepmann, F. Mathematical modeling of drug delivery. *Inter. J. of Pharm*. **2008**, 364, 328-342.
[39] Felice, B.; Prabhakaran, M. P.; Zamani, M.; Rodríguez, A. P.; Ramakrishna, S. Electrosprayed poly(vinyl alcohol) particles: preparation and evaluation of their drug release profile. *Polym. Int*. **2015**, 64: 1722-1732.
[40] Blanchard, J.; Sawchuk, R. J.; Brodie, B. B. (eds): Principles and Perspectives in Drug Bioavailability. Basel, Karger, **1979**, pp 20-58.
[41] Ryu, S. R.; Noda, I.; Jung, Y. M. What is the origin of positional fluctuation of spectral features: true frequency shift or relative intensity changed of two overlapped bands? *Appl. Spectrosc*. **2010**, 64: 1017-1021.
[42] Guirguis, O. W.; Moselhey, M. T. H. Thermal and structural studies of poly(vinyl alcohol) and hydroxypropyl celulose blends. *Natural Sci*. **2012**, 4: 57-67.
[43] Kiziltepe, T.; Ashley, J. D.; Stefanick, J. F.; Qi, Y. M.; Alves, N. J.; Handlogten, M. W.; Suckow, M. A.; Navari, R. M.; Bilgicer, B. Rationally engineered nanoparticles target multiple myeloma cells, overcome cell-adhesion-mediated drug resistance, and show enhanced efficacy in vivo. *Blood Cancer J*. **2012**, 2, e65.
[44] Liu, K.; Wang, Z.; Wang, S.; Liu, P.; Qin, Y.; Ma, Y.; Li, X..; Huo, Z. Hyaluronic acid-tagged sílica nanoparticles in colon câncer therapy: therapeutic efficacy evaluation. *Int. J. of Nanomedicine*. **2015**, 10: 6445-6454.

CAPÍTULO 2: Electrospun PVA-Dacarbazine nanofibers: novel nano brain-implant for treatment of glioblastoma

O artigo será submetido ao periódico Materials Science and Engineering: C

Electrospun PVA-Dacarbazine nanofibers: novel nano brain-implant for treatment of glioblastoma

Luiza Steffens[ab], Ana Moira Morás[b], Pablo Ricardo Arantes[b], Kevin Masterson[a], Zhi Cao[a], Michael Nugent[a], Dinara Jaqueline Moura[b]

a- Athlone Institute of Technology, Materials Research Institute, Athlone, Co. Westmeath, Ireland
b- Laboratory of Genetic Toxicology, Federal University of Health Sciences of Porto Alegre – UFCSPA, Sarmento Leite, 245, Lab.714, Porto Alegre, Rio Grande do Sul, Brazil

* Corresponding author. Address: Federal University of Health Sciences of Porto Alegre – UFCSPA, Sarmento Leite, 245, Lab.714, Porto Alegre, Rio Grande do Sul, Brazil
E-mail address: dinaram@ufcspa.edu.br (Dinara Jaqueline Moura, PhD)

ABSTRACT

Malignant glioblastoma (GB) treatment consists of resection surgery followed by radiotherapy and chemotherapy. Despite several implications, such as systemic toxicity and low efficacy, CT continues to be used for GB therapy. Aiming to overcome the blood brain barrier (BBB) limitations, one of the most promising approaches is the use of drug delivery systems (DDS) to treat the cancer cells *in situ*. Dacarbazine (DTIC) is an antitumor agent that has limited application given its high toxicity to healthy cells. However, it is effective against GB recurrent cells. In this study, DTIC polymeric nanofibers (NF) were successfully prepared, characterized and the anticancer efficacy was determined. This system demonstrated a high drug loading of 83.9 ± 6.5%, good stability and mechanical properties and sustained release with improved drug release in tumor pH (6.8). This controlled release prolonged the uptake of GB improving DTIC antitumor effects such as DNA damage and cell death by apoptosis. Molecular dynamics simulations revealed that DTIC interact with PVA, possibly explaining controlled release of the drug. Therefore, DTIC NF brain-implant could be a promising drug delivery system for GB therapy.

Key-words: Electrospinning. Dacarbazine. Nanofibers. Polyvinyl alcohol. Glioblastoma.

1. INTRODUCTION

Currently, standard therapy of malignant glioblastoma (GB) consists of resection followed by radiotherapy and adjuvant chemotherapy (CT). Several problems are related to CT including systemic toxicity, non-effective drug concentrations in the tumor site due to the blood brain barrier (BBB) and inability to sustain therapeutic drug concentration in the tumor site [1]. To overcome the BBB limitations, one of the most promising approaches is the use of drug delivery systems (DDS) to transport CT drugs to tumor.

Eventually, a high proportion of tumor recurs [2]. Recurrent GB are less responsive to CT than the original tumor and extremely invasive. This means that GB can recur and invade functional brain areas however, a second surgical resection is risked [3].

Despite the application of numerous treatment strategies, GB remains an incurable disease and the patients' overall survival is between 12 and 15 months after initial diagnosis [3]. Autopsy studies suggest that recurrent GB are mainly local and appear within 2 centimeters of the initial tumor site [4]. Therefore, localized and controlled CT directly into the tumor site can provide an alternative DDS in GB treatment.

The CT drug, dacarbazine (DTIC), is a well-tolerated imidazotetrazine derivate with established efficacy in recurrent GB [5]. However, DTIC presents some severe limitations. The CT drug is unstable and has poor solubility, DTIC is usually administered intravenously and this route is painful and usually the patients become non-compliant. Additionally, DTIC absorption is normally erratic and the drug induces severe cytotoxicity to healthy tissues [6]. To improve the treatment efficacy with DTIC, directly DDS could be administered during surgery, with systemic side effects reduction associated with a prevention of tumor recurrence.

Due to its biocompatibility, polymeric DDS are one of the most encouraging approaches for use in tumor treatment [7], since it exhibits low toxicity and controlled release properties, which makes this system a suitable DTIC delivery choice. In this regard, DDS using polymeric micro and nanoproducts has been intensely studied to treat GB because of its potential for sustained release [8,9,10,11,12,13,14,15,16]. Our research group focus is on the study of polyvinyl alcohol (PVA), which has an excellent history of biomedical applications [17,18,19]. PVA is an interesting option to design nanoproducts, since presents low cytotoxic and is biodegradable.

Here, we report the development and characterization of polymeric brain-implant prepared using PVA electrospun nanofibers for the controlled release of DTIC and its *in silico* and *in vitro* evaluation. We employed a combination of quantum mechanics (QM) calculations, molecular modelling techniques and molecular dynamics (MD) simulations to study conformational properties, such as the interaction and the dynamics of PVA in presence of DTIC. Improvements on the parameters of DTIC torsional angles were achieved. Our molecular dynamics (MD) simulations analysis showed the interaction of PVA with DTIC which can justify the controlled release. The PVA-DTIC *in vitro* analysis showed that it is effective in inducing cytotoxicity in GB cells.

2. MATERIALS AND METHODS

2.1 Materials

PVA (Mw 78K, 90% hydrolyzed), dacarbazine (DTIC), rhodamine-B, ethanol, acetic acid, methanol, isopropanol (IPA), 3-(4,5-dimethylthiazol-2-yl)-2,5-diphenyltetrazolium bromide (MTT), paraformaldehyde, triton X-100, tryptone soy broth (TSB) and fluid thioglycolate medium (FTM) were obtained from Sigma e Aldrich. Dulbeco's Modified Eagle Medium (DMEM), fetal bovine serum (FBS), phosphate-buffered saline (PBS), L-glutamine, trypsin-EDTA, antibiotics (penicillin and streptomycin) and Trypan blue were purchased from Gibco Life Sciences. Dead Cell Apoptosis Kit with annexin V FITC and PI was acquired from Invitrogen.

2.2 PVA nanofibers preparation

PVA hydrogels were made by dissolving PVA at 5% concentration (wt/vol), and dacarbazine (10 mg) or rhodamine (10 mg) in distilled water (dH_2O), at 90°C with continuous stirring until the whole solubilization of the polymer, after the solutions were colder ethanol (10%) was added. The solutions were electrospun using a blunt-end 20-gauge needle. The flow rate was set 0.5 mL/h using 10 kV. The needle tip to collector distance was 5 cm. Neat PVA hydrogel was also prepared and electrospun for comparison purposes.

2.3 Analysis of nanofiber size and morphology

By using scanning electron microscope (SEM, Tescan Mira XMU, TESCAN, Brno, CZ), the morphology of the NFs was observed. Back scattered electron mode was used with magnifications ranged from 10kX to 30kX. Previous to the analysis, the NFs were sputtered with gold. For NF size analysis, the ImageJ software was used (ImageJ Version 1.48v) and more than 200 NFs were analyzed to extract the mean diameter.

2.4 Solid-state NMR

The stability of the drug subsequent to encapsulation in PVA NFs was assessed using nuclear magnetic resonance (NMR) spectroscopy. The evaluation was performed using Bruker 400 MHz Avance III HD equipped with a 3.2 mm H/X

CPMAS probe.

2.5 Mechanical properties

The NFs mechanical properties of the NFs was measured by using a Discovery HR-2 rheometer (TA instruments, DE, USA). The experiments were performed by using the parallel plate method. As a heating component, a Peltier plate was used and as the top geometry, a 60 mm steel plate was used. The samples were loaded on the Peltier plate after 15 minutes in PBS buffer (pH 6.8 and 7.4). After an equilibration step, the viscoelastic properties: elastic modulus (G') and viscous modulus (G'') as function of frequency were measured through frequency sweep testes over a range from 0.01 to 10 Hz. To build flow curves of apparent viscosity data of each sample, steady shear evaluations were performed in the shear rate range 1 – 100 s^{-1}.

2.6 Determination of loaded amount and encapsulation efficiency of DTIC

To measure the percent encapsulation efficiency (EE%) and the total amount of loaded DTIC, DTIC-NFs were completely dissolved in dH_2O and the quantity of released DTIC was measured by ultraviolet (UV) light on Shimadzu UV 1280 spectrometer at 323 nm. The EE (%) of the DTIC was determined as follows:

$$EE(\%) = \frac{actual\ amount\ of\ loaded\ DTIC\ in\ NFs}{theoretical\ amount\ of\ loaded\ DTIC\ in\ NFs} X100$$

2.7 *In vitro* drug release studies

Drug dissolution profiles were achieved using a Distek Model 2500 Dissolution System (Distek, Inc., NJ, USA). The samples were tested in PBS (pH 7.4 or 6.8) at 37°C. 900 ml of dissolution media were used per vessel and the stir rate was established to 50 rpm. Samples were taken at set intervals and evaluated by UV light on Shimadzu UV 1280 spectrometer at 323 nm.

2.8 Fourier transform infrared spectral study

Attenuated total reflectance Fourier transform infrared spectroscopy (ATR-FTIR) were taken to investigate the possible chemical interactions between DTIC after conjugating with PVA. The study was performed on a Perkin Elmer Spectrum One fitted with a universal ATR sampling accessory. All samples were evaluated in the

spectral range of 4000-650 cm^{-1} using 4 scan per sample cycle. Following analysis was carried out using Spekwin32 software.

2.9 Thermal properties

The physical state of DTIC entrapped into the NFs was characterized using differential scanning calorimeter (DSC TAQ2000 from TA instruments). The sample weights were measured (between 5 and 10 mg) and encapsulated in sealed aluminum pans. The temperature ramped was set from 20°C to 270°C at a rate of 10°C/min with an empty pan as a reference. All results were plotted as a function of heat flow (W/g) against temperature (°C).

2.10 Nomenclature and software

The IUPAC proposed recommendations for nomenclature and symbols were used. Regarding MD simulations, the GROMACS 2018 simulation suite [20] was employed, along with the GROMOS 53A6 force field [21] and the GROMOS 53A6GLYC force field [22,23]. For DTIC imidazole ring, the parameters of previous work were chosen [24]. For the manipulation and construction of the whole molecule of PVA the Assemble! [25] tool was used. This tool makes it easier the simulation of polymeric systems in Gromacs. Using either a GUI or console commands, Assemble! [25] allows for the creation of polymers from monomer building blocks with a user-defined force field. For the manipulation and visualization of structures, the softwares VMD [26] and PyMOL [27] were employed.

2.11 Generation of new torsional parameter for DTIC

The QM torsional profile for the dihedrals within the DTIC structure were obtained using Gaussian03 [28]. Compounds similar to DTIC were chosen for these analyzes (more details are described in results). These QM calculations were carried out using the scan routine combined with the convergence criterion tight, at MP2 level with the 6-31G* basis set, obtaining the relative energy associated with the rotation of dihedral by increments of 30º. Analogue MM calculations were performed in GROMACS 2018, using the force field parameter set 53A6, as described previously [22,23,29]. The QM and MM profiles were fitted in Rotational Profiler server [30], providing proper torsional parameters for MM calculations to yield a torsional profile similar to the QM. These new parameters were then implemented in the DTIC

topology for MD simulations.

2.12 Parametrization strategy and topology construction

In order to describe PVA-DTIC interaction through molecular mechanics' techniques, a set of molecules commonly found in GROMOS 53A6 [21] and the GROMOS 53A6GLYC [22,23] force fields were selected to act as building blocks in this work. Topologies were constructed for PVA using the potentials for bond stretching, bond-angle bending, improper dihedral deformation and proper dihedral, as well as van der Waals interactions terms retrieved directly from GROMOS53A6 [21] and the GROMOS 53A6GLYC [22,23] set. Moreover, in order to maintain compatibility with the general GROMOS force field, and due to its highly charged nature, the potentials for the DTIC imidazole ring were adapted from previous study [24], that used GROMOS force field to simulate the dynamical behavior of aromatic rings (including an imidazole) mostly commonly used in drug design. All MD simulations and analyses were performed using the GROMACS simulation suite [31], version 2018 [32]. Each DTIC molecule was analyzed separately on the systems studied.

2.13 Molecular Dynamics Simulations

The PVA chosen for the study is the PVA with molecular weight 78K, which corresponds to a polymer with 1765 units. The system was constructed using the Assemble! tool [25], with the concentration of experimental data: 1 molecule of PVA (1765 units) was considered as 5% and the DTIC as 0.1%, resulting on eight molecules of the drug for 1 molecule of PVA. Two structures were constructed, PVA with eight molecules of DTIC and eight drug molecules in water. As previously described [33,34,35], in order to randomize the structure and relax local stresses further, the PVA chain was subjected to the steepest descent energy minimization and 1 ns of molecular dynamics pre-equilibration of the polymer around the drug. Following the pre-equilibration steps, the dodecahedron box was then solvated with SPC water model [36] and periodic boundary conditions. Before this process, to retain the physiological ionic strength 0.15 M NaCl was added to the aqueous solution. The LINCS algorithm [37] was chosen to constrain covalent bond lengths. This way, an integration step of 2 fs was applied. As for the electrostatic interactions,

calculations were performed by the particle mesh Ewald (PME) method [38]. The pressure barostat chosen was Parrinello–Rahman [39,40], with a 2.0 ps coupling constant, while the temperature thermostats chosen were V-rescale (NVT step) [41] and Nosé–Hoover (NPT equilibration and production MD) [42,43], with a coupling constant of $\tau = 0.5$. Constant temperature of 298 K and constant pressure of 1 atm were also implemented. Steepest Descent algorithm was used in the energy minimizations performed. First, two simulations of equilibration were performed with position restraints: an NVT and an NPT of 2 ns and 5 ns, respectively. Subsequently, 500 ns of unrestrained NPT MD simulations were performed for each system (DTIC and PVA-DTIC), generating the production run from which data were collected. Each system was simulated in three independent runs, with different starting velocities, to filter low probability conformational events [44,45]. For analysis, coordination number is the total number of neighbors of a nitrogen atom on a DTIC imidazole ring, extracted from optimal binding distance calculated by radial distribution function.

2.14 Nanofiber Sterilization and Sterility Validation

NF samples were sterilized prior to cell culture applications. NF were immersed in 100% IPA for 1 hour into a sterile petri dish. Then, samples were put in the over at 60°C for 1 hour. The sterilization method was validated following USP protocol 71 [The United States pharmacopeia, USP 34, NF 29], with minor adjustments. *Staphylococcus aureus* (ATCC 25923), *Candida albicans* (ATCC 10231) and *Aspergillus niger* (ATCC 6275) were chosen as test microorganisms for assessing aerobic, anaerobic and fungal growth conditions respectively. TSB was used as aerobic and fungal growth media, and FTM was used as anaerobic growth media. Both sterilized NF and untreated NF were assessed. Samples of NFs were dissolved in PBS and transferred to test tubes of growth media (sterility assay) and growth media with 100 cfu of appropriate microorganism (method suitability). Positive control tubes of growth media were inoculated with 100 cfu of appropriate test microorganism and negative (sterility) control tubes with only growth media were prepared. Tests tubes were incubated at either 37°C (aerobic, anaerobic) or 25°C (fungal) for a total of 14 days. All tubes were examined daily for growth or changes in turbidity.

2.15 Cell uptake

The GB cells (U87MG) were kindly provided by Dr. Brona Murphy (Department of Physiology and Medical Physics, Royal College of Surgeons in Ireland). Cells were cultured in DMEM supplied with 10% FBS and antibiotics at 37°C in a humidified atmosphere containing 5% CO_2. To perform the experiments two different pH of the media: 6.8 and 7.4 were used. The cellular uptake of NFs was studied on cells in a time-dependent manner. The fluorescent dye loaded in the NFs was rhodamine-B (Rho-B). The cells were treated with Rho-B/NFs (1 mg/mL) and incubated for several time points. After treatment, cells were washed three times with PBS to remove unbound NFs and fixed in methanol. Fluorescence images were acquired using the Leica DM 2000 confocal microscope with a x40 oil lens (Leica Microsystems, Ireland). Image acquisition was performed by LAS V3.8 software (Leica) and fluorescence analysis was carried out using ImageJ software (ImageJ Version 1.48v).

2.16 Cell viability evaluation

The NFs cytotoxicity potential was determined by using MTT colorimetric assay. Cells were treated with several blank and DTIC-loaded NFs formulations at several concentrations during 1 or 5 days. After treatment, cells were incubated with MTT for 3 hours at 37°C. To dissolve the formazan crystals, DMSO was added to each well. The absorbance was recorded at 540 nm in a microplate reader (BioTek Synergy HT, Swindon, UK), and percentage of residual cell viability was determined. The cell viability was calculated using the control cells as 100%.

2.17 DNA damage evaluation

After treatment, cells were trypsinized, fixed with 3.7% paraformaldehyde for 15 min and permeabilized with 0.5% (v/v) Triton X-100 in PBS for 15 min followed by blocking with 10% (v/v) FBS in PBS for 1 h. Then, the samples were incubated overnight at 4°C with following antibody at a dilution of 1:75: Alexa Fluor 488 Mouse anti-H2AX (pS-139) (BD Biosciences, SP, Brazil). The samples were added in a glass slide and each slide was dropwise added with Hoechst 33258 stain (ThermoFisher Scientific, SP, Brazil), covered with a coverslip, and mounted with

nail polish. The slides were stored at −20 °C until used for microscopic observation. Finally, the cells were imaged using an INCell analyser 2200 (GE Heathcare Life Sciences, Piscataway, NJ, USA).

2.18 Cell death analysis

After treatment, cells were trypsinized, collected, resuspended in 100 µL of binding buffer 1x with 3 µL Annexin V-FITC plus 1 µL of PI (100 µg/mL) and incubated at room temperature for 15 min. After this period of incubation, 400 µL of binding buffer were added. Data were collected and analyzed using a FACS Calibur flow cytometer (Becton Dickinson, San Jose, CA, USA) with CellQuest software. A total of 10.000 events per sample were collected.

2.19 Statistical analysis

Quantitative data were expressed as the mean value ± standard deviation (SD). Statistical analysis was carried out using one-way analysis of variance (ANOVA) following by Tukey post-test or two-way ANOVA following by Bonferroni post-test using GraphPad Prism 5 software (La Jolla, CA, USA). Statistically significant results were considered when the P-value < 0.05.

3. RESULTS AND DISCUSSION

3.1 Development and characterization of electrospun nanofibers

With the objective of achieving a more potent DDS to treat GB, in the present research, DTIC-encapsulated NF were developed to accomplish a controlled release of the drug. The NFs morphology evaluated by SEM is show in figure 1A. The average fiber diameter revealed that the NFs had 275.3 ± 96.2 nm (figure 1B).

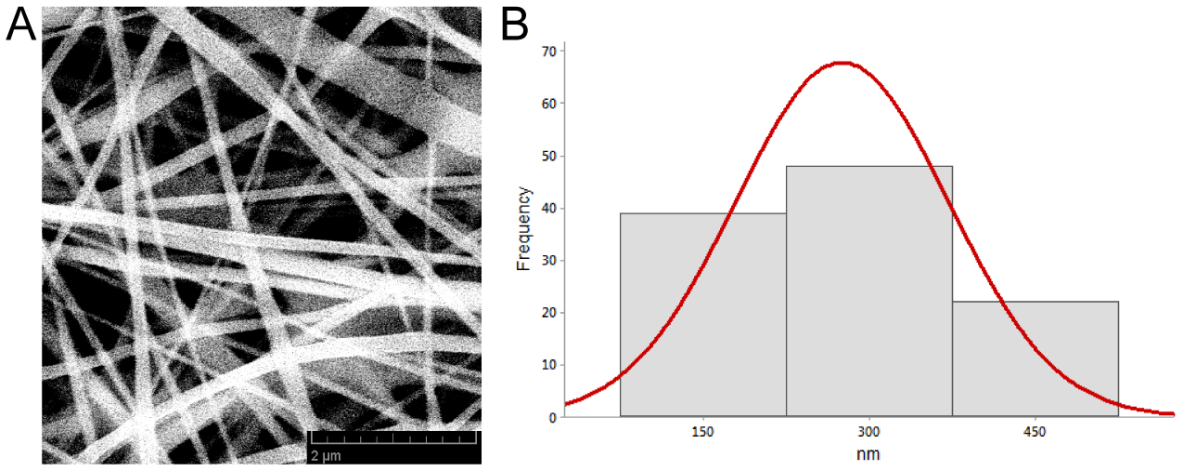

Figure 1: Characterization of the NFs **(A)** SEM images of NFs with 10 kx of magnification **(B)** Fiber diameter distribution of the NFs.

The stability of DTIC after encapsulation into the NFs, determined by ^{13}C NMR spectrum, to PVA hydrogel (figure 2A), PVA powder (Supplementary 1A) and PVA NF (figure 2B), reveal a sharp peak related to CH_2 (around 45 ppm) and three typical peaks (I, II and III) of CH (between 60 and 80 ppm). No significant differences were found in PVA NFs. The DTIC powder spectrum exhibited peaks ranging from 36 to 165 ppm. These peaks shifted toward 34 to 162 ppm after encapsulation in PVA-NFs, which can br result of weak interactions including hydrogen bonds between DTIC and the PVA-NF [46,47,48]. However, no significant variance was observed in the spectrums of DTIC powder and DTIC NFs. The results suggested the stability of DTIC moreover, this means that DTIC bioactivity is preserved after NF encapsulation [46].

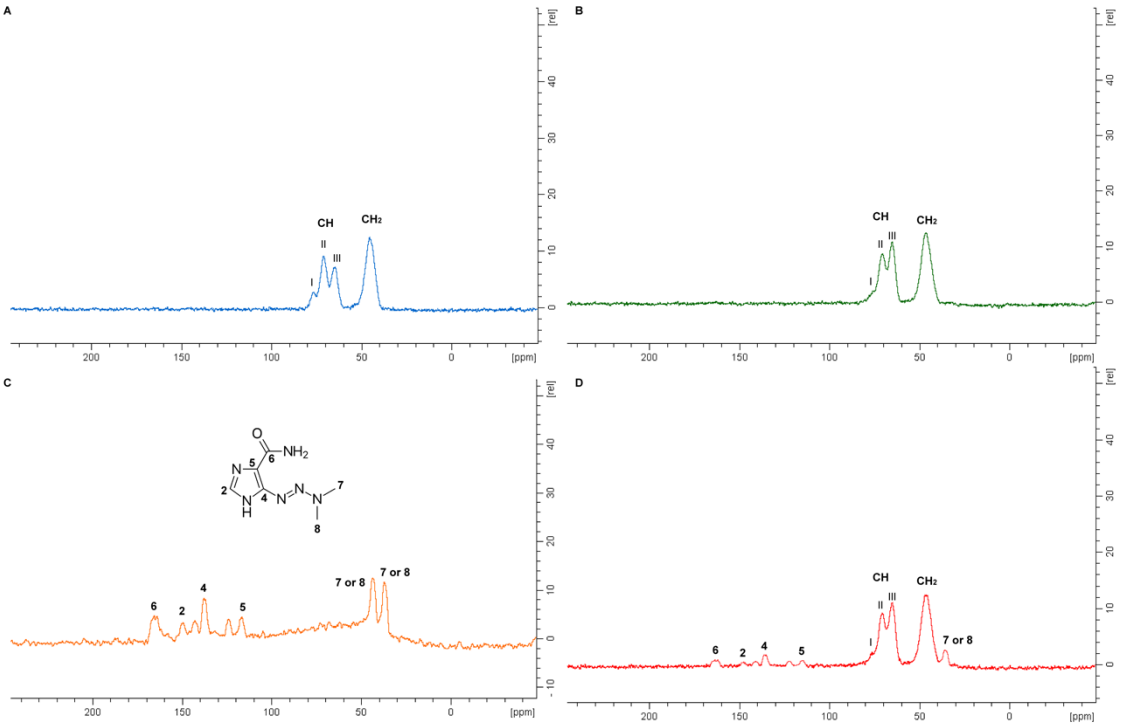

Figure 2: ^{13}C NMR spectra of **(A)** PVA hydrogel **(B)** PVA NF **(C)** DTIC powder and **(D)** DTIC loaded NFs.

It is well known that GB maintain an acidic extracelular (6.5-6.8) pH [49,50]. This pH stimulates tumor progress and increases the CT resistance. The increased extracellular acidification in tumors is due to the metabolic alteration in the cells because they switch from oxidative phosphorylation to glycolysis (Warburg effect), in which the cells release lactate and H^+ [49,50]. Highest tumor invasion sites correspond to lowest pH sections [51]. Therefore, it is assumed that acidic pH stimulates invasive tumor progress and metastasis. Given the application of the NF as a brain implant to treat brain cancer, we performed some analyses using two different pHs: acid, 6.8 and physiological, 7.4.

Rheological properties of the NFs were measured through oscillatory tests to determine the dependence of viscoelastic properties with frequency and through steady state experiments to determine the viscosity of NF as a function of shear rate. Figure 3A shows the flow curves at 37°C of the DTIC NF and Blank NF after 15 min of incubation in buffers with pH 6.8 and 7.4. The Blank NFs and DTIC NFs presented similar viscosities with the apparent viscosity decreasing over several order of magnitudes with increasing shear rates. The viscoelastic properties elastic

(G') and viscous (G'') moduli at 37°C, recorded from 0.01 to 10 Hz, are represented in figure 3B. The NFs showed similar G' and G'' values, also, they were frequency-dependent and varied up to several orders of magnitude within the rage of studied frequencies. The DTIC NF (pH 7.4) showed the highest values of G' and G'', with the curves exhibiting a cross-over point around 0.5 Hz (i.e. G'=G''), beyond which the viscoelastic become predominantly elastic (G'>G''). Similar outcomes were found by Yang et al (2017), when studying electrospinning solutions [52].

NFs are controlled release nanoproducts with swelling properties. The water absorption during the swelling leads to expansion of the polymer, this expansion direct affects the drugs diffusion and significantly impacts the release kinetics. The capacity of drugs to migrate through the polymer matrix and the macromolecular relaxation of the polymer can be analyzed to determine the release rate of polymeric NFs [53]. Figures 3C and D show the swelling profiles evaluation of PVA NFs under different pHs. The results suggested that the alteration of pH from 6.8 to 7.4 has resulted in a diffusion rate reduction. This result can be justified by the intensification of ionic strength that is expected to neutralize the acetate groups negative charges [53].

Therefore, swelling analysis suggested that PVA NFs were sensitive to pH alteration, in the pH range assessed. Some researchers have described PVA as almost neutral after pH stimuli, however the insertion of PVA moieties normally improves its pH sensitivity [54]. Moreover, the addition of DTIC decreased the swelling, given the formation of weak interactions between the PVA polymer chain and the drug. Consequently, it is PVA NFs could be used in controlled release system.

The resulting drug release from the NFs depends on the polymer used in the nanoproduct formulation. In this study, the NFs provided a continuous release profile for DTIC over 5 days (figures 3E, F, G). DTIC EE (%) was recorded as 83.9 ± 6.5%, which implied that a substantial amount of DTIC was encapsulated in the NFs. The sustainability of DTIC in the NFs and hydrogels was calculated by *in vitro* drug release in physiological pH (pH 7.4) and tumor pH (pH 6.8) at different time intervals (figures 3E, F, G). The release percentages of DTIC NFs in acid pH were higher in comparison with neutral pH, which is in accordance with the swelling results. This

suggested that the performance of the DTIC NFs is suitable for GB management and it is a promising approach to achieve a sustained drug delivery for GB therapy. In order to achieve an appropriate treatment using antitumor drugs, an initial burst is fundamentally required, together with a sustained drug release aiming to treat the cells that survived in the early stage [55]. The release profile of DTIC NFs displayed an initial burst release (around 58% in pH 6.8 and 33% in pH 7.4) followed by a sustained release during six days. The burst release can be explained due to the diffusion of DTIC absorbed in the polymeric matrix or present at the NF surfaces and owing to the nanopores present in the NF surfaces resulted from the solvent evaporation during the electrospinning [56,57,58]. Given that DTIC is a hydrophobic drug, the drug release could be a function of PVA matrix erosion and DTIC diffusion [57]. To analyze the release profiles of the samples, *in vitro* release kinetics models were used. The samples were modelled on the hypothesis that DTIC was uniformly distributed in the NFs and hydrogels, in this system the drug is loaded into the matrix by a simple combination of both [57].

The drug release results were investigated using Korsmeyer-Peppas model, in which it is calculated the Log cumulative percentage of drug released versus log of time, and using Higuchi model, where the cumulative percentage of drug released is plotted against the square root of time [59].

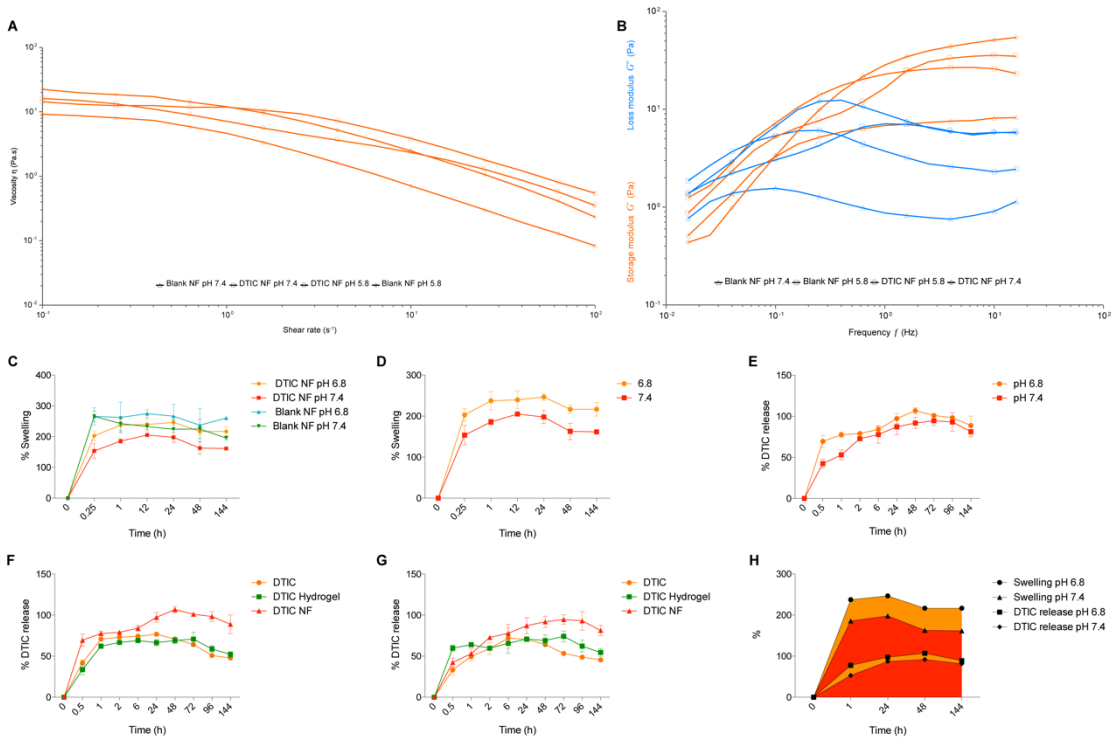

Figure 3: NFs mechanical and release properties. **(A)** Flow curves of NFs; **(B)** Frequency dependence of elastic (G') and viscous (G'') moduli of NFs; **(C)** Swelling studies of Blank and DTIC NFs in pHs 6.8 and 7.4; **(D)** Swelling percentage of DTIC NFs; **(E)** DTIC release of NFs; **(F)** DTIC release of samples in pH 6.8; **(G)** DTIC release of samples in pH 7.4; **(H)** Percentage of swelling and DTIC release of DTIC NFs in pHs 6.8 and 7.4.

Table 1: Release behavior of DTIC loaded formulations and DTIC in powder form.

Sample		Model			
		Korsmeyer-Peppas		Higuchi	
DTIC	pH 6.8	n	0.0083	K	71.528
		R^2	0.6901	R^2	0.5316
	pH 7.4	n	0.0117	K	73.897
		R^2	0.5192	R^2	0.6742
DTIC NF	pH 6.8	n	0.2330	K	78.399
		R^2	0.9353	R^2	0.5402
	pH 7.4	n	0.2250	K	21.606
		R^2	0.9576	R^2	0.9845
DTIC Hydrogel	pH 6.8	n	0.0626	K	166.66
		R^2	0.7418	R^2	0.8653
	pH 7.4	n	0.0338	K	115.27
		R^2	0.9091	R^2	0.9265

Where, R^2 is the regression coefficient, K is the Higuchi rate constant and n is the release or, slope exponent.

Figure 4A and figure S1B displays the FTIR spectra of PVA NF, PVA hydrogel and PVA powder. All PVA main peaks associated to acetate and hydroxyl groups were observed. The bands detected between 3500 and 3000 cm^{-1} are related to O-H stretching from the intramolecular and intermolecular hydrogen bonds. Additionally, the band observed between 2900 and 2860 cm^{-1} are due to C-H stretching from alkyl groups and finally, the peaks between 1745 and 1730 cm^{-1} are related to C=O and C-O stretching from acetate groups from PVA [51]. The intensity of the carbonyl groups was found stronger in PVA NF, suggesting that the PVA degree of hydrolysis is lower in the NF. In addition, the intensity of the 1141 cm^{-1} peak is influenced by the crystalline part of the chains of the polymer, and the results clearly showed that this peak is missing in the NF. The degree of crystallinity of a polymer is a result of the uniform arrangement of its chains within the network structure; a crystalline polymer degrades slower than an amorphous one, while the amorphous is more

suitable for drug delivery systems [60]. Moreover, no significant changes were observed for DTIC NF when compared to Blank NF (figure 4B), indicating that there are strong chemical interactions between DTIC and the polymer that could modify drug structure [60].

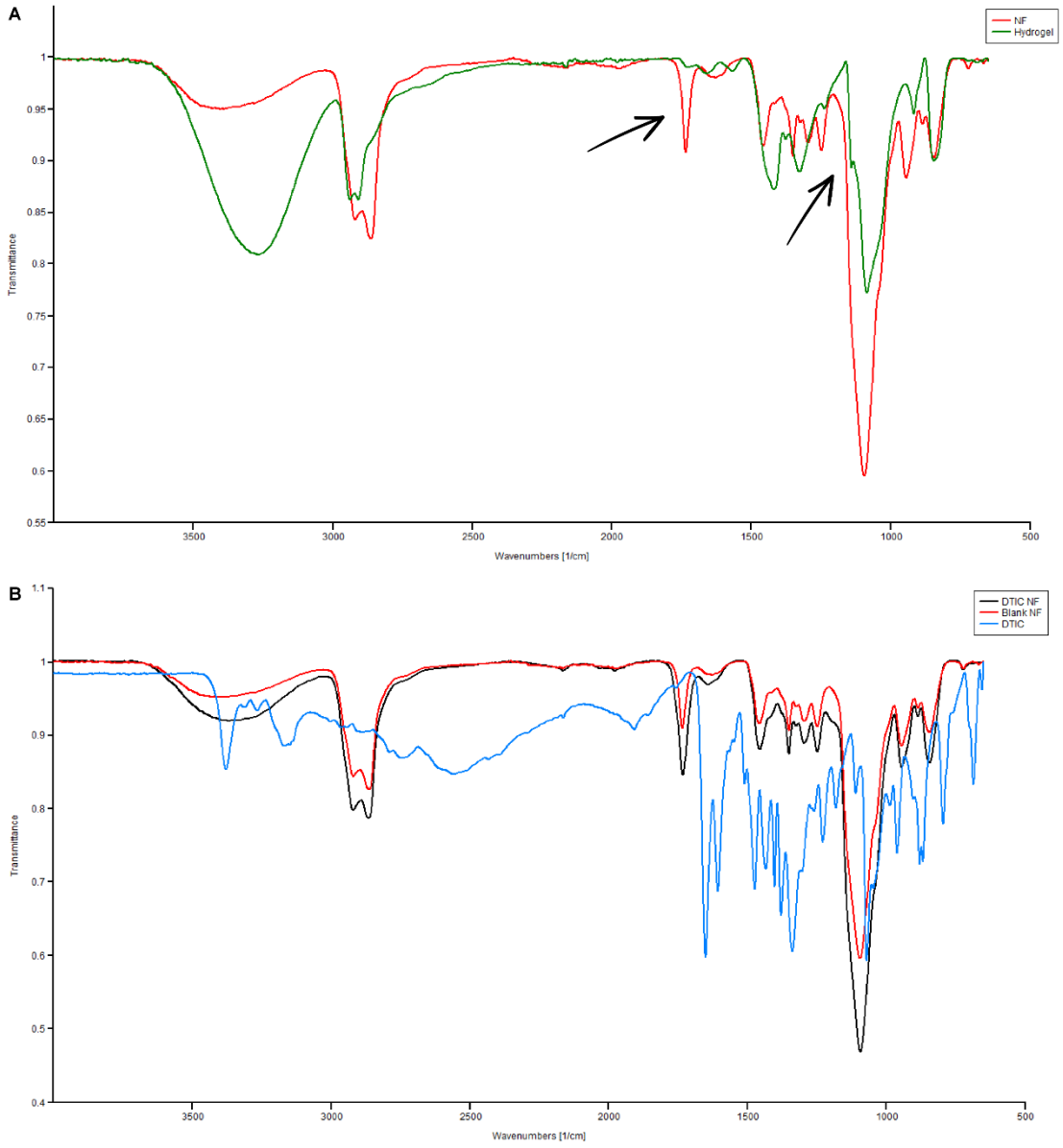

Figure 4: FTIR spectra obtained from **(A)** PVA control samples: Blank NF and PVA hydrogel **(B)** Blank NFs, DTIC NPs and DTIC in powder form.

A thermogram of PVA hydrogel is shown in figure 5A, in which the sharp peak at 220°C characterizes the melting point (Tm). The PVA α-relaxation (glass transition

– Tg) is displayed in the step change at around 30°C to the hydrogel, Blank NF, DTIC NF and PVA powder (figures 5A, B and D and supplementary 1C). The β-relaxation can be seen at 116, 102, 81 and 77°C to PVA powder, PVA hydrogel, Blank NF, and DTIC NF, respectively. These transitions are probably due to microcrystallites or the evaporation of water [61].

The NFs (figures 5B and 5D) moreover showed an exothermic peak around 170°C probably due to the removal of chemically adsorbed alcohol and water. Another study suggested that this phenomenon could happen given the decomposition of residual organic matter and the hydroxide groups given the chemical rearrangement after the electrospinning process [62]. The DTIC powder thermogram (figure 5C) exhibits a sharp exothermic peak at 212°C corresponding to its Tm, demonstrating its crystalline inherent characteristic [6]. DTIC NF shows endothermic melting peak at 218°C, this suggests that DTIC is present in non-crystalline form in the NF formulation, which can be related to formation of a drug amorphous state. It is known that transforming the drug's physical state from crystalline to amorphous leads to high-energy state and high disorder. This results in faster dissolution due to the increased solubility [60,63], that is in accordance with the drug release analysis (figure 3F and G) and the FTIR analysis (figure 4).

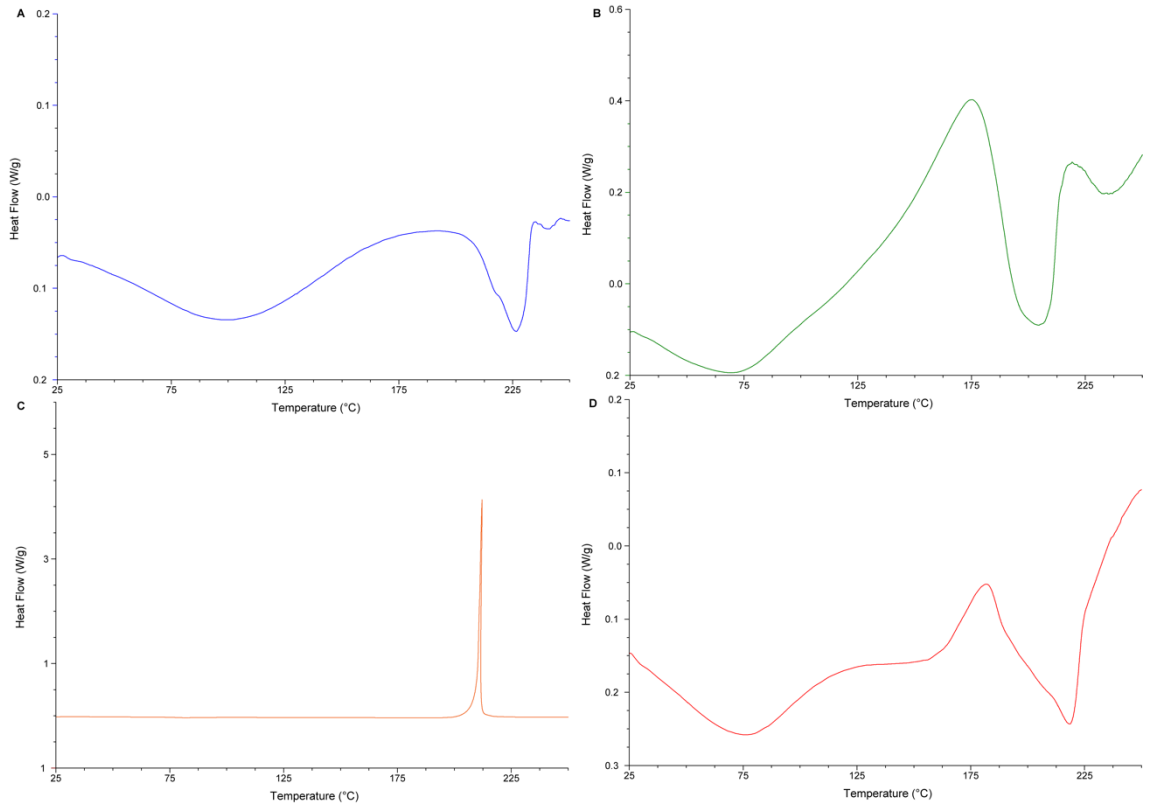

Figure 5: DSC thermogram obtained from **(A)** PVA hydrogel **(B)** Blank NFs **(C)** DTIC in powder form **(D)** DTIC NFs.

3.2 Torsional potential and force field calibration for DTIC

While some of the torsional potentials were preserved from the GROMOS 53A6 parameter set for PVA, the conformation of the DTIC was reevaluated based on fitting to QM data. The functional form of the potential energy term, associated with the torsion around dihedral angle m, is given in GROMOS by:

$$V_{\varphi,m} = k_{\varphi,m}[1 + \cos\delta_m \cos(n_m \varphi_m)]$$

where φ_m is the dihedral angle value, nm the multiplicity of the term, δ_m the associated phase shift, and $k_{\varphi,m}$, the corresponding force constant, which are applied. It is worth noting that a given dihedral angle may be described by more than one torsional potential energy term with different multiplicities and/or phase shifts. The compounds 1, 2 and 3 (figure 6) were chosen due to their similarity to DTIC, and these parameters were then implemented in the DTIC topology for MD simulations. Accordingly, the classical energy profiles obtained from Compound 1, 2 and 3 angles rotations were compared to energy profiles obtained from QM

calculations. Analyses of the dihedral angle showed important divergences between QM-calculated and GROMOS 53A6 energy profiles for dihedral angles (figure 6). Although, the Compound 1 presents the same minimum-energy geometry, at 180°, the conformational barriers obtained for the current GROMOS 53A6 parameters are too high to properly describe the rotation of the dihedral correctly. Additionally, on Compound 2, the 90° and 240° conformers are described as the energy local minimum, instead of a global maximum (figure 6). The barriers obtained for Compound 3 also show divergences, counting with two conformers at 90° and 270°, described as the local minimal, instead of energy global maximum (figure 6). On the basis of these data, eight new torsional dihedral potentials associated with the rotation of the dihedrals angles were obtained by fitting the corresponding classical energy profiles to energy profiles obtained from QM calculations (figure 6). The resulting potentials (table 2), were shown to adequately reproduce the QM-obtained energy profile related to such torsion.

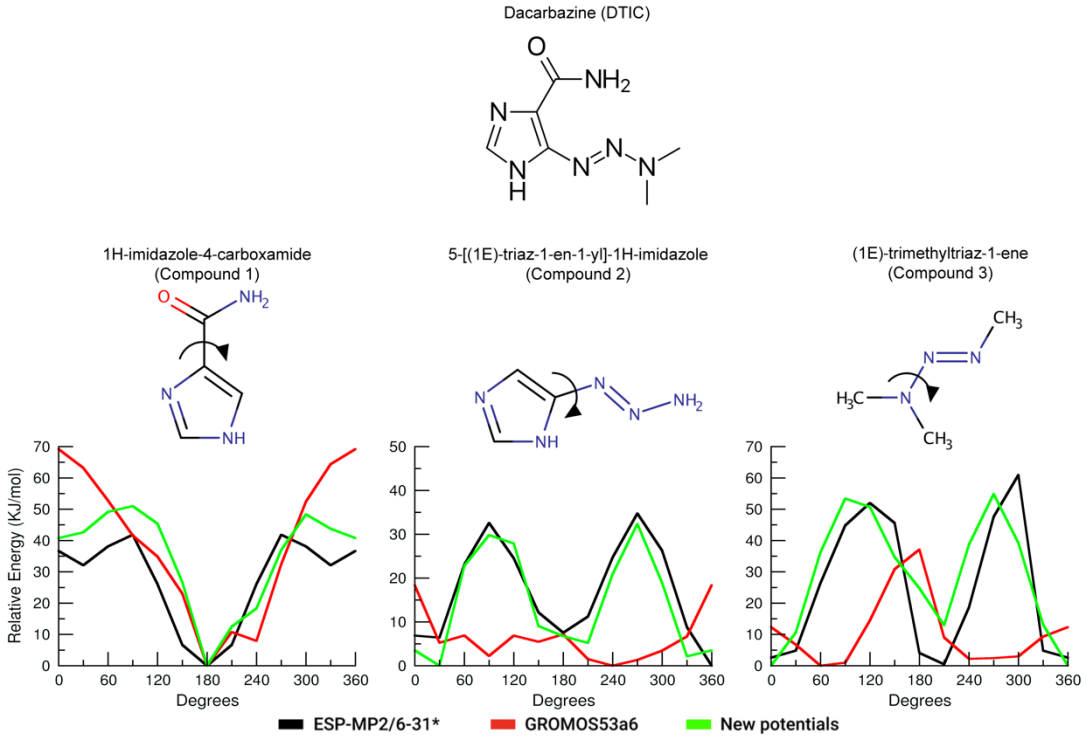

Figure 6: Comparison of energy profiles calculated at classical (GROMOS53A6) and QM (MP2/6-31G*) levels in the gas phase. The fitting has generated parameters that reproduce well the QM potential energy in the MM calculations.

Table 2: Torsional parameters obtained based on QM calculations.

Compound	δ	$k_{\phi,m}$	n
Compound 1	0	7.893	0
	0	-14.201	1
	0	-11.795	2
Compound 2	0	18.121	0
	0	-5.252	1
	0	-18.737	2
Compound 3	0	24.150	0
	0	-32.380	2

3.3 Polymeric Network and Drug Interaction

In order to evaluate the PVA-DTIC interaction, two systems were simulated: (1) DTIC and (2) PVA-DTIC in water. Each system was simulated in three independent runs to filter low probability conformational events [38,39], and the obtained data is presented as an average of these three simulations.

Regarding the possibility of PVA interaction with the drug, we explored the exposition of all DTIC molecules to solvent with different techniques. These include, the coordination number (CN) of water molecules, total energetic contribution for the interaction between PVA-DTIC and solvent-accessible surface area (SASA) surrounding DTIC (figure 7A and figure S4), as well visual examination of drug during the MD simulations (figure 7B). Accordingly, when complexed to polymer, DTIC exposition to solvent is diminished (figure 7A-B and figure S4 C-G) and the interaction energy of drug with PVA is closer to energy the interaction of DTIC with water (figure 7A and figure S4 C-G). When compared the two systems (PVA-DTIC and DTIC in water), the drug total energy interaction with water is smaller on system with PVA, showing the influence of PVA on DTIC. Not only that, the coordination number (CN) of water molecules are in agreement with SASA results (figure 7A and figure S4 C-G), reinforcing the drug complexation with PVA. The visual examination (figure 7B) confirm the interaction of polymer with DTIC, possibly through hydrogens bonds. This picture shows the polymer folding and binding scaffold for the drug. It is noticeable that not all drug molecules, during the MD simulations, interact with PVA (figure S4 A and B). This behavior could explain the controlled release system

of the DTIC, some molecules are accessible to solvent and others are complexed with PVA and will be release more slowly.

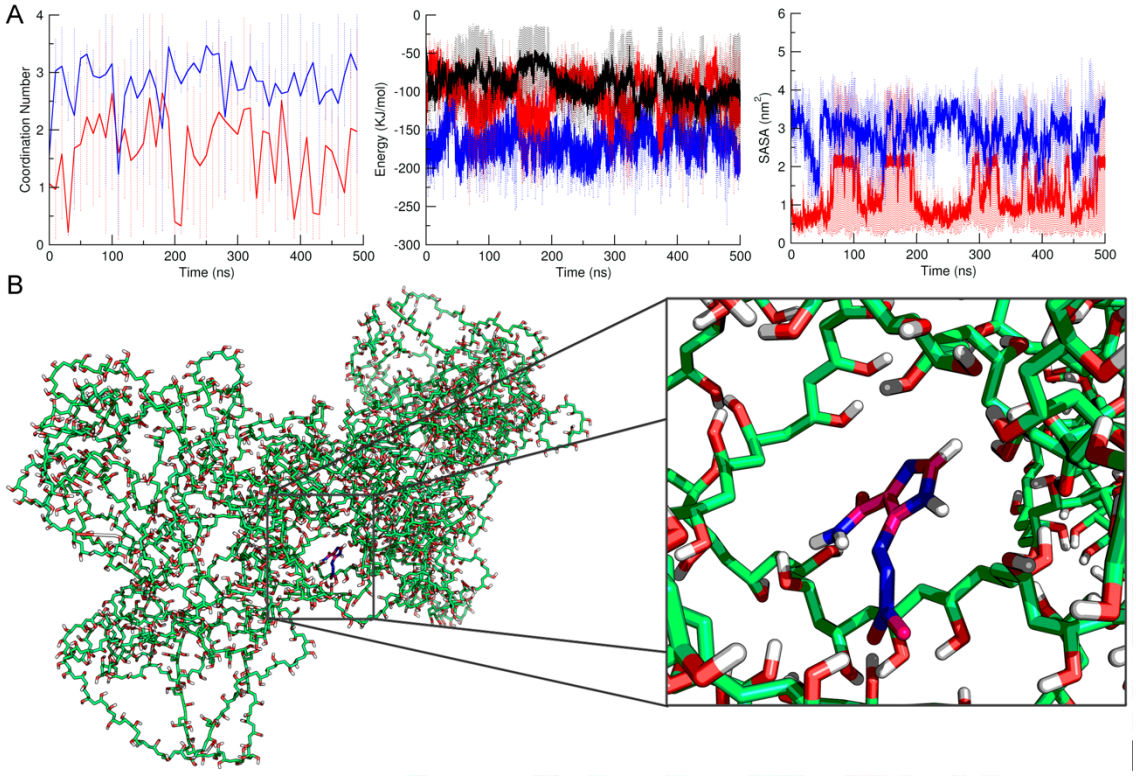

Figure 7: (**A**) Coordination number of water molecules (CN) on nitrogen atom of DTIC imidazole ring, total interaction energy between PVA-DTIC and PVA-Water and average of solvent accessible surface area (SASA) on drug during the molecular dynamics simulations. In blue the system of DTIC in water, in red and black the system with PVA-DTIC in water. The black line is total interaction energy between PVA-DTIC and in red and blue total interaction energy between Water-DTIC in each system. Each point in the graphs represents the average of three simulations for each system. (**B**) Interaction between the polymer and the DTIC. The PVA and the drug are presented as sticks highlighted in green and pink, respectively. The frame was retrieved at 250 ns of MD simulations.

3.4 Nanofiber Sterility Validation

Preceding cell testing, it is essential to certify absolute sterility of the samples. Aiming to analyze if the sterilization procedure used in DTIC NF was efficient, we contaminated it with bacteria and used IPA for decontamination. The inoculated tubes exhibited growth after 2 days' incubation in aerobic and anaerobic growth conditions, whereas the fungal growth conditions displayed growth following 5 days' incubation. The TSB inoculated with *S. aureus* and incubated at 37°C exhibited

strong growth, causing very evident turbidity throughout the media with growth formations observed at the bottom of the tubes. TSB tubes inoculated with *A. niger* at 25°C became turbid with some growth observed at the top of the media. The FTM inoculated with *C. albicans* displayed positive signs of anaerobic growth, with large, white formations on the bottom of the test tubes. There was no observable growth in any of the un-inoculated tubes, including those containing the non-treated nanofibers. These results show that the IPA sterilization method was adequate in eliminating bacterial and fungal contaminants (figure S2-3).

3.5 Cell uptake profile

Rhodamine-B (Rho) was added into the NFs to investigate the cellular uptake potential of the NFs. Figure 8 shows the cell uptake after 6, 24 and 48 hours of exposition of Rho solution and Rho-NF. Rho-NF showed an increased uptake mostly after 24 hours of treatment and a continuous uptake until 48 hours. In opposition, Rho solution uptake is higher after 6 hours and then decreased in the following time. The results indicated that the controlled release of the NF is in accordance if the cell uptake.

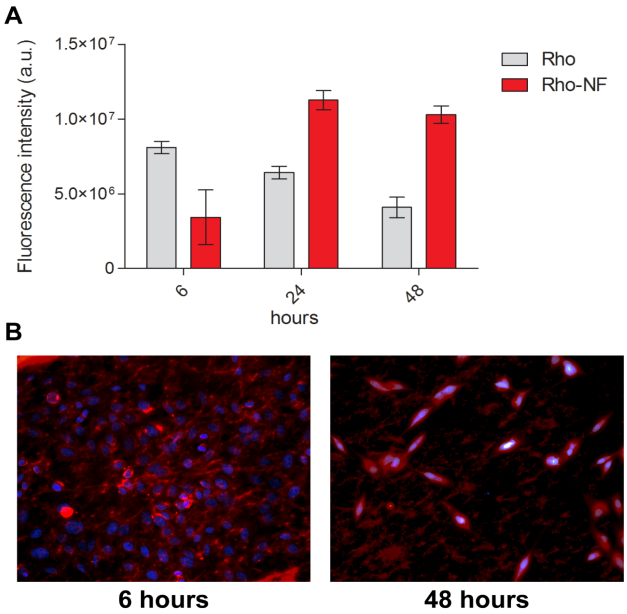

Figure 8: Cell Uptake evaluation **(A)** Fluorescence intensity of Rho-NF and Rho solution (**B)** Cells images of Rho-NF treatment after 6 and 48 hours of exposure. Results are exhibited as mean fluorescence intensity of cells treated with Rho solution or with Rho-NFs ± SD.

3.6 Cytotoxicity, DNA damage and cell death analysis

The cytotoxic effect of DTIC NFs was evaluated in GB cells by using MTT assay in media with pH 6.8 (figure 9A) and pH 7.4 (figure 9B). The results clearly showed that the blank NF is not cytotoxic, since the percentage of cell viability was greater than 90% after 1 day and 5 days of treatment. The absence of cytotoxicity indicates a biocompatibility, as well as, that its use would be suitable for the treatment of cancer. In other hand, DTIC NF significantly decreased the cell viability in both pHs and it was statistical different from DTIC alone in the pH 6.8 media, decreasing the viability after 5 days (figure 9A), indicating that the NFs improved the efficacy of DTIC after a prolonged exposure. However, the comparison between the NFs in the different medium was not significant (figure 9C).

Figure 9D shows the cells images over exposition to Blank NF, DTIC NF and DTIC alone in pH 6.8 media. Traditionally, GB cell lines propagate faster with longer protrusions and grow as monolayers. It is possible to observe that after 1 day of treatment with DTIC NFs the cells formed multilayer spheroids and started to grow extremely slowly given that only small members of cells could migrate outside their spheres.

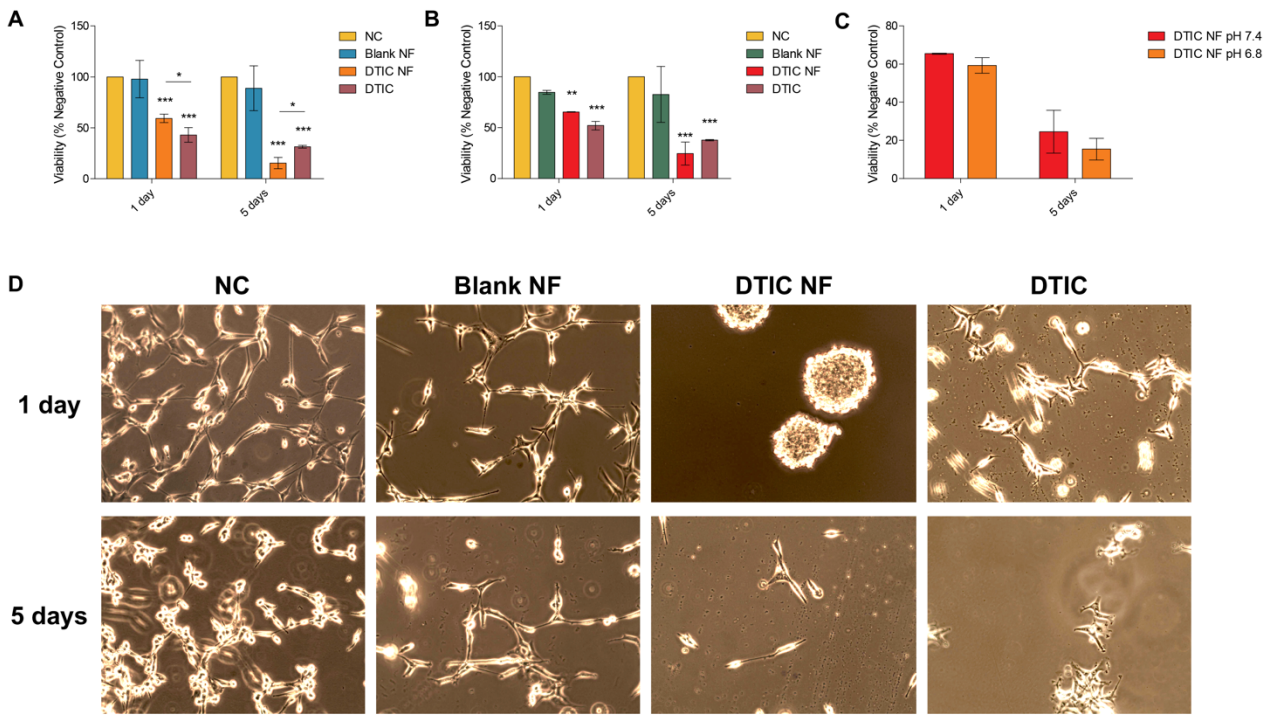

Figure 9: Cytotoxic effects of Blank NF, DTIC NF and DTIC in U87 cells after 1 and

5 days' exposure by MTT assay **(A)** Cytotoxic evaluation in pH 6.8 media and **(B)** pH 7.4 media **(C)** Comparison between treatment of DTIC NFs in pH 6.8 and 7.4 media **(D)** Cells images over exposition to Blank NF, DTIC NF, DTIC and without treatment in pH 6.8 media. Results are expressed as mean viability percentage in treated cells compared to negative control (NC) ± SD. Statistical analyses were performed using two-way ANOVA and Bonferroni post-test. Data was considered significant different when compared to NC at $*p < 0.05$ and $***p < 0.001$.

It is known that DTIC is an agent that causes DNA damage given its methylation and cell cycle arrest [64], which can results in double-strand break (DSB). When DSB establishes in DNA, several molecules of histone H2AX existing in the chromatin flanking the DSB site and they are phosphorylated (γ). The γH2AX foci usually increases in size rapidly for half an hour after formation and remains until the repair of the break [65]. Confocal microscopy showed significantly more γH2AX foci percentage in cells treated with DTIC NF compared to NC and DTIC (figure 10A-B) after 1 and 5 days of treatment. Figure 10C shows cells images without treatment and over exposition to DTIC and DTIC NF. The white arrows show γH2AX foci, indicating that over DTIC NF exposition there is more DNA damage.

Moreover, previous studies have demonstrated that DTIC treatment results in cell death through apoptosis [64,66]. Therefore, the present study evaluated, using Annexin V assay, whether DTIC NFs increases cell death pathways rate when compared to DTIC. As shown in figure 10D and 8E, cells treated with DTIC NFs presented a higher apoptosis and late apoptosis percentages (19.9 and 32.8%, respectively) when compared to DTIC by itself (15.8 and 14.2%, respectively), after 5 days. Additionally, when compared to the negative control, DTIC NF presented 7-fold increase in the apoptosis and 3.1-fold increase in the late apoptosis, while DTIC presented 2.1-fold and 3-fold increase, respectively. Thus, data from DNA damage and cell death indicate that the NF facilitated drug uptake and enhanced accumulation of DTIC into the GB cells improving its genotoxic and cytotoxic effects.

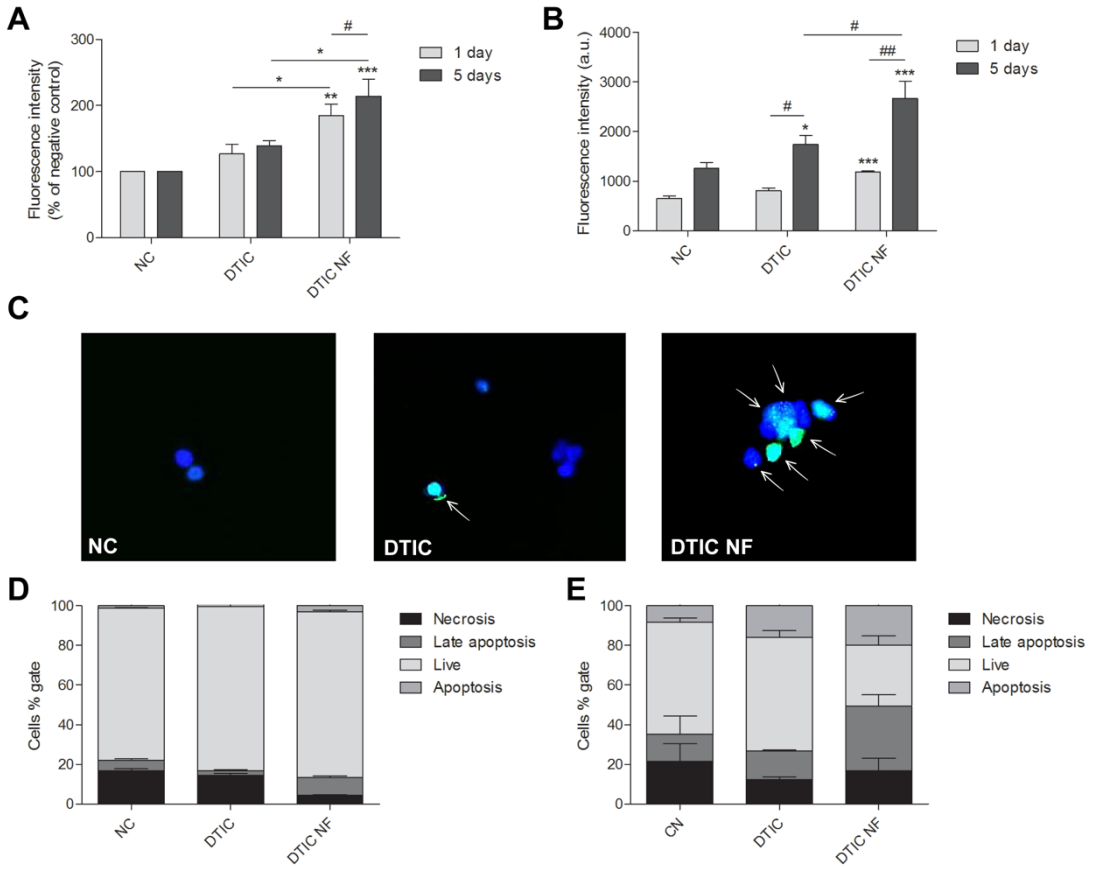

Figure 10: DNA damage and cell death evaluation. γH2AX fluorescence intensity in U87 cells after 1 and 5 days' treatments. **(A)** Fluorescence intensity percentage of negative control; **(B)** Fluorescence intensity arbitrary units; **(C)** Cells images over exposition to DTIC, DTIC NF, and without treatment. White arrows indicate γH2AX foci; **(D)** Type of cell death analysis after 1 day of exposure and **(E)** after 5 days of exposure. Results are expressed as mean in treated cells compared to negative control (NC) ± SD. Statistical analyses were performed using one-way ANOVA and Tukey post-test when # and two-way ANOVA and Bonferroni post-test when *. Data was considered significant different when compared to NC at *or#$p < 0.05$, **or##$p < 0.01$ and ***or###$p < 0.001$.

4. CONCLUSION

Despite its moderate effect, DTIC continues to be used for cancer treatment. Given its limited efficacy and several side effects there appears to be a need for the development of effective drug delivery strategies. In this study, DTIC polymeric NF were successfully prepared, characterized and its anticancer efficacy was determined. This system demonstrated a high drug loading, which extended drug release and allowed prolonged exposure of the GB cells to the treatment improving its antitumor effects. The present work demonstrated, through a series of molecular

dynamics simulations, that DTIC is able to interact with PVA, as well as explaining the extended drug release. These results represent the first atomic level indication of PVA-DTIC complexation. The *in vitro* results suggested this approach as efficient against GB cell, therefore DTIC NF drug delivery system could be a promising vector for a novel brain implant therapeutic therapy.

Acknowledgments

This study was supported in parts by grants from the Athlone Institute of Technology research and development funding, GOI-IES (Government of Ireland International Education Scholarship) and CAPES (Coordenação de Aperfeiçoamento de Pessoal de Nível Superior, Brazil).

Conflict of Interest

The authors declare that there are no conflicts of interest.

Statement of authors' contributions to manuscript

L.S., P.R.A., A.M.M., K.M., and Z.C. conducted the experiments; L.S., P.R.A., D.J.M. and M.N. wrote the paper. All authors read and approved the final manuscript.

Supplementary

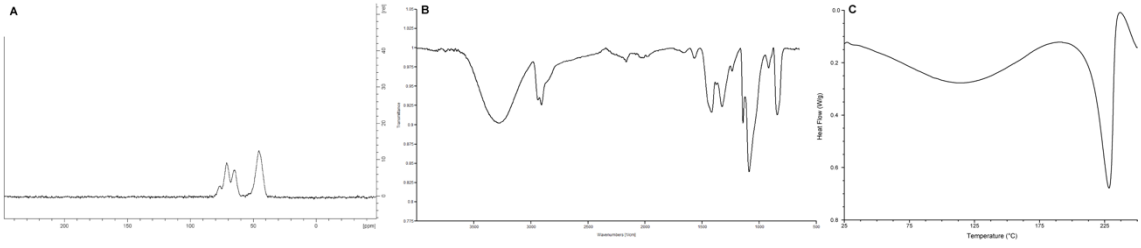

Figure 1: PVA powder analysis. (**A**) NMR, (**B**) FTIR and (**C**) DSC.

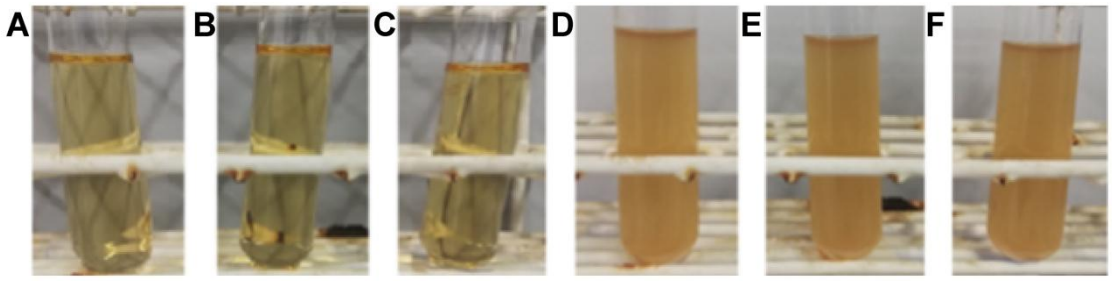

Figure 2: Test tubes of TSB incubated at 37 °C for 14 days. Test microorganism used was *S. aureus*. (**A**) Negative (Sterility) control, (**B**) Untreated NF (**C**) Sterilized NF (**D**) Positive (Growth) control of *S. aureus* (**E**) Untreated NF + *S. aureus* (**F)** Sterilized NF + *S. aureus*.

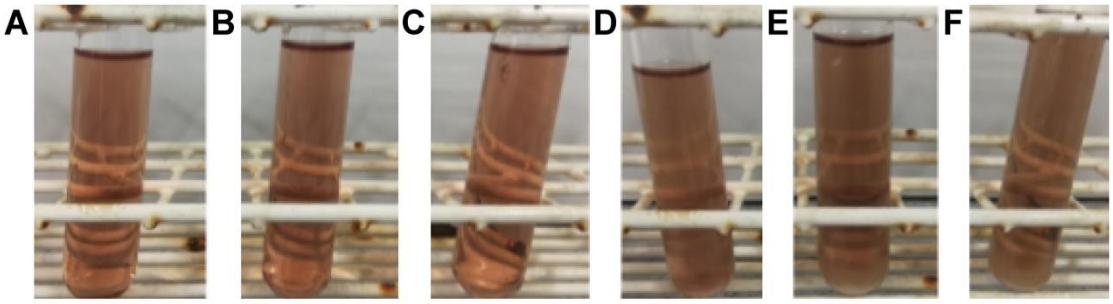

Figure 3: Test tubes of FTM incubated at 37 °C for 14 days. Test microorganism used was *C. albicans*. (**A**) Negative (Sterility) control, (**B**) Untreated NF (**C**) Sterilized NF (**D**) Positive (Growth) control of *C. albicans* (**F**) Untreated NF + *C. albicans* (**E**) Sterilized NF + *C. albicans*.

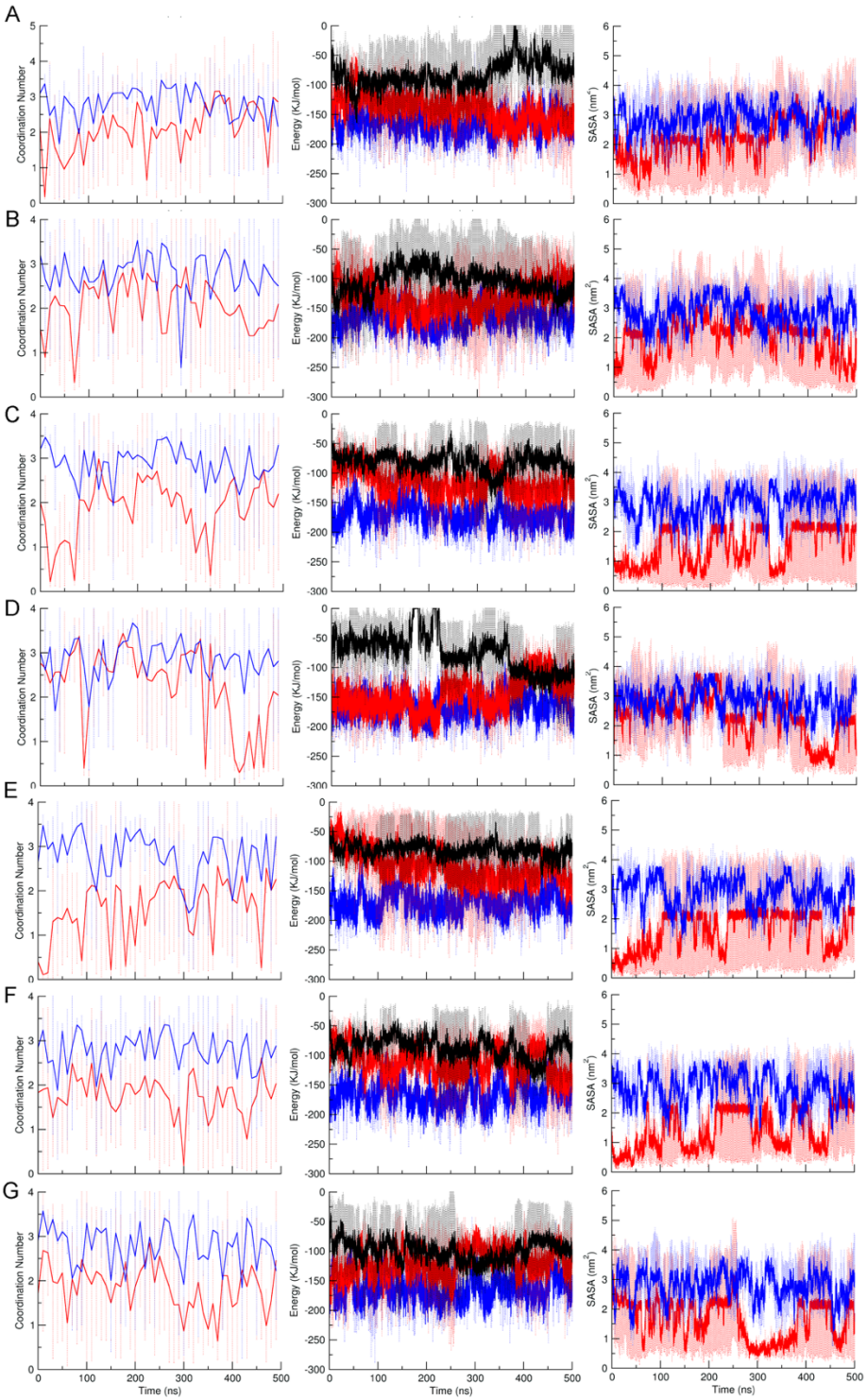

Figure 4: Coordination number of water molecules (CN) on nitrogen atom of DTIC imidazole ring, total interaction energy between PVA-DTIC and PVA-water and average of solvent accessible surface area (SASA) on drug during the molecular dynamics simulations. In blue the system of DTIC in water, in red and black the system with PVA-DTIC in water. The black line is total interaction energy between PVA-DTIC and in red and blue total interaction energy between water-DTIC in each system. Each point in the graphs represents the average of three simulations for each system. (**A-G**) other drug molecules present in the systems studied.

References

1. Siegal, T. (2013) Which drug or drug delivery system can change clinical practice for brain tumor therapy? Neuro. Oncol. 15, 656-669.
2. Stupp, R., Hegi, M.E., Mason, W.P., van den Bent, M.J., Taphoorn, M.J.B., Janzer, R.C. et al. (2009) Effects of radiotherapy with concomitant and adjuvant temozolomide versus radiotherapy alone on survival in glioblastoma in a randomised phase III study: 5-year analysis of the EORTC-NCIC trial. Lancet Oncol. 10, 459–466.
3. Weller, M., Cloughesy, T., Perry, J.R., Wick, W. (2013) Standards of care for treatment of recurrent glioblastoma--are we there yet? Neuro-oncology. 15, 4–27.
4. Campos, B., Olsen, L.R., Urup, T., Poulsen, H.S. (2016) A comprehensive profile of recurrent glioblastoma. Oncogene. 1-7.
5. Fazeny-Dorner, B., et al. (2003) Survival with dacarbazine and fotemustine in newly diagnosed glioblastoma multiforme. British J of Cancer 88, 496-501.
6. Di Bei, J.M. & Bi-Botti, C.Y. (2009) Formulation of Dacarbazine-Loaded Cubosomes—Part I: Influence of Formulation Variables. AAPS PharmSciTech. 10(3), 1032-9.
7. Pourgholi, F. et al. (2016) Nanoparticles: Novel vehicles in treatment of Glioblastoma. Biomedic&Pharmacot. 77, 98-107.
8. Ahmed, F. et al. (2006) Biodegradable polymersomes loaded with both paclitaxel and doxorubicin permeate and shrink tumors, inducing apoptosis in proportion to accumulated drug. J. Control. Release 116, 150–8.
9. Ranganath, S. H. & Wang, C.H. (2008) Biodegradable microfiber implants delivering paclitaxel for post-surgical chemotherapy against malignant glioma. Biomaterials 29, 2996–3003.
10. Kumar Naraharisetti, P. et al. (2007) *In vivo* performance of implantable biodegradable preparations delivering Paclitaxel and Etanidazole for the treatment of glioma. Biomaterials 28, 886–94.
11. Hernán Pérez de la Ossa, D. et al. (2013) Local delivery of cannabinoid-loaded microparticles inhibits tumor growth in a murine xenograft model of glioblastoma multiforme. PLoS One8, e54795.
12. Scott, A.W. et al. (2011) Intracranial microcapsule drug delivery device for the treatment of an experimental gliosarcoma model. Biomaterials 32, 2532–9.
13. Kim, G.Y. et al. (2007) Resorbable polymer microchips releasing BCNU inhibit tumor growth in the rat 9L flank model. J. Control. Release 123, 172–178.
14. Hua, M.Y. et al. (2011) The effectiveness of a magnetic nanoparticle-based delivery system for BCNU in the treatment of gliomas. Biomaterials 32, 516–27.
15. Ramachandran, R. et al. (2014) A Polymer-Protein Core–Shell Nanomedicine for Inhibiting Cancer Migration Followed by Photo-Triggered Killing. J. Biomed. Nanotechnol. 10, 1401–1415.
16. Ramachandran, R. et al. (2017). Theranostic 3-Dimensional nano brain-implant for prolonged and localized treatment of recurrent glioma. Scientific reports, 7, 43271. doi:10.1038/srep43271.

17. Chen, W. et al. (2015) Charge-conversional and reduction-sensitive poly(vinyl alcohol) nanogels for enhanced cell uptake and efficient intracellular doxorubicin release. J. Controlled Release. 205, 15-24.
18. De Lima, G.G. et al. (2015) A novel pH-sensitive ceramic-hydrogel for biomedical applications. Polym Advan Tech. 26, 1439-46.
19. Canillas, M. et al. (2016) Bioactive Composites Fabricated by Freezing-Thawing Method for Bone Regeneration Applications. Polym Phys. 54, 761-73.
20. Pronk, S., et al. (2013) GROMACS 4.5: A high-throughput and highly parallel open source molecular simulation toolkit. Bioinformatics, 29(7), 845–854. doi: 10.1093/bioinformatics/btt055
21. Oostenbrink, C., Villa, A., Mark, A. E., & van Gunsteren, W. F. (2004) A biomolecular force field based on the free enthalpy of hydration and solvation: the GROMOS force-field parameter sets 53A5 and 53A6. Journal of computational chemistry, 25(13), 1656–76. doi: 10.1002/jcc.20090
22. Pol-Fachin, L., Rusu, V. H., Verli, H., & Lins, R. D. (2012) GROMOS 53A6 GLYC, an Improved GROMOS Force Field for Hexopyranose-Based Carbohydrates. Journal of Chemical Theory and Computation, 8(11), 4681–4690. doi: 10.1021/ct300479h
23. Pol-Fachin, L., Verli, H., & Lins, R. D. (2014) Extension and validation of the GROMOS 53A6(GLYC) parameter set for glycoproteins. Journal of computational chemistry, 35(29), 2087–95. doi: 10.1002/jcc.23721
24. Polêto, M. D., et al. (2018). Aromatic Rings Commonly Used in Medicinal Chemistry: Force Fields Comparison and Interactions With Water Toward the Design of New Chemical Entities. Frontiers in Pharmacology, 9, 395. Retrieved from http://journal.frontiersin.org/article/10.3389/fphar.2018.00395/full doi: 10.3389/fphar.2018.00395
25. Degiacomi, M. T., Erastova, V., & Wilson, M. R. (2016) Easy creation of polymeric systems for molecular dynamics with Assemble! Computer Physics Communications, 202, 304–309. Retrieved from https://www.sciencedirect.com/science/article/pii/S0010465516000187 doi: 10.1016/J.CPC.2015.12.026
26. Humphrey, W., Dalke, A., & Schulten, K. (1996) VMD: Visual molecular dynamics. Journal of Molecular Graphics, 14(1), 33–38. doi: 10.1016/0263-7855(96)00018-5
27. Delano, W. L. (n.d.) PyMOL: An Open-Source Molecular Graphics Tool (Tech. Rep.). Retrieved from https://www.ccp4.ac.uk/newsletters/newsletter40/11_pymol.pdf
28. Frisch, M. J., et al. (n.d.) Gaussian 09 Revision E.01.
29. Arantes, P. R., et al. (2019) Development of GROMOS- Compatible Parameter Set for Simulations of Chalcones and Flavonoids. The Journal of Physical Chemistry B, 123(5), 994–1008. Retrieved from http://pubs.acs.org/doi/10.1021/acs.jpcb.8b10139 doi: 10.1021/acs.jpcb.8b10139
30. Rusu, V. H., Baron, R., & Lins, R. D. (2014) Pitomba: Parameter interface for oligosaccharide molecules based on atoms. Journal of chemical theory and computation, 10(11), 5068–5080.

31. Van der Spoel, D., & Lindahl, E. (n.d.) Brute-Force Molecular Dynamics Simulations of Villin Headpiece: Comparison with NMR Parameters. The Journal of Physical Chemistry B(40), 11178–11187. doi: 10.1021/jp034108n
32. Abraham, M. J., et al. (2015) GROMACS: High performance molecular simulations through multi-level parallelism from laptops to supercomputers. SoftwareX , 1, 19– 25. doi: 10.1016/j.softx.2015.06.001
33. Kyrychenko, A., Pasko, D. A., & Kalugin, O. N. (2017) Poly(vinyl alcohol) as a water protecting agent for silver nanoparticles: The role of polymer size and structure. Physical Chemistry Chemical Physics, 19(13), 8742– 8756. Retrieved from http://dx.doi.org/10.1039/C6CP05562A doi:10.1039/c6cp05562a
34. Tallury, S. S., & Pasquinelli, M. A. (2010a) Molecular dynamics simulations of flexible polymer chains wrapping single-walled carbon nanotubes. Journal of Physical Chemistry B, 114(12), 4122–4129. doi: 10.1021/jp908001d
35. Tallury, S. S., & Pasquinelli, M. A. (2010b) Molecular dynamics simulations of polymers with stiff backbones interacting with single-walled carbon nanotubes. Journal of Physical Chemistry B, 114(29), 9349–9355. doi: 10.1021/jp101191j
36. Berendsen, H. J. C., Grigera, J. R., & Straatsma, T. P. (1987) The Missing Term in Effective Pair Potentials. Journal of Physical Chemistry, 91(24), 6269– 6271. doi: 10.1021/j100308a038
37. Hess, B., Bekker, H., Berendsen, H. J. C., & Fraaije, J. G. E. M. (1997) LINCS: A linear constraint solver for molecular simulations. Journal of Computational Chemistry, 18(12), 1463–1472. doi: 10.1002/(SICI)1096-987X(199709)18:12<1463::AID-JCC4>3.0.CO;2-H
38. Darden, T., York, D., & Pedersen, L. (1993) Particle mesh Ewald: An N-log(N) method for Ewald sums in large systems. The Journal of Chemical Physics, 98(12), 10089. doi: 10.1063/1.464397
39. Parrinello, M. (1981) Polymorphic transitions in single crystals: A new molecular dynamics method. Journal of Applied Physics, 52(12), 7182. doi: 10.1063/1.328693
40. Nosé, S., & Klein, M. L. (1983) Constant pressure molecular dynamics for molec- ular systems. Molecular Physics, 50(5), 1055–1076.
41. Bussi, G., Donadio, D., & Parrinello, M. (2007) Canonical sampling through velocity rescaling. The Journal of chemical physics, 126(1), 014101. doi: 10.1063/1.2408420
42. Nosé, S. (1984) A molecular dynamics method for simulations in the canonical ensemble. Molecular Physics, 52(2), 255–268. doi: 10.1080/00268978400101201
43. Hoover, W. G. (1985) Canonical dynamics: Equilibrium phase-space distributions. Physical Review A, 31(3), 1695–1697. doi: 10.1103/PhysRevA.31.1695
44. Nemec, M., & Hoffmann, D. (2017) Quantitative Assessment of Molecular Dynamics Sampling for Flexible Systems. Journal of Chemical Theory and Computation, 13(2), 400–414. Retrieved from http://pubs.acs.org/doi/10.1021/acs.jctc.6b00823 doi: 10.1021/acs.jctc.6b00823

45. Perez, J. J., Tomas, M. S., & Rubio-Martinez, J. (2016) Assessment of the Sampling Performance of Multiple-Copy Dynamics versus a Unique Trajectory. Journal of Chemical In- formation and Modeling, 56(10), 1950–1962. Retrieved from http://pubs.acs.org/doi/10.1021/acs.jcim.6b00347 doi: 10.1021/acs.jcim.6b00347
46. Vashisth, P., Kumar, N., Sharma, M., Pruthi, V. (2015) Biomedical applications of ferulic acid encapsulated electrospun nanofibers. Biotechnology Reports, 8, 36-44.
47. Zhoun B, Shen M, Banyai I, Shi, X. (2016) Structural characterization of PEGylated polyethylenimine-entrapped gold nanoparticles: An NMR study. Analyst. 141, 5390-5397.
48. Al-Badr A & Mansour MA. (2016) Dacarbazine, Comprehensive profile. 323-377.
49. Honasoge, A. & Sontheimer, H. (2013) Involvement of tumor acidification in brain cancer pathophysiology. Front Physiol 4, 316, doi:10.3389/fphys.2013.00316.
50. Rao, J. U., Coman, D., Walsh, J. J., Ali, M. M., Huang, Y., Hyder, F. (2017) Temozolomide arrests glioma growth and normalizes intratumoral extracelular pH. Scientific Reports 7, 7865. doi:10.1038/s41598-017-07609-7.
51. Estrella, V. et al. (2013) Acidity generated by the tumor microenvironment drives local invasion. Cancer Res 73, 1524–1535, doi:10.1158/0008-5472.CAN-12-2796.
52. Yang, W., Sousa, A. M. M., Li, X., Tomasula, P. M., Liu, L. (2017) Electrospinning of Guar Gum/Corn Starch Blends. SOJ Materials Science & Engineering. 5(1), 1-7.
53. Mansur, H.S. et al. (2008) FTIR spectroscopy characterization of poly(vinyl alcohol) hydrogel with different hydrolysis degree and chemically crosslinked with formaldehyde. Mater. Sci. Eng. C. 28, 539-548.
54. Peppas, N.A., Bures, C.D. (2006) Glucose-Responsive Hydrogels, Encyclopedia of Biomaterials and Biomedical Engineering. Taylor & Francis.
55. Vashisth, P., Singh, R.P., Pruthi, V. (2015) A controlled release system for quercetin from biodegradable poly(lactide-co-glycolide)-polycaprolactone nanofibers and its in vitro antitumor activity. J. Bioactive and Comp. Polymers. 1-13.
56. Cao, Y. et al. (2017) Drug release from core-shell PVA/silk fibroin nanoparticles fabricated by one-step electrospraying. 7, 11913.
57. Li, X. et al. (2013) Electrospun polyvinyl-alcohol nanofibers as oral fast-dissolving delivery system of caffeine and riboflavin. Col. and Surf. B: Biointer. 103, 182-188.
58. Chen, P. et al. (2010) A controlled release system of titanocene dichloride by electrospun fiber and its antitumor activity in vitro. Eur. J. Pharm. Biopharm. 76, 413-420.
59. Budiasih, S. et al. (2014) Optimization of polymer concentration for designing of oral matrix controlled release dosage form. UK J. of Pharm. and Biosci. 5, 54-61.

60. El-Feky, G.S. et al. (2015) Utilization of crosslinked starch nanoparticles as a carrier for indomethacin and acyclovir drugs. J. Nanomed. Nanotechnol. 6, 254.
61. Nugent, M. et al. (2005) Investigation of a novel freeze-thaw process for the production of drug delivery hydrogels. J. of Mater. Sci. Mater. in Med. 16, 1149-1158.
62. Dejene, F.B. et al. (2011) Optical properties of ZnO nanoparticles synthesized by varying the sodium hydroxide to zinc acetate molar ratios using a sol-Gel process. Cent. Eur. J. Phys. 9(5), 1321-1326.
63. Lopez, F.L. et al. (2004) Amorphous Formulations of Indomethacin and Griseofulvin Prepared by Electrospinning. Mol. Pharmaceutics. 11(12), 4327-4338.
64. Al-Gatati, A. & Aliwaini, S. (2017) Combined pitavastatin and dacarbazine treatment activates apoptosis and autophagy resulting in synergistic cytotoxicity in melanoma cells. Oncology letters 14, 7993-7999.
65. Nakamura, A. et al. (2006) Techniques for γ-H2AX Detection. Methods in Enzymology 409, 236-250.
66. Sanada, M. et al. (2007) Modes of actions of two types of anti-neoplastic drugs, dacarbazine and ACNU, to induce apoptosis. Carcinogenesis 28, 2657-2663.

CAPÍTULO 3: Nek1-inhibitor and temozolomide-loaded nanofibers as a co-therapy strategy for glioblastoma treatment

O artigo será submetido ao periódico Materials Science and Engineering: C

Nek1-inhibitor and temozolomide-loaded nanofibers as a co-therapy strategy for glioblastoma treatment

Luiza Steffens[ab], Ana Moira Morás[b], Jeferson Gustavo Henn[b], Pablo Ricardo Arantes[b], Mabilly Cox Holanda de Barros Dias[a], Zhi Cao[a], Michael Nugent[a], Dinara Jaqueline Moura[b*]

a. Athlone Institute of Technology, Materials Research Institute, Athlone, Co. Westmeath, Ireland
b. Laboratory of Genetic Toxicology, Federal University of Health Sciences of Porto Alegre – UFCSPA, Sarmento Leite, 245, Lab.714, Porto Alegre, Rio Grande do Sul, Brazil

* Corresponding author. Address: Federal University of Health Sciences of Porto Alegre – UFCSPA, Sarmento Leite, 245, Lab.714, Porto Alegre, Rio Grande do Sul, Brazil
E-mail address: dinaram@ufcspa.edu.br (Dinara Jaqueline Moura, PhD)

ABSTRACT

Malignant glioblastoma (GB) is the most prevalent brain tumor in adults, with an overall survival of less than 15 months. The GB standard therapy includes surgery followed by radiotherapy and adjuvant chemotherapy with temozolomide (TMZ). However, this approach has proved ineffective. Therefore, localized and controlled approaches that treat recurrent GBs straight into tumor site provides an alternative to enhance chemotherapy efficacy and reduce systemic toxicity. Moreover, the discovery of powerful genetic and protein targets has stimulated clinical development of these therapy approaches to treat patients with GB. Nek1 is a protein related to DNA repair and mitosis. Recently, it was shown that Nek1 might be a novel and important oncotarget in glioma cells and its role in the GB malignance seems to be related to cell growth and TMZ-resistance promotion. In this study we report a polyvinyl alcohol (PVA) nanofiber (NF) brain-implant prepared using electrospinning for the controlled release of TMZ and Nek1 inhibitor (iNek1) and evaluation of its *in vitro* efficacy. We incorporated TMZ in lipid nanoparticles (NPs). These carriers presented mean size of 519.5 ± 52 nm, zeta potential was found to be -31.6 ± 0.7 mV and encapsulation efficiency (EE%) of 79.8 ± 6.8. Then we produced TMZ + iNek-PVA NF with distribution size of 2900 ± 1142 nm and iNek1-PVA with TMZ NPs inside distribution size of 2723 ± 684 nm. In the ^{1}H and ^{13}C NMR studies no shifting peaks were observed, therefore these results suggested the stability of the drugs into the formulations and because of that, TMZ and iNek1 bioactivities are probably preserved after encapsulation into NF and NP. The nanoproducts presented adequate viscosity and mechanical properties observed by using rheometer analysis. The EE% of TMZ into the NP was 79.8 ± 6.8 and the EE% of iNek1 into the NFs was 79.2 ± 7.3. The NFs with dissolved TMZ presented an EE% of 75.2 ± 5.9. The resulting drug release from the nanoproducts provided a continuous release profile of TMZ and iNek1 over 8 days and showed that NP inside of NF presented a slower release of TMZ when compared to TMZ + iNek- NF. Before cell testing we performed NF sterility analysis by using isopropanol (IPA) and we found 100% of efficacy. Aiming to verify if Nek1 responds to TMZ treatment we

analyzed the expression of Nek1 in GB cells. The results showed a translocation of Nek1 to nucleus and a small increase of its expression. The cytotoxic effect of nanoproducts was evaluated and TMZ + iNek1 NF and TMZ NP + iNek1 NF showed great efficacy at all treatment points (2 days, 5 days and 5 days + 2 days of recover). Consequently, the produced NF brain-implants could be a promising drug delivery system for GB therapy.

Key-words: Electrospinning. Temozolomide. Nima-related kinase 1. Nanoparticles. Nanofibers. Polyvinyl alcohol. Glioblastoma.

1. INTRODUCTION

Malignant glioblastoma (GB) is the most prevalent brain tumor in adults, with an overall survival of less than 15 months (Norouzi et al, 2016; Tseng et al, 2016; Brodbelt et al, 2015; Rape et al, 2014). Currently, surgery followed by radiotherapy and adjuvant chemotherapy are considered as the standard therapy for GB patients (Tseng et al, 2015; Huang et al, 2016; Siegal et al, 2013). However, GB presents high capacity to infiltrate in normal tissue and this makes almost impossible to remove completely the tumor through surgical resection. After resection, the recurrent GB invasive cells are able to form tumors within few centimeters of the original site (Weller et al, 2013; Tseng et al, 2015; Huang et al, 2016; Sawyer et al, 2006). In addition, the presence of the blood-brain barrier (BBB) and its tight capillary cellular junctions restricts efficient drug delivery to the brain making chemotherapy inefficacious (Sun et al, 2017; Irani et al, 2017; Wei et al, 2014; Fan et al, 2015; Park et al, 2017). Several drugs fail to achieve therapeutic concentrations at the tumor site, even at toxic systemic level concentrations (Tseng et al, 2015; Tseng et al, 2013). Therefore, localized and controlled approaches that treat recurrent GBs straight into tumor site provides an alternative to enhance chemotherapy efficacy and reduce systemic toxicity (Ranganath & Wang, 2008; Han et al, 2017; Kuramitsu et al, 2015; Hirschberg et al, 2013).

Due to its biocompatibility, polymers are one of the most promising resources to use in the production of drug delivery systems (DDS) (Di Bei & Bi-Botti, 2009). Several DDS, such as micro and nanoproducts and wafers have been developed to provide adequate drug release into the tumor site (Ahmed et al, 2006; Ranganath & Wang,

2008; Kumar et al, 2007; Hérnan et al, 2013; Scott et al, 2011; Kim et al, 2007; Hua et al, 2011, Ramachandran et al, 2014; Ramachandran et al, 2017; Ranganath & Wang, 2008; Irani et al, 2017; Játiva & Cena, 2017; Cheng et al, 2014; Mangraviti et al, 2016). Nevertheless, given the high interstitial pressure in the brain, micro and nanoparticles can be easily expelled from the target site, and also, these products usually present burst release of loaded drugs and this can cause neurotoxicity (Irani et al, 2017). Additionally, hydrogels and wafers have low surface areas resulting in inappropriate and inconsistent drug dissolution (Ranganath & Wang, 2008; Norouzi, 2018). Recently, nanofibers (NF) produced by using electrospinning have attracted attention as a novel alternative approach for drug delivery in the brain tumor. Our research group focus is the research of polyvinyl alcohol (PVA). PVA is a noteworthy choice for designing NFs, since this polymer is biodegradable and presents very low toxicity (Pourgholi et al, 2016; Ahmed et al, 2006; Ranganath & Wang, 2008). Newly, we produced Dacarbazine-PVA NFs to treat glioblastomas and this product showed great mechanical and delivery properties (data not published).

Temozolomide (TMZ) is an alkylating agent and is currently used for the treatment of GB by oral administration (Denny et al, 1994). Adjuvant therapy with TMZ after surgery has been widely accepted as the most effective and well-tolerated option (Akbar et al, 2009). To improve the therapy efficacy with TMZ and decreased its side effects such as hematologic toxicities (Stupp et al, 2005; Corsa et al, 2006; Mutter & Stupp, 2006; Vera et al, 2004), directly DDS can be administered to prevent tumor recurrence. Moreover, the discovery of powerful genetic and protein targets has stimulated clinical development of these therapy approaches to treat patients with GB (Zhu et al, 2016). Lack of success in the clinic has been attributed to the inability of conventional vectors to achieve tumor site throughout highly disseminated tumors, however, it is extremely import to bio-functionalize the DDS with oncotargets (Westphal et al, 2011). Nek1 is member of Nek family kinases (Patil el al, 2013; White & Quarmby, 2009). The role of Nek1 has been related to mitosis (Patil el al, 2013; White & Quarmby, 2009) and in DNA damage repair (Surpili et al., 2003; Liu et al., 2013; Spies et al., 2016). More recently was showed that Nek1 might be a novel and important oncotarget of glioma cells since its role in the GB malignance is related to cell growth and TMZ-resistance (Zhu et al, 2016).

The aim of this study was to develop and characterize a PVA NF brain-implant prepared using electrospinning with stearic acid NP for the controlled release of Nek1 inhibitor (iNek1) and TMZ, respectively, and to evaluate its effectiveness in glioblastoma cells.

2. MATERIALS AND METHODS

2.1 Materials

PVA (Mw 146-168K, 90% hydrolyzed), Temozolomide, rhodamine-B, curcumin, Ethanol, methanol, Isopropanol, 3-(4,5-dimethylthiazol-2-yl)-2,5-diphenyltetrazolium bromide (MTT), paraformaldehyde, Triton X-100, tryptone soy broth (TSB) and fluid thioglycolate medium (FTM) were obtained from Sigma and Aldrich. Dulbeco's Modified Eagle Medium (DMEM), fetal bovine serum (FBS), phosphate-buffered saline (PBS), L-glutamine, trypsin-EDTA, antibiotics (penicillin and streptomycin) and Trypan blue were purchased from Gibco Life Sciences. Jun N-terminal kinase (JNK) Inhibitor II used as inhibitor of Nek1 was obtained from Merck Millipore.

2.2 Preparation of temozolomide based nanocarriers

TMZ-loaded stearic acid nanocarriers were produced by solvent diffusion method according to Hafeez (2017) with minor modifications. TMZ (10% wt/wt) and stearic acid were suspended in an organic phase prepared using acetone:ethanol mixture (1:1). Then, the aqueous phase was prepared by heating up to 70°C distilled water (dH_2O) on a continuous stirring. Finally, the organic phase was mixed into the aqueous phase during 30 min. After cooling at room temperature the mixture, it was ultrasounded during 5 min and froze overnight. Later, the mixture was lyophilized in a freeze dryer (Heto, LyoLab 3000). For comparison proposes Blank nanocarriers were prepared by using only stearic acid.

2.3 Particle size and zeta potential

Particle Size analysis and Zeta potential analysis was carried out on the Beckman Coulter Delsa Nano C. For particle sizing, the sample was run 9 times to ensure that results were statistically relevant. Analysis was carried out on the measured

autocorrelation functions using the Non-negative Least Square algorithm. Very large aggregate results (above 5 μm) were removed from the analysis as the fitting and algorithm cannot provide accurate results at this size. For Zeta potential, the sample was run 3 times (as each run is repeated 10 times and averaged to provide the result). The applied voltage on the electrodes of the cell was 60 mV.

2.4 Preparation of nanofibers

PVA hydrogel solutions were produced by mixing PVA at 10% concentration (wt/vol) in dH_2O, at 90°C with continuous stirring, after solubilization, 10% of ethanol 10% was added. Then, different solutions were prepared by adding known amounts of TMZ, Nek1 inhibitor (iNek1) solution in DMSO or nanocarriers into the PVA solution. For details see below the table 1:

Table 1: Hydrogels solutions.

10% PVA solution	Composition
1	-
2	Stearic acid nanocarriers (Blank NP)
3	TMZ
4	iNek1
5	TMZ + iNek1
6	TMZ + stearic acid nanocarrier (TMZ NP) + iNek1

The solutions were electrospun using a blunt-end 26-gauge needle and it distance to the collector plate was set 5 cm. The flow rate was set 0.5 mL/h using 9 kV.

2.5 Analysis of nanofiber size and morphology

The morphology of the nanoproducts were analyzed by using scanning electron

microscope (SEM) (Tescan Mira XMU SEM, TESCAN, Brno, CZ). Back scattered electron mode was used with magnifications ranged from 10 kX to 30 kX. Firstly, the NP and NF were sputtered with gold. For NF mean diameter size analysis, 200 NF were observed in the ImageJ software (ImageJ Version 1.48v). Fluorescence images of the NFs were acquired using the Leica DM 2000 confocal microscope with a x40 oil lens (Leica Microsystems, Ashbourne, Ireland). Image acquisition was performed by LAS V3.8 software (Leica) and fluorescence analysis was carried out using ImageJ software (ImageJ Version 1.48v).

2.6 Solid-state NMR

The stability of the drugs after encapsulation in PVA NFs or stearic acid NP were evaluated using nuclear magnetic resonance (NMR) spectroscopy. The assessment was executed using Bruker 400 MHz Avance III HD equipped with a 3.2mm H/X CPMAS probe.

2.7 Mechanical properties

The mechanical properties of the NFs were measured by using a Discovery HR-2 rheometer (TA instruments, DE, USA). The analysis was accomplished by using the parallel plate method. The samples were loaded on the Peltier plate after 30 minutes in PBS buffer. After an equilibration step, the viscoelastic properties: elastic modulus (G') and viscous modulus (G'') as function of frequency were measured through frequency sweep testes over a range from 1 to 40 Hz. The flow curves of apparent viscosity data of each sample were produced using steady shear evaluations were performed in the shear rate range 1 – 50 s^{-1}.

2.8 Determination encapsulation efficiency of TMZ and iNek1

To quantity the percent encapsulation efficiency (EE%) of loaded-TMZ and iNek1 nanoproducts, NF or NP were completely dissolved in DMSO and the amount of released drug was measured by ultraviolet (UV) light on Shimadzu UV 1280 spectrometer at 328 and 407 nm, respectively. The EE% was determined as follows:

$$EE\% = \frac{actual\ amount\ of\ drug\ release\ in\ nanoproduct}{theoretical\ amount\ of\ loaded\ drug\ in\ nanoproduct} X100$$

2.9 *In vitro* drug release studies

In vitro drug release profiles were evaluated using a Distek Model 2500 Dissolution System (Distek, Inc., NJ, USA). NF and NP were tested in PBS (pH 6.8 and 7.4) at 37°C. The stir rate was set to 50 rpm and 300 ml of dissolution media were used per vessel. The amount of 3 mL of samples were taken at set intervals and assessed by UV light on Shimadzu UV 1280 spectrometer.

2.10 Nanofiber Sterilization and Sterility Validation

Isolated colonies of *Escherichia coli* (*E. coli*) (NC 12241) and *Staphylococcus aureus* (*S. aureus*) (NC 12981) from stock strains cryogenized on -80°C freezer were obtained through isolation seeding and grown overnight. Each colony of each bacteria, were separately suspended in 5 mL of sterile PBS (Phosphate buffered saline solution) and standardized with Spectrophotometer by 0.5 McFarland scale (1.5×10^8 CFU/mL in 600 nm wavelength). After that, 50 µL of standardized bacterial suspension were add into each polymer sample (1 cm^2 each sample) on 3 cm^2 diameter sterile plates. Contaminated samples were sterilized by total immersion in 500 µL of isopropyl alcohol 70% for a few seconds, and subsequently drained. Serial dilution of samples was conducted in a 96-well sterile microplate previously filled with 270 µL of sterile PBS until the 5^{th} well. Each sample was dispersed into 1 mL of sterile PBS and briefly mixed. From this dilution, 30 µL was taken out and transferred to the 1^{st} well in microplate, briefly mixed, being now the 10^{-1} dilution. And this went through until the 10^{-5} dilution. This procedure was repeated for each sample separately. From each dilution 100 µL was taken and inoculated through spread plate method in agar plate with 20 mL of solid Nutrient agar (NA) with a bent rod at once. Other three replicates were made with micro drop technique (10 µL) in NA plates. Plates were then incubated at 37°C for 24 hours. After the first reading, the plates were left on incubator for 2 weeks to analyze the growth possibility and no growth was observed on sterilized plates.

2.11 Nek1 protein expression

The GB cells (U87MG) were cultured in DMEM supplied with 10% FBS and antibiotics at 37°C in a humidified atmosphere containing 5% CO_2. Cell were submitted to a treatment with TMZ (75 µM) for 24 h. After treatment, U87 cells were

trypsinized, fixed with 3.7% paraformaldehyde for 15 min and permeabilized with 0.5% (v/v) Triton X-100 in PBS for 15 min followed by blocking with 10% (v/v) FBS in PBS for 1 h. Then, the samples were incubated overnight at 4°C with following diluted antibodies: 1:100 Alexa Fluor 488 Mouse anti-γH2AX (pS-139) (BD Biosciences, SP, Brazil), 1:50 anti-vinculin-FITC (Sigma-Aldrich Ltda., SP, Brazil) and 1:100 anti-Nek1 (Sigma-Aldrich Ltda., SP, Brazil), the secondary antibody for Nek1 staining was anti-rabbit Alexa Fluor 594 at a dilution of 1:500. The samples were added in a glass slide and each slide was dropwise added with Hoechst 33258 stain (ThermoFisher Scientific, SP, Brazil), covered with a coverslip, and mounted with nail polish. The slides were stored at −20°C until used for microscopic observation. Finally, the cells were imaged using an INCell analyser 2200 (GE Heathcare Life Sciences, Piscataway, NJ, USA). Protein extracts were also prepared by using lysis buffer and western blot was performed, then the membranes were blocked with 5% skim milk in TTBS for 1 hour and incubated overnight at 4°C with following antibodies at a dilution of 1:500 anti-Nek1 (Sigma-Aldrich Ltda., SP, Brazil) and anti-β-actin (Santa Cruz Biotechnology, SP, Brazil). The secondary antibodies used were 1:3000 mouse anti-rabbit and goat anti-mouse (Santa Cruz Biotechnology, SP, Brazil). The membranes were incubated with Luminol-based Enhanced Chemiluminescent (ECL) mix and exposed to films to develop.

2.12 Cell viability evaluation

To perform the experiments two different pH of the media: 6.8 and 7.4 were used. The drugs screening and the NFs cytotoxicity potential was determined by using MTT colorimetric assay. Firstly, TMZ and iNek1 solutions diluted in DMSO were tested during 48 h aiming to select the IC_{50} for using in the following experiments. After this screening, cells were treated with several NFs formulations at the IC_{50} previously determined and with the neat drugs during 2, 5 and 5+2 recovery days. After treatment, cells were incubated with MTT for 3 hours at 37°C. Then, to dissolve the formazan crystals, DMSO was added to each well. The absorbance was recorded at 540 nm in a microplate reader (BioTek Synergy HT, Swindon, UK), and percentage of residual cell viability was determined. The cell viability was calculated using the control cells as 100%.

2.13 Statistical analysis

The results were expressed as the mean value ± standard deviation (SD). Statistical analysis was perfomed using one-way analysis of variance (ANOVA) following by Tukey post-test when * or two-way ANOVA following by Bonferroni post-test when # using GraphPad Prism 5 software (La Jolla, CA, USA). Statistically significant results were considered when the P-value < 0.05.

3. RESULTS AND DISCUSSION

3.1 Nanocarriers Preparation and Characterization

In this study, we have incorporated TMZ in nanostructured lipid NPs by using the emulsion method. TMZ is poorly soluble in water, has stunted half-life in blood circulation along with side effects (Stupp et al, 2005; Corsa et al, 2006; Mutter & Stupp, 2006; Vera et al, 2004). Considering these characteristics of TMZ, the current study was designed for the controlled release of TMZ for *in loco* delivery. Morphology and particle size and its distribution play preliminary role in the evaluation of NP formulations (Zeng et al, 2016). NP size has a significant effect on the release of the drug. In our experiments, TMZ NPs presented mean size of 519.5 ± 52 nm and circular shape analyzed by SEM (figure 1). Additionally, the NP surface charge determines its interaction with biological environments and its interaction with biologically active compounds (Giri et al, 2014). In general, optimum colloidal stability, where there is no particle aggregation, is greater when zeta potential is more positive or negative, around ± 45 mV (Krai et al, 2017). Zeta potential of TMZ NP was found to be -31.6 ± 0.7 mV. Therefore, we anticipated a high stability and efficacy in the produced nanocarriers.

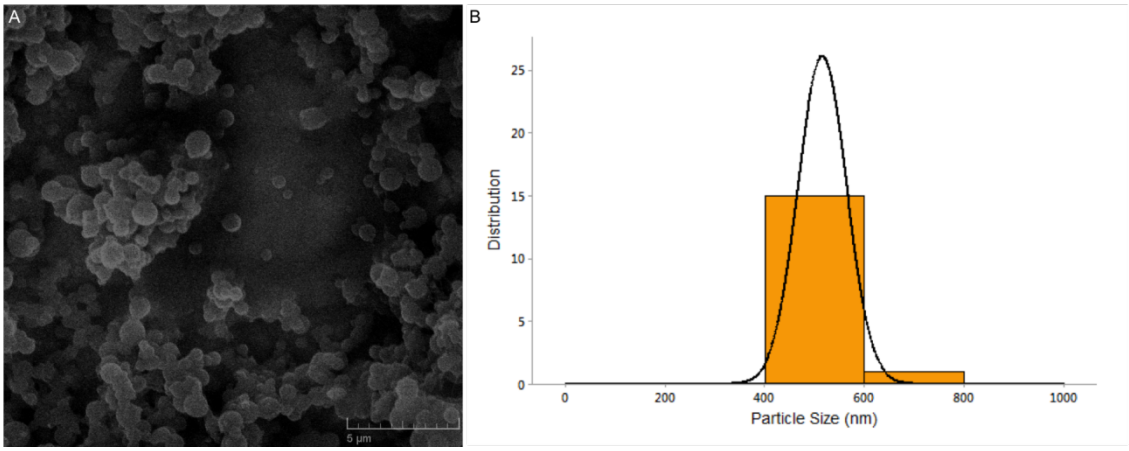

Figure 1: TMZ NP characterization (A) SEM of TMZ NP. (B) NP size distribution. The experiment was repeat 9 times.

It is known the Nek1 plays an important role in DNA damage signaling and that the inhibition of this protein increases apoptosis in glioma cells during TMZ treatment (Lio et al, 2013; Spies et al, 2016; Zhu et al, 2016). Therefore, we hypothesis that if we inhibit Nek1 and then treat the tumor with TMZ with a slow and controlled release DDS the treatment efficacy would improve. Given that, we produced PVA and Nek1 inhibitor (iNek1) hydrogel solutions with TMZ NP, then NF were developed by using electrospinning (figure 2).

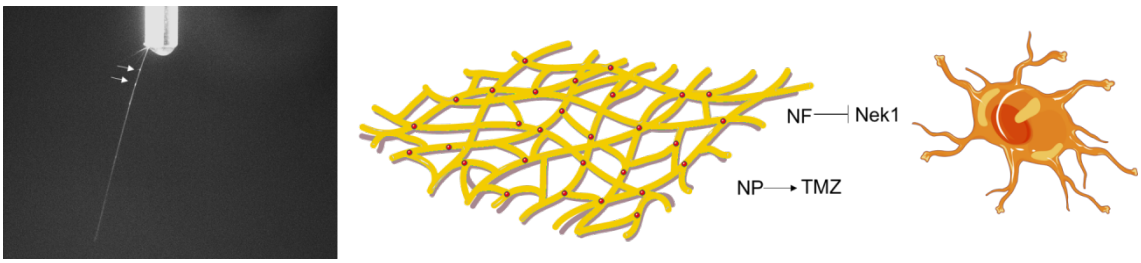

Figure 2: Electrospun of NF with NP. White arrows show the NP inside of the NF during electrospinning producing NF with iNek1 and TMZ NP aiming to first inhibit Nek1 and then release TMZ from the NP.

The NF were characterized according their morphology and size using SEM (figure 3). NF made with TMZ and iNek1 mixture presented distribution size of 2900 ± 1142 nm (figures 3A and E), while iNek1 NF with TMZ NP showed distribution size of 2723 ± 684 nm (figures 3B and F). Figure 3C shows NF after 2 h of swelling in PBS where the NF increased size 2-fold showing no significant water uptake which would

be related to increased size during the application *in situ*. Figure 3D shows curcumin NF with NP inside which could be used in future localized cell uptake *in vivo* studies.

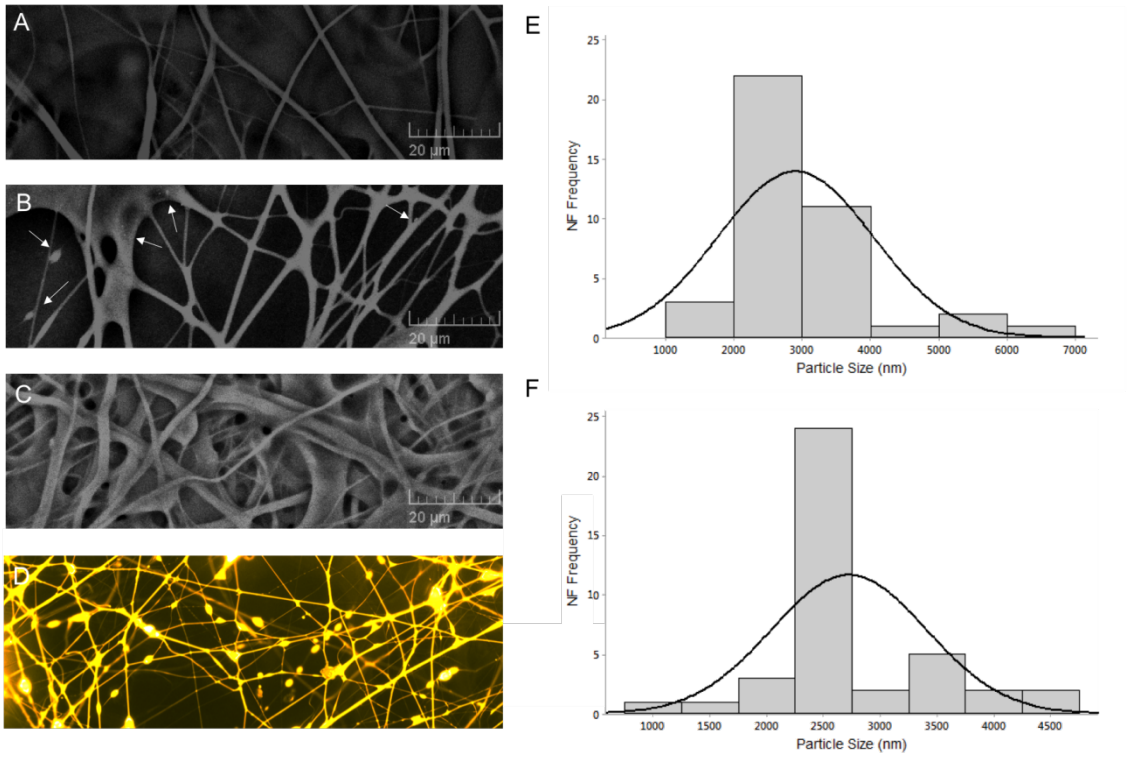

Figure 3: NF morphology and distribution. (A) iNek1 + TMZ NF (B) iNek1 NF with TMZ NP (C) NF after swelling test (D) NF with curcumin (E) iNek1 + TMZ NF size distribution (F) iNek1 NF with TMZ NP size distribution.

The stability of the drugs after nanoencapsulation was examined by using NMR studies. Figure 4A and B shows the results of both ^{1}H and ^{13}C NMR analysis of NP samples. In the ^{1}H study it was observed that peaks of TMZ in the 1.9 ppm position is presented in the TMZ NP without shift position (figure 4A). In the ^{13}C analysis (figure 4B), stearic acid blank NP presented peaks in 14.7 ppm (C11), 32.5 ppm (C3) and 182.1 ppm (C1) the other carbon peaks were not obtained. TMZ NP presented these three peaks of stearic acid and peaks related to TMZ: 36.8, 128.1, 137.1, 140.3 and 164.9 ppm (Laszcz et al., 2013). Figure 4C presents ^{13}C NMR of the produced nanoproducts. PVA presents four fingerprints peaks: a peak associated to CH_2 (around 45 ppm) and three CH peaks (between 60 and 80 ppm); it is possible to observe these peaks in all NF samples. No significant peaks related to the drugs are visible given that the concentrations are very low however, the TMZ NP + iNek1 NF sample presents the peaks related to stearic acid. In the ^{1}H NMR

analysis (figure 4D) it is possible to observe disperse peaks of TMZ NP and pure TMZ around 1.9 to 8 ppm and two peaks around 2.5 and 3.4 ppm related to iNek1. When closed analyzed, the NF with drugs present a disperse peak of TMZ and a peak around 3.4 ppm of iNek1. No shifting peaks were observed, therefore these results suggested the stability of the drugs into the formulations and because of that, TMZ and iNek1 bioactivities are probably preserved after encapsulation into NF and NP (Vashisth et al., 2015).

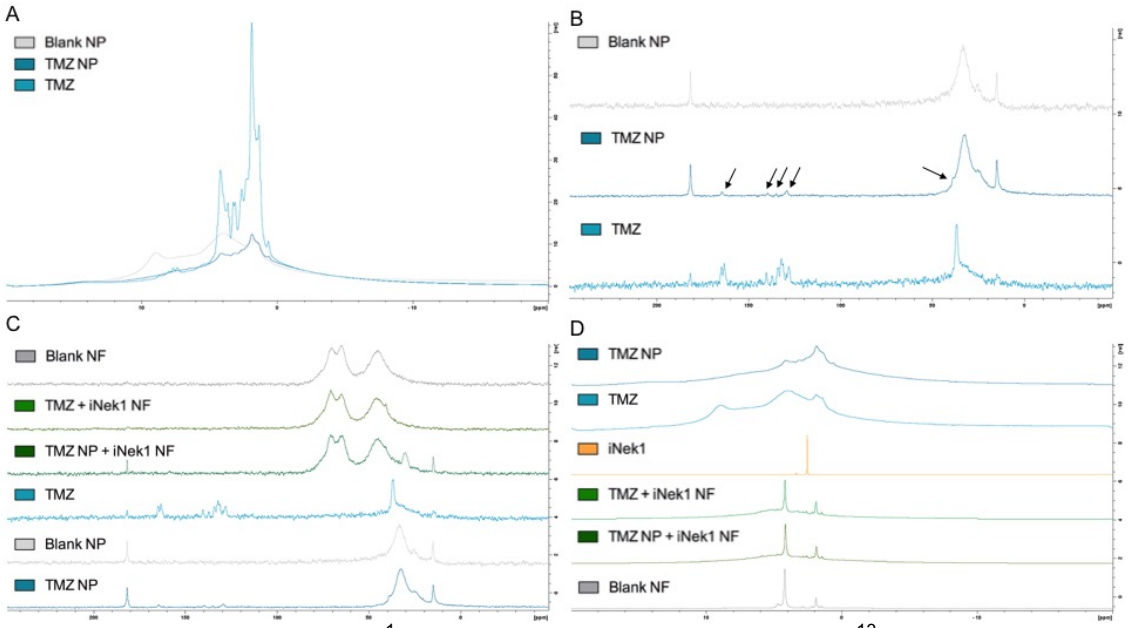

Figure 4: NMR evaluation. (A) ^{1}H NMR of NP samples and TMZ (B) ^{13}C NMR of NP samples and TMZ (C) ^{13}C NMR of nanoproducts and drugs (D) ^{1}H NMR of nanoproducts and drugs.

Subsequently, we decided to investigate the rheological properties of the samples. The experiment was used to analyze the viscosity of NF as a function of shear rate and the oscillatory tests therefore it was possible to determine if the viscoelasticity was depended of frequency. Figure 5A shows flow curves at 37°C of blank NF, TMZ + iNek1 NF and TMZ NP + iNek1 NF. The blank NFs and TMZ NP + iNek1 NF demonstrated similar profile of viscosities with the apparent viscosity increasing with increasing shear rates however, TMZ + iNek1 NF presented decreasing viscosity with increasing shear rates. The viscoelastic properties elastic (G') and viscous (G'') moduli at 37°C, recorded from 10 to 40 Hz, are observed in figure 5B. The NF present similar frequency-dependent G' and G'' values. The TMZ+iNek1 NF showed

the highest values of G' and G'', with the curves exhibiting a cross-over point around 20 Hz, after this frequency the viscoelastic was mainly elastic.

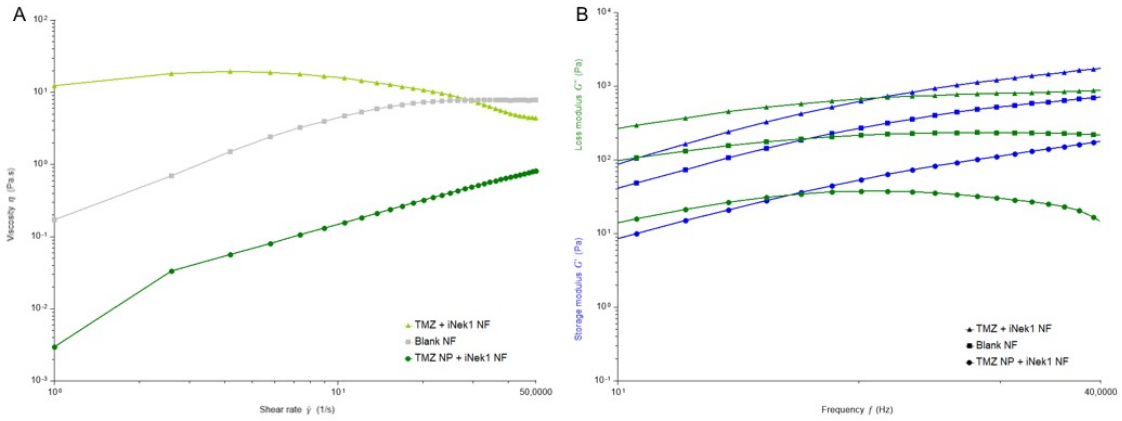

Figure 5: Mechanical properties. (A) Flow curves of NFs (B) Frequency dependence of elastic (G') and viscous (G'') moduli of NFs.

To investigate the total percentage amount of encapsulated drugs into the nanoproducts, the samples were totally dissolved in DMSO and the EE% was measured by using absorbance values. The EE% of TMZ into the NP was 79.8 ± 6.8 and the EE% of iNek1 into the NFs was 79.2 ± 7.3. The NFs with dissolved TMZ presented an EE% of 75.2 ± 5.9. These results suggested that the methodologies used to produce the nanoproducts are efficient because each EE% were found to be higher than 50%.

Given that GB presents an acidic extracellular pH around 6.8 (Honasoge & Sontheimer, 2013), we decided to investigate if the drugs using two different pH: 6.8 and 7.4. GB cells usually change them metabolic route from oxidative phosphorylation to glycolysis and when it happens the cells release lactate and H+, moreover the acid pH is being related to tumor progression and resistance (Honasoge & Sontheimer, 2013; Estrella et al., 2013).

The resulting drug release from the nanoproducts provided a continuous release profile of TMZ and iNek1 over 8 days (figure 6). TMZ and iNek1 presented 50% of released after 1 day in the TMZ + iNek1 NFs in both pH: 6.8 (figure 6A) and 7.4 (figure 6C) however, the TMZ NP + iNek1 NF samples presented 50% of TMZ released after 3 days in pH 6.8 (figure 6B) and 6 days in pH 7.4 (figure 6D). This observation shows the interesting approach of NP inside of NF to slow the release

of TMZ. Additionally, we tested the TMZ release from NPs and it was not observed a significant difference (figure 6E). Although PVA is considered a neutral polymer, previous results (data not published) from our research group found PVA to increase its swelling and release properties in physiological pH when compared to acid pH. Similar results were found by Mansur et al., 2008.

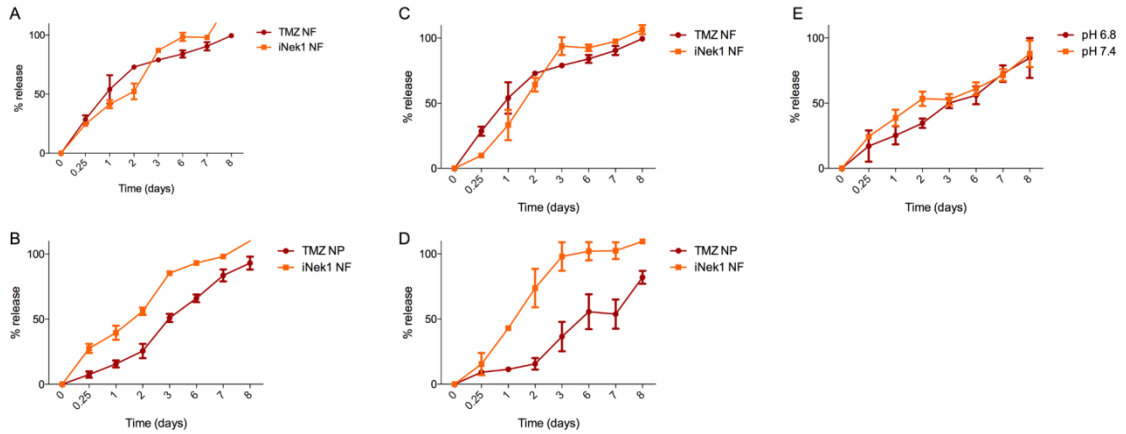

Figure 6: Drug release studies during 8 days. (A-B) pH 6.8 buffer and (C-D) pH 7.4 buffer. (A) TMZ + iNek1 NF (B) TMZ NP + iNek1 NF (C) TMZ + iNek1 NF (D) TMZ NP + iNek1 NF (E) TMZ nanocarries in different pHs.

3.2 Nanofiber Sterility Analysis

Prior to cell testing, it is necessary to ensure complete sample sterility. In order to evaluate if the sterilization process used in nanoproducts was effective, NF were contaminated with bacteria and IPA was used for decontamination. There was no observable growth in any of the plates of the sterilization groups. These results suggest that IPA sterilization process was suitable in removing bacterial contaminants (figure 7).

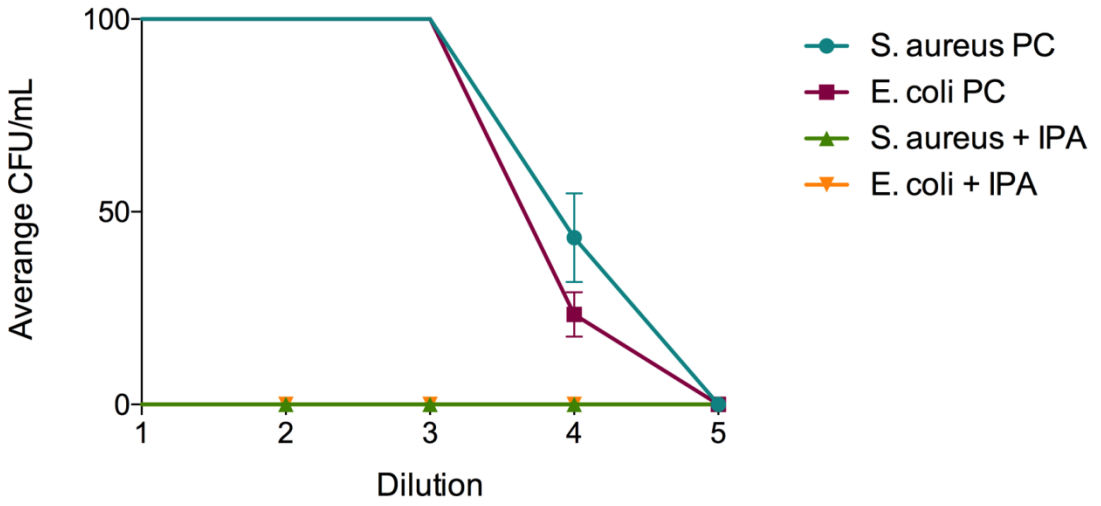

Figure 7: Serial dilutions of NF suspension contaminated with bacteria after and without (positive control – PC) sterilization by using IPA.

3.3 Efficacy in glioblastoma therapy

Aiming to verify if Nek1 responds to TMZ treatment we analyze the expression of Nek1 in GB cells (figure 8). Cells were treated with TMZ and co-incubate with vinculin and Nek1 antibodies and the localization of Nek1 was observed. Results showed a significant increase of Nek1 expression in nucleus (figures 8A B and E) meaning that Nek1 translocated to nucleus after TMZ treatment probably because its role in the DNA damage repair (DDR) signaling (Lio et al, 2013). During DNA damage repair caused by TMZ there is a formation of double-strand break (DSB) in the DNA and when a DSB establishes in DNA the histone 2AX flaks the damage site and it is phosphorylated. Owing to γH2AX foci usually increases after DSB formation (Nakamura et al., 2006), its expression was also verified after TMZ treatment the intensity of fluorescence of γH2AX and Nek1 increased (figures 8C, D and F). Nek1 expression was also analyzed by using western blot and the results showed an increased expression although not significant.

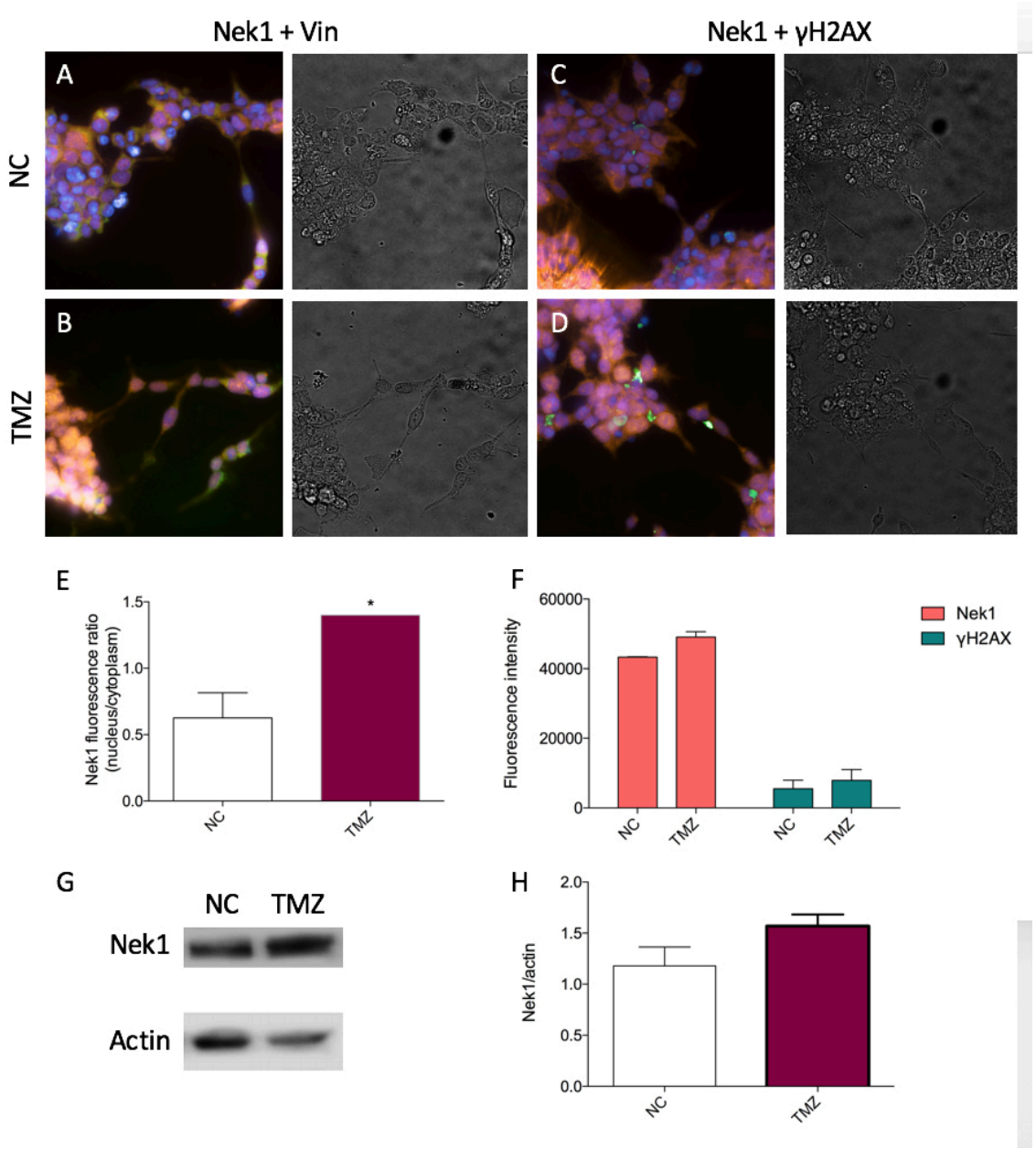

Figure 8: Nek1 and γH2AX expression analysis in GB cells (A-D) Immunofluorescence evaluation of Nek1 and Vinculin where the first image is a merge and the second is the bright field (A) without treatment and with (B) TMZ treatment. Immunofluorescence evaluation of Nek1 and γH2AX (A) without treatment and with (B) TMZ treatment. (E) Nek1 fluorescence intensity quantification in the nucleus divide by the fluorescence in the cytoplasm (F) Nek1 and γH2AX fluorescence intensity quantification (G) Nek1 expression by western blot analysis (H) Nek1 expression quantification normalized by actin expression. Results are expressed as mean in treated cells compared to negative control (NC) ± SD. Statistical analyses were performed using one-way ANOVA and Tukey post-test. Data was considered significant different when compared to NC at * < 0.05, ** < 0.01 and *** < 0.001.

In this work we used an ATP-mimetic inhibitor (Moraes et al., 2015) to inhibit Nek1 aiming to improve GB treatment *in vitro*. This compound was validated by reducing Nek1 kinase activity in almost 30% at a 50 μM concentration and its binding site was

identified by *in silico* docking at the ATP-binding site (Moraes et al., 2015). A screening of TMZ and iNek1 concentrations was perform to find the IC_{50} of these drugs. Figure 9A and B show a dose-response curve of both drugs, TMZ and iNek1, with IC_{50} of 76.3 and 54.4 μM, respectively.

The cytotoxic effect of nanoproducts was evaluated in U87 cells by using MTT assay in pH 6.8 media at three different treatment points: 2 days, 5 days and 5 days + 2 days of recover (change of media) and the drugs IC_{50} previously found. The results (figure 9D-F) visibly showed that the blank NF is not cytotoxic, since the percentage of cell viability was greater than 90% after all treatments. However, these NF may not facilitate cell grown and this can explain the cell dead in the controls. TMZ and iNek1 solutions were significant different after 2 days ($p>0.05$), 5 and 5 days + 2 days recover ($p>0.01$), TMZ NP, TMZ NF and iNek1 NF were statistically significant at all points ($p>0.05$ for 2 days treatment and $p>0.01$ for 5 and 5 days + recover). Moreover, TMZ + iNek1 NF and TMZ NP + iNek1 NF showed great efficacy at all treatment points ($p>0.0001$). When close analyzed, it was possible to observe that in comparison with TMZ + iNek1 co-treatment, TMZ NP + iNek1 NF were more effective against GB cells (figure 9C). Figures 9G-N showed cells images after 5 days + recover, and it's possible to notice that TMZ + iNek1 NF and TMZ NP + iNek1 NF great induce cell dead with almost no cells in the wells (figure 9M and N).

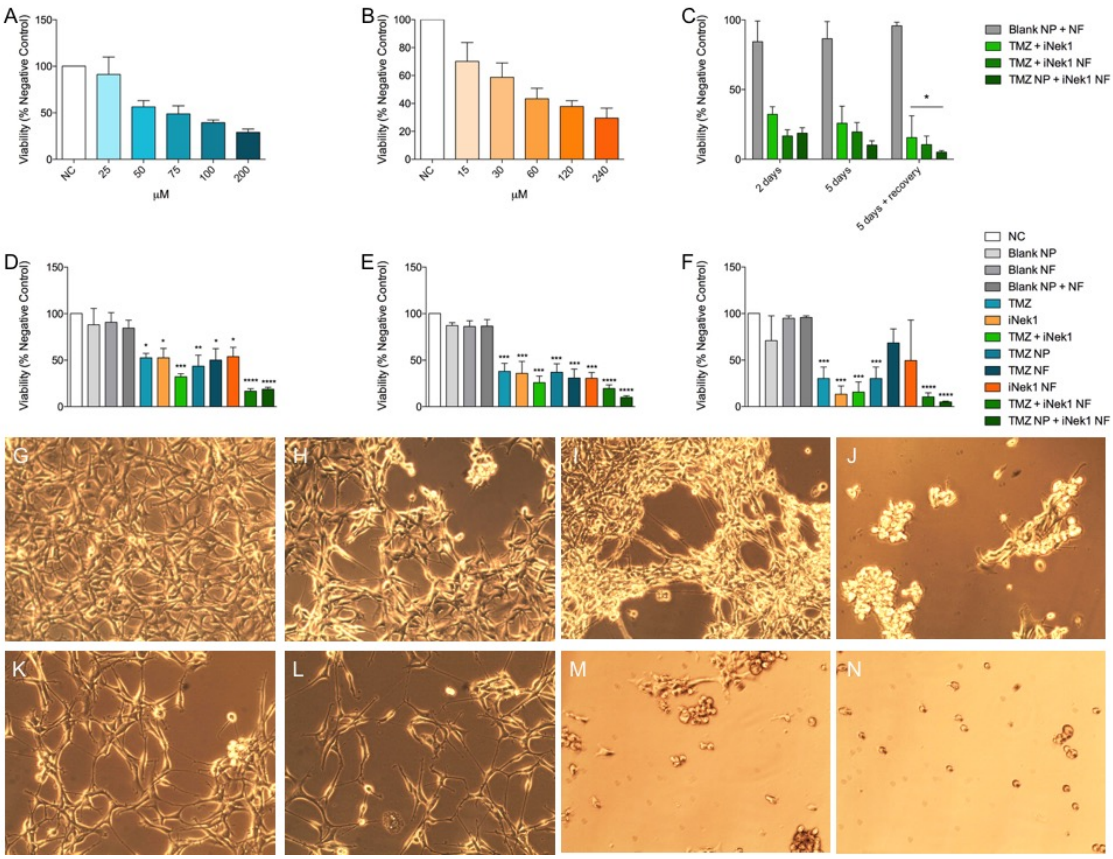

Figure 9: GB cell viability analysis (A) TMZ concentrations' screening (B) iNek1 concentrations' screening (C) Viability analysis of co-treatment of TMZ + iNek1 with and without the formulations (D) Viability analysis of all formulations after 2 days of exposure (E) 5 days of exposure (F) 5 days of exposure + 2 days of recover (G-N) Cells images after treatment (G) Negative control (H) Blank NF (I) Blank NP (J) TMZ NP (K) TMZ NF (L) iNek1 NF (M) TMZ and iNek1 NF (N) TMZ NP + iNek1 NF. Results are expressed as mean in treated cells compared to negative control (NC) ± SD. Statistical analyses were performed using one-way ANOVA and Tukey post-test when *. Data was considered significant different when compared to NC at * < 0.05, ** < 0.01, *** < 0.001 and **** < 0.0001.

It is interesting to observe that co-treatment of TMZ + iNek1 significantly decreased cell viability when compared to TMZ even without a formulation (figure 9). This result suggests the importance of Nek1 in GB response to therapy. Currently, it is known that Nek1 is required for activing DNA damage response pathway through ATR activation (Liu et al., 2013; Melo-Hanchuk et al., 2017), moreover Nek1 expression has an anti-apoptotic effect through phosphorylation and deactivation of the mitochondrial voltage dependent anion channel (VDAC1) (Chen et al., 2009; Chen et al., 2010; Chen et al., 2014). In addition, other DNA damage-related proteins, e.g. Rad54 and Mre11, are associated with Nek1 (Surpili et al., 2003; Liu et al., 2013; Spies et al., 2016). This implies the importance of inhibiting this protein during therapies that involves DNA damage. Recent studies revealed Nek1 as an important

oncotarget of GB cells and its knockdown significant decreased cell viability with co-treatment of TMZ (Zhu et al, 2016). Our results strongly suggest that Nek1 inhibition could improve therapy and, additionally, its role in GB malignancy should be further elucidated.

When a formulation was tested (TMZ + iNek1 NF and TMZ NP + iNek1 NF), cell viability decreased further after 5 days of treatment + 2 days after media replacement, showing that for a prolonged and sustained treatment it is important to use a DDS to control the release of a drug.

4. CONCLUSION

Given that GB presents high capacity of tumor recurrence, consequently, localized and controlled approaches of treatment provide an alternative to enhance chemotherapy efficacy and reduce systemic toxicity. In addition, GB resistance is related to oncotargets' expressions and their inhibition could improve tumor treatment. One of these oncotargets is Nek1, a kinase related to cell growth and TMZ-resistance. In this study, brain-implants prepared using TMZ NP and iNek1 polymeric NF were designed, produced, characterized and its *in vitro* effectiveness was evaluated. This approach revealed adequate mechanical properties and high drug loading concentration, which prolonged TMZ and iNek1 release and permitted sustained drug exposure of the GB cells improving TMZ and iNek1 antitumor effects. This system could be a promising approach for a novel *in situ* therapy. Our forthcoming study aims *in vivo* efficacy evaluation and further improvement of the nanoproduct production development.

Acknowledgments

This study was supported in parts by grants from the Athlone Institute of Technology research and development funding, GOI-IES (Government of Ireland International Education Scholarship), CAPES (Coordenação de Aperfeiçoamento de Pessoal de Nível Superior, Brazil) and FAPERGS (Fundação de Apoio a Pesquisa do Rio Grande do Sul, Grant n° 17/2551-0001388-3).

Conflict of Interest

The authors declare that there are no conflicts of interest.

Statement of authors' contributions to manuscript

L.S., A.M.M., J.G.H., M.C.H.B. and Z.C. conducted the experiments; L.S., M.N. and D.J.M. wrote the paper. All authors read and approved the final manuscript.

REFERENCES

Ahmed, F. et al. (2006) Biodegradable polymersomes loaded with both paclitaxel and doxorubicin permeate and shrink tumors, inducing apoptosis in proportion to accumulated drug. J. Control. Release 116, 150–8.

Akbar, U. et al. (2009) Delivery of temozolomide to the tumor bed via biodegradable gel matrices in a novel model of intracranial glioma with resection. J Neurooncol 94: 203.

Brodbelt, A. et al. (2015) Glioblastoma in England: 2007–2011. Eur. J. Cancer 51, 533-542.

Chen, Y. et al. (2009) Nek1 regulates cell death and mitochondrial membrane permeability through phosphorylation of VDAC1. Cell Cycle 8, 257–267.

Chen, Y. et al. (2010) Phosphorylation by Nek1 regulates opening and closing of voltage dependent anion channel 1. Biochem. Biophys. Res. Commun. 394, 798–803.

Chen, Y. et al. (2014) Increased Nek1 expression in renal cell carcinoma cells is associated with decreased sensitivity to DNA-damaging treatment. Oncotarget 5, 4283–4294.

Cheng, Y. et al. (2014) Multifunctional nanoparticles for brain tumor imaging and therapy. Adv. Drug Deliv. Rev. 66, 42–57.

Corsa, P. et al. (2006) Temozolomide and radiotherapy as first-line treatment of high-grade gliomas. Tumori 92:299–305.

Denny, B.J. et al. (1994) NMR and molecular modeling investigation of the mechanism of activation of the antitumor drug temozolomide and its interaction with DNA. Biochemistry 33:9045–9051.

Di Bei, J.M. & Bi-Botti, C.Y. (2009) Formulation of Dacarbazine-Loaded Cubosomes—Part I: Influence of Formulation Variables. AAPS PharmSciTech. 10(3):1032-9.

Estrella, V. et al. (2013) Acidity generated by the tumor microenvironment drives local invasion. Cancer Res 73, 1524–1535, doi:10.1158/0008-5472.CAN-12-2796.

Fan, C. et al. (2015) Drug-loaded bubbles with matched focused ultrasound excitation for concurrent blood–brain barrier opening and brain-tumor drug delivery. Acta Biomater. 15, 89–101.

Giri, K. et al. (2014) Understanding protein-nanoparticle interaction: a new gateway to disease therapeutics. Bioconjug. Chem. 25(6), 1078–1090.

Hafeez, A. & Kazmi, I. (2017) Dacarbazine nanoparticle topical delivery system for the treatment of melanoma. Sci. Reports. 7, 16517.

Han, D. et al. (2017) In-vitro evaluation of MPA-loaded electrospun coaxial fiber membranes for local treatment of glioblastoma tumor cells. J. Drug Deliv. Sci. Technol. 40, 45–50.

Hirschberg, H. (2013) Photo-activated cancer therapy: potential for treatment of brain tumors. In Optical Methods and Instrumentation in Brain Imaging and Therapy. pp. 253–271, Springer, New York, NY.

Hernán Pérez de la Ossa, D. et al. (2013) Local delivery of cannabinoid-loaded microparticles inhibits tumor growth in a murine xenograft model of glioblastoma multiforme. PLoS One8, e54795.

Honasoge, A. & Sontheimer, H. (2013) Involvement of tumor acidification in brain cancer pathophysiology. Front Physiol 4, 316, doi:10.3389/fphys.2013.00316.

Hua, M.Y. et al. (2011) The effectiveness of a magnetic nanoparticle-based delivery system for BCNU in the treatment of gliomas. Biomaterials 32, 516–27.

Huang, D. et al. (2016) A potential nanofiber membrane device for filling surgical residual cavity to prevent glioma recurrence and improve local neural tissue reconstruction. PLOS ONE 11, e0161435.

Irani, M. et al. (2017) The sustained delivery of temozolomide from electrospun PCL-Diol-b-PU/gold nanocomposite nanofibers to treat glioblastoma tumors. Mater. Sci. Eng. C 75, 165–174.

Játiva, P. & Cena, V. (2017) Use of nanoparticles for glioblastoma treatment: a new approach. Nanomedicine 12, 2533–2554.

Kim, G.Y. et al. (2007) Resorbable polymer microchips releasing BCNU inhibit tumor growth in the rat 9L flank model. J. Control. Release 123, 172–178.

Krai, J. et al. (2017) Doxazosin nanoencapsulation improves its in vitro antiproliferative and anticlonogenic efects on breast cancer cells. Biomed. Pharmacother. 94, 10–20.

Kumar Naraharisetti, P. et al. (2007) *In vivo* performance of implantable biodegradable preparations delivering Paclitaxel and Etanidazole for the treatment of glioma. Biomaterials. 28, 886–94.

Kuramitsu, S. et al. (2015) Double-edged sword in the placement of Carmustine (BCNU) wafers along the eloquent area: a case report. NMC Case Rep. J. 2, 40–45.

Laszca, M. et al. (2013) Identification and Physicochemical Characteristics of Temozolomide Process-Related Impurities. Molecules. 18, 15344-15356.

Lio, S. et al. (2013) Nek1 kinase associates with ATR–ATRIP and primes ATR for efficient DNA damage signaling. PNAS. 110, 2175-2180.

Liu, S. et al. (2013) Nek1 kinase associates with ATR-ATRIP and primes ATR for efficient DNA damage signaling. Proc. Natl. Acad. Sci. USA 110, 2175–2180.

Mangraviti, A. et al. (2016) Nanobiotechnology-based delivery strategies: new frontiers in brain tumor targeted therapies. J. Control. Release 240, 443–453.

Mansur, H.S. et al. (2008) FTIR spectroscopy characterization of poly(vinyl alcohol) hydrogel with different hydrolysis degree and chemically crosslinked with formaldehyde. Mater. Sci. Eng. C. 28, 539-548.

Melo-Hanchuk, T.D. et al. (2017) NEK1 kinase domain structure and its dynamic protein interactome after exposure to Cisplatin. Sci. Reports. 7, 5445.

Moras, E.C. et al. (2015) Kinase Inhibitor Profile for Human Nek1, Nek6, and Nek7 and Analysis of the Structural Basis for Inhibitor Specificity. Molecules. 20, 1176-1191.

Mutter, N. & Stupp, R. (2006) Temozolomide: a milestone in neuro-oncology and beyond? Expert Rev. Anticancer Ther. 6:1187–1204.

Nakamura, A. et al. (2006) Techniques for γ-H2AX Detection. Methods in Enzymology 409, 236-250.

Norouzi, M. et al. (2016) Injectable hydrogel-based drug delivery systems for local cancer therapy. Drug Discov. Today 21, 1835–1849.

Park, J. et al. (2017) Evaluation of permeability, doxorubicin delivery, and drug retention in a rat brain tumor model after ultrasound-induced blood-tumor barrier disruption. J. Control. Release 250, 77–85.

Patil, M. et al. (2013) Nek1 interacts with Ku80 to assist chromatin loading of replication factors and S-phase progression. Cell Cycle 12, 2608-2616.

Pourgholi, F. et al. (2016) Nanoparticles: Novel vehicles in treatment of Glioblastoma. Biomedic&Pharmacot. 77, 98-107.

Ramachandran, R. et al. (2014) A Polymer-Protein Core–Shell Nanomedicine for Inhibiting Cancer Migration Followed by Photo-Triggered Killing. J. Biomed. Nanotechnol. 10, 1401–1415.

Ramachandran, R. et al. (2017). Theranostic 3-Dimensional nano brain-implant for prolonged and localized treatment of recurrent glioma. Scientific reports, *7*, 43271. doi:10.1038/srep43271.

Rape, A. et al. (2014) Engineering strategies to mimic the glioblastoma microenvironment. Adv. Drug Deliv. Rev. 79, 172–183.

Ranganath, S.H. & Wang, C. (2008) Biodegradable microfiber implants delivering paclitaxel for post-surgical chemotherapy against malignant glioma. Biomaterials 29, 2996–3003.

Sawyer, A.J. et al. (2006) New methods for direct delivery of chemotherapy for treating brain tumors. Yale J. Biol. Med. 79, 141–152.

Scott, A.W. et al. (2011) Intracranial microcapsule drug delivery device for the treatment of an experimental gliosarcoma model. Biomaterials 32, 2532–9.

Spies, J. et al. (2016) Nek1 Regulates Rad54 to Orchestrate Homologous Recombination and Replication Fork Stability. Molecular Cell. v. 62, n. 6, p. 903-917.

Stupp, R. et al. (2005) Radiotherapy plus concomitant and adjuvant temozolomide for glioblastoma. N Engl J Med 352:987–996.

Sun, C. et al. (2017) Noninvasive nanoparticle strategies for brain tumor targeting. Nanomedicine 13, 2605–2621.

Surpili, M. J. et al. (2003) Identification of proteins that interact with the central coiled-coil region of the human protein kinase NEK1. Biochemistry 42, 15369–15376.

Tseng, Y. et al. (2013) Sustainable release of carmustine from biodegradable poly[(d,L)-lactide-co-glycolide] nanofibrous membranes in the cerebral cavity: in vitro and in vivo studies. Expert Opin. Drug Deliv. 10, 879–888.

Tseng, Y. et al. (2015) Concurrent delivery of carmustine, irinotecan, and cisplatin to the cerebral cavity using biodegradable nanofibers: in vitro and in vivo studies. Colloids Surf. B: Biointerfaces 134, 254–261.

Tseng, Y.Y. et al. (2016) Advanced interstitial chemotherapy combined with targeted treatment of malignant glioma in rats by using drug-loaded nanofibrous membranes. Oncotarget 7, 59902–59916.

Vashisth, P. et al. (2015) Biomedical applications of ferulic acid encapsulated electrospun nanofibers. Biotechnology Reports, 8, 36-44.

Vera, K. et al. (2004) Dose-dense regimen of temozolomide given every other week in patients with primary central nervous system tumors. Ann Oncol 15, 161–171.

Weller, M. et al. (2013) Standards of care for treatment of recurrent glioblastoma--are we there yet? Neuro-oncology. 15, 4–27.

Westphal, M. & Lamszus, K. (2011) The neurobiology of gliomas: from cell biology to the development of therapeutic approaches. Nat Rev. Neurosci. 12, 495-508.

White, M.C. & Quarmby, L.M. (2009) The NIMA-family kinase, Nek1 affects the stability of centrosomes and ciliogenesis. BMC Cell Biol 9, 29.

Wei, X. et al. (2014) Brain tumor-targeted drug delivery strategies. Acta Pharm. Sin. B 4, 193–201.

Zeng, Z. et al. (2016) Graphene Oxide Quantum Dots Covalently Functionalized PVDF Membrane with Significantly-Enhanced Bactericidal and Antibiofouling Performances. Sci. Rep. 6, 20142.

Zhu, J. et al. (2016) Frequent Nek1 overexpression in human gliomas. Biochem Biophys Res Comm 476, 522-527.

CONSIDERAÇÕES FINAIS

O GB é uma doença extremamente agressiva, no entanto, a atual terapia para tratar GBs não sugere resultados eficientes e a cura é uma realidade distante. O uso da nanotecnologia pode ser visto como uma abordagem promissora para a terapia GB; no entanto, existem várias respostas desconhecidas que precisam ser mais investigadas. Pesquisadores ainda não conhecem todos os possíveis efeitos quando utilizam abordagens DDS, como parâmetros de toxicidade e eficácia. Hoje em dia, cânceres como o GB, que são particularmente malignos e muito resistentes à QT, podem ser tratados com nanocarreadores que melhoram a eficácia. Atualmente, existem diversos vetores que estão sendo investigados, no entanto, apenas algumas formulações que usam essa abordagem inovadora estão comercialmente disponíveis. Mesmo assim, os nanocarreadores são uma estratégia promissora para a entrega efetiva de medicamentos com liberação estável nos locais do tumor por um período sustentado.

O presente estudo visou desenvolver e caracterizar nanoprodutos de PVA produzidos pela técnica de eletrofiação para o tratamento de GBs. As NP produzidas contendo DTIC apresentaram boa encapsulação do fármaco, aumento da solubilidade do sistema e liberação controlada e prolongada acarretando o aumento da eficácia da droga uma vez que células tratadas com estas NP apresentaram menor viabilidade.

Tendo em vista que o GB pode recorrer e invadir áreas funcionais do cérebro, a segunda ressecção cirúrgica é arriscada. Estudos de autópsia sugerem que os GB recorrentes são principalmente locais e aparecem dentro de 2 centímetros do local inicial do tumor. Portanto, QT localizada e controlada diretamente no local do tumor fornece um DDS alternativo para o tratamento do GB. Com o objetivo de superar as limitações da BHE, uma das abordagens mais promissoras é o uso de DDS para tratar as células cancerígenas *in loco*. Para melhorar a eficácia do tratamento com DTIC e TMZ, implantes cerebrais foram produzidos visando a durante a cirurgia. Esta abordagem pode reduzir significativamente os efeitos colaterais sistêmicos e pode prevenir a recorrência do tumor. Neste estudo, NF foram preparadas, caracterizadas e sua eficácia anticancerígena foi determinada. Estes sistemas

demonstraram uma elevada percentagem de encapsulação, estabilidade prolongada e propriedades mecânicas e perfil de libertação contínua dos fármacos com maior liberação do fármaco no pH do tumor. Isto sugere que o desempenho das NF é apropriado para o manejo do GB e é uma abordagem promissora para alcançar uma entrega controlada do medicamento para a terapia GB. Além disso, as NF mostraram um aumento da absorção celular. Ainda, tendo em vista a liberação controlada, os efeitos antitumorais dos fármacos aumentaram significativamente tanto para a NF com DTIC quanto para a NF com TMZ e iNek1.

Visando analisar a atividade de DTIC, este estudo avaliou a formação de γH2AX. Os resultados de microscopia confocal demonstraram significativamente mais *foci* de γH2AX em células tratadas com DTIC NF em comparação com o controle negativo e DTIC em solução após 1 e 5 dias de tratamento. Este dano foi acompanhado por um aumento da apoptose. Células tratadas com DTIC NF apresentaram maior percentual de apoptose e apoptose tardia quando comparadas ao DTIC. Assim, os dados do dano ao DNA e da morte celular indicam que a NF facilitou a absorção do fármaco e aumentou o acúmulo de DTIC nas células do GB, melhorando seus efeitos genotóxicos e citotóxicos. Ainda, as NF com co-tratamento de TMZ e iNek1 diminuíram consideravelmente a viabilidade celular. Portanto, os implantes cerebrais produzidos são um sistema promissor para administração de medicamentos na terapia de GB.

Embora muitos estudos como este tenham estabelecido bons resultados, investigações adicionais são essenciais para desenvolver DDS bem-sucedidos. A este respeito, desenvolver nanocarreadores com superfícies biofuncionalizadas e alvos moleculares se faz necessário para melhorar a entrega *in vivo*. Além disso, desenvolver nanocarreadores funcionalizados pode fornecer múltiplos alvos e superar os problemas de BHE.

Outros aspectos importantes que precisam ser melhor compreendidos durante a fabricação do DDS são:

(a) o microambiente do GB, pois é importante elucidar as implicações moleculares que podem afetar o carreador;

(b) as respostas do sistema imunológico.

Devem ser realizados ensaios clínicos para analisar as características farmacológicas das formulações e a biodistribuição. Somente com esses tipos de avaliações é possível obter terapias otimizadas. Em geral, também é essencial desenvolver métodos inteligentes que possam avaliar os resultados da formulação do DDS. Isso é extremamente necessário para entender as interações celulares após a captação do transportador e as mudanças no microambiente tumoral.

Além disso, análises de dinâmica molecular, *docking* computacional e modelagem molecular podem ser estratégias úteis para avaliar o comportamento das células e suas alterações moleculares após o tratamento com carreadores, uma vez que essas abordagens podem predizer as alterações dinâmicas durante a terapia do câncer. Finalmente, abordagens baseadas na nanotecnologia podem ser usadas para melhorar e direcionar a entrega de drogas conhecidas e novas para o manejo de várias doenças humanas. Pode-se concluir que os dias são prósperos para estratégias baseadas em nanotecnologia.

PERSPECTIVAS

Avaliação da inibição *in vitro* de Nek1 em células U87MG frente ao tratamento com o inibidor.

Determinação da resposta imune (pela medida de citosinas pró e anti-inflamatórias) frente ao tratamento com as formulações.

Investigação do potencial terapêutico dos nanoprodutos *in vivo* utilizando ratos *Wistar* com implantes tumorais. O projeto *in vivo* foi aprovado pelo CEUA-UFCSPA (protocolo n° 236/18).

Desenvolvimento de nanoprodutos biofuncionalizados com marcadores de superfície, como por exemplo marcados de células-tronco tumorais: CD133, CD44 e CD15.

REFERÊNCIAS BIBLIOGRÁFICAS

Aftab, S. *et al.* (2018) Nanomedicine: An effective tool in cancer therapy, Int J Pharm. 540, pp. 132–149. doi: 10.1016/j.ijpharm.2018.02.007.

Agarwal, A. *et al.* (2011) Remote triggered release of doxorubicin in tumors by synergistic application of thermosensitive liposomes and gold nanorods, ACS Nano 5, pp. 4919–4926.

Alifieris, C. & Trafalis, D.T. (2015) Glioblastoma multiforme: Pathogenesis and treatment, Pharmacol Ther. 152, pp. 63-82. doi: 10.1016/j.pharmthera.2015.05.005.

Allen, T.M. & Cullis, P.R. (2004) Drug delivery systems: entering the mainstream. Science 303, pp. 1818–1822.

American Association of Neurosciences Nurses (2014) Care of the adult patient with a brain tumor. Disponível em: https://www.abta.org/healthcare-professionals/clinical-practice-guidelines/. Acesso em: 27 de março de 2019.

Aminabhavi, T.M. & Deshmukh, A.S. (2016) Polysaccharide-based hydrogels as biomaterials, In: Polymeric Hydrogels as Smart Biomaterials. Springer, pp. 45–71.

Aminabhavi, T., Dharupaneedi, S. & More, u. (2017) The role of nanotechnology and chitosan-based biomaterials for tissue engineering and therapeutic delivery. Chitosan Based Biomater. Tissue Eng Therap. 2, pp. 1–29.

Baghirov, H. *et al.* (2017) ultrasound-mediated delivery and distribution of polymeric nanoparticles in the normal brain parenchyma and melanoma metastases, Cancer Research, 77, pp. 1–18. doi: 10.1158/1538-7445.AM2017-3109.

Bagó, J.R. *et al.* (2016) Electrospun nanofibrous scaffolds increase the efficacy of stem cell-mediated therapy of surgically resected glioblastoma. Biomaterials 90, 116–125.

Barani, I.J. & Larson, D.A. (2015) Radiation therapy of glioblastoma, Cancer Treat and Research. 163, pp. 49-73. doi: 10.1007/978-3-319-12048-5_4.

Baumann, F. *et al.* (2004) Combined thalidomide and temozolomide treatment in patients with glioblastoma multiforme, J Neurooncol. 67, pp. 191-200.

Baronzio, G., Gramaglia, A. & Fiorentini G. (2009) Current Role and Future Perspectives of Hyperthermia for Prostate Cancer Treatment, In Vivo. 23, pp. 143-146.

Bazak, R. *et al.* (2015) Cancer active targeting by nanoparticles: a comprehensive review of literature, J Cancer Res Clin Oncol. 141, pp. 769-784. doi: 10.1007/s00432-014-1767-3.

BC Cancer Agency Management Guidelines (2018) BC Cancer Protocol Summary for Concomitant (Dual Modality) and Adjuvant Temozolomide for Newly Diagnosed Malignant Gliomas with Radiation. Disponível em: <http://www.bccancer.bc.ca/health-professionals/clinical-resources/chemotherapy-protocols/neuro-oncology>. Acesso em: 27 de março de 2019.

Bischoff, P., Altmeyer, A. & Dumont, F. (2009) Radiosensitising agents for the radiotherapy of cancer: advances in traditional and hypoxia targeted radiosensitisers, Expert Opin Ther Pat. 19, pp. 643-662. doi: 10.1517/13543770902824172.

Brandes, A.A. *et al.* (2008) Glioblastoma in adults, Crit Rev Oncol Hematol. 67, pp. 139-152. doi: 10.1016/j.critrevonc.2008.02.005.

Bregy, A. *et al.* (2013) The role of Gliadel wafers in the treatment of high-grade gliomas. Expert Rev. Anticancer Ther. 13, pp. 1453–1461.

Brennan, C.W. *et al.* (2013) The somatic genomic landscape of glioblastoma, Cell. 10, pp. 462-477. doi: 10.1016/j.cell.2013.09.034.

Cabada, T.F. *et al.* (2012) Induction of cell death in a glioblastoma line by hyperthermic therapy based on gold nanorods, Int J Nanomed. 7, pp. 1511.

Campos B, Olsen LR, Urup T, Poulsen HS. (2016) A comprehensive profile of recurrent glioblastoma. Oncogene. 1-7.

Canillas M, *et al.* (2016) Bioactive Composites Fabricated by Freezing-Thawing Method for Bone Regeneration Applications. Polym Phys. 54, pp. 761-773.

Cao, Y. *et al.* (2017) Drug release from core-shell PVA/silk fibroin nanoparticles fabricated by one-step electrospraying. Sci. Rep. 7, 11913.

Cardoso, F.L. et al (2010) Looking at the blood-brain barrier: molecular anatomy and possible investigation approaches. Brain Res. Rev. 64, pp. 328-363.

Chai, Z. *et al.* (2017) A facile approach to functionalizing cell membrane-coated nanoparticles with neurotoxin-derived peptide for brain-targeted drug delivery, J Control Release. Elsevier, 264, pp. 102–111. doi: 10.1016/j.jconrel.2017.08.027.

Charnley, N. West, C. & Price, P. (2009) Assessment of Drug Resistance in Anticancer Therapy by Nuclear Imaging in Drug Resistance in Cancer Cells, Springer. pp. 295-313.

Chen, J., McKay, R.M. & Parada, L.F. (2012) Malignant glioma: lessons from genomics, mouse models, and stem cells, Cell. 30, pp. 36-47. doi: 10.1016/j.cell.2012.03.009.

Chen W, *et al.* (2015) Charge-conversional and reduction-sensitive poly(vinyl alcohol) nanogels for enhanced cell uptake and efficient intracellular doxorubicin release. J. Controlled Release. 205, pp. 15-24.

Chen, Y. *et al.* (2014) Increased Nek1 expression in Renal Cell Carcinoma cells is associated with decreased sensitivity to DNA-damaging treatment. Oncotarget. 5(12), pp. 4283-4294.

Cheng, Y. *et al.* (2011) Deep penetration of a PDT drug into tumors by noncovalent drug-gold nanoparticle conjugates, J Am Chem Soc. 133, pp. 2583–2591.

Ching, J. *et al.* (2015) A novel treatment strategy for glioblastoma multiforme and glioma associated seizures: increasing glutamate uptake with PPARγ agonists, J Clin Neurosci. 22, pp. 21-28. doi: 10.1016/j.jocn.2014.09.001.

Cho, K., *et al.* (2008) Therapeutic Nanoparticles for Drug Delivery in Cancer, 14, pp. 1310-1316. doi: 10.1158/1078-0432.CCR-07-1441.

Choi, B. D. *et al.* (2009) EGFRvIII-targeted vaccination therapy of malignant glioma. Brain Pathol, 19, pp. 713-23.

Cole, A.J. *et al.* (2011) Magnetic brain tumor targeting and biodistribution of long-circulating PEG-modified, cross-linked starchcoated iron oxide nanoparticles. Biomaterials 32, pp. 6291–6301.

Couvreur, P. *et al.* (2002) Nanocapsule technology: a review, Crit Rev Ther Drug Carrier Syst. 19, pp. 99-134.

Danhier, F. *et al.* (2012) PLGA-based nanoparticles: an overview of biomedical applications. J Control Release 161, pp. 505–522.

Davis, M. E. (2016) Glioblastoma: Overview of Disease and Treatment, Clin J Oncol Nurs. 20, pp. S2-S8. doi: 10.1188/16.CJON.S1.2-8.

De Lima GG, *et al.* (2015) A novel pH-sensitive ceramic-hydrogel for biomedical applications. Polym Advan Tech. 26, pp. 1439-46.

Di Bei JM & Bi-Botti CY. (2009) Formulation of Dacarbazine-Loaded Cubosomes—Part I: Influence of Formulation Variables. AAPS PharmSciTech. 10(3), pp. 1032-1039.

Dikpati, A. *et al.* (2012) Targeted drug delivery to CNS using nanoparticles. J of Adv Pharmaceut Sci. 2, pp. 179-191.

Dilnawaz F. *et al.* (2012) The transport of non-surfactant based paclitaxel loaded magnetic nanoparticles across the blood brain barrier in a rat model, Biomaterials. 33, pp. 2936-51. doi: 10.1016/j.biomaterials.2011.12.046.

Elsamadicy, A. A. (2017) Prospect of rindopepimut in the treatment of glioblastoma. Expert Opin Biol Ther, 17, pp. 507-513.

Fang, C. *et al.* (2016) Temozolomide Nanoparticles for Targeted Glioblastoma Therapy, HHS Public Access. 7(12), pp. 6674–6682. doi: 10.1021/am5092165.

Fazeny-Dorner B, *et al.* (2003) Survival with dacarbazine and fotemustine in newly diagnosed glioblastoma multiforme. British J of Cancer 88, pp. 496-501.

Felice, B. *et al.* (2015) Electrosprayed poly(vinyl alcohol) particles: preparation and evaluation of their drug release profile. Polym. Int. 64, pp. 1722-1732.

Ferlay, J. *et al.* (2015) Cancer incidence and mortality worldwide: sources, methods and major patterns in GLOBOCAN 2012, 136, pp. 359-386. doi: 10.1002/ijc.29210.

Frenot, A. & I. S. Chronakis. (2003) Polymer nanofibers assembled by electrospinning. Curr. Opin. Colloid., 8, pp. 64-75.

Ganguly, K. *et al.* (2014) Polysaccharide-based micro/nanohydrogels for delivering macromolecular therapeutics, J Control Release 193, pp. 162–173.

Geldenhuys, W. *et al.* (2011) Brain-targeted delivery of paclitaxel using glutathione-coated nanoparticles for brain cancers. J Drug Target. 19, pp. 837–845.

Gelperina, S. *et al.* (2010) European Journal of Pharmaceutics and Biopharmaceutics Drug delivery to the brain using surfactant-coated poly(lactide-co-glycolide) nanoparticles: Influence of the formulation parameters, Eur J of Pharm and Biopharm. Elsevier B.V., 74(2), pp. 157–163. doi: 10.1016/j.ejpb.2009.09.003.

Ghorani, B. & Tucker, N. (2015) Fundamentals of electrospinning as a novel delivery vehicle for bioactive compounds in food nanotechnology. 51, pp. 227-240.

Gilbert, M. R. *et al.* (2014) A randomized trial of bevacizumab for newly diagnosed glioblastoma. N Engl J Med, 370, pp. 699-708.

Gilchrist, R. *et al.* (1957) Selective inductive heating of lymph nodes, Ann Surg. 146, pp. 596.

Glaser, T. *et al.* (2017) Targeted nanotechnology in glioblastoma multiforme, Frontiers in Pharm, 8, pp. 1–14. doi: 10.3389/fphar.2017.00166.

Gong, W. *et al.* (2011) Improving efficiency of adriamycin crossing blood brain barrier by combination of thermosensitive liposomes and hyperthermia, Biol Pharm Bull. 34, pp. 1058-64.

Greineder, C.F. *et al.* (2016) Molecular engineering of high affinity single-chain antibody fragment for endothelial targeting of proteins and nanocarriers in rodents and humans. J Control Release 226, pp. 229–237.

Greiner, A. & J. H. Wendorff (2007) Electrospinning: A Fascinating Method for the Preparation of Ultrathin Fibers. Angewandte Chemie International Edition, 46, pp. 5670-5703.

Gu, G. *et al.* (2013) PEG-co-PCL nanoparticles modified with MMP-2/9 activatable low molecular weight protamine for enhanced targeted glioblastoma therapy. Biomaterials 34, pp. 196-208.

Gullotti, E & Yeo, Y. (2009) Extracellularly activated nanocarriers: a new paradigm of tumor targeted drug delivery, Mol Pharm. 6, pp. 1041-1051. doi: 10.1021/mp900090z.

Guo, G. *et al.* (2011) Preparation of curcumin loaded poly (e-caprolactone)–poly (ethylene glycol)–poly (e-caprolactone) nanofibers and their in vitro antitumor activity against Glioma 9L cells. Nanoscale 3, pp. 3825-3832.

Guo, J. *et al.* (2011) Aptamer-functionalized PEG–PLGA nanoparticles for enhanced anti-glioma drug delivery. Biomaterials 32, pp. 8010-8020.

Grupta, R. & Sharma, D. (2019) Evolution of Magnetic Hyperthermia for Glioblastoma Multiforme Therapy. ACS Chem Neurosci. 10, pp. 1157-1172.

Han, D. *et al.* (2017) In-vitro evaluation of MPA-loaded electrospun coaxial fiber membranes for local treatment of glioblastoma tumor cells. J. Drug Deliv. Sci. Technol. 40, pp. 45-50.

Haseloff, R.F. *et al.* (2015) Transmembrane proteins of the tight junctions at the blood-brain barrier: structural and functional aspects, Semin Cell Dev Biol. 38, pp. 16-25. doi: 10.1016/j.semcdb.2014.11.004.

He, H. *et al.* (2011) PEGylated Poly(amidoamine) dendrimer-based dual-targeting carrier for treating brain tumors, Biomaterials 32, pp. 478-487.

Hegi, M.E. *et al.* (2008) Correlation of O6-methylguanine methyltransferase (MGMT) promoter methylation with clinical outcomes in glioblastoma and clinical strategies to modulate MGMT activity, J Clin Oncol. 1, pp. 4189-4199. doi: 10.1200/JCO.2007.11.5964.

Hildebrandt, B. *et al.* (2002) The cellular and molecular basis of hyperthermia, Crit Rev Oncol Hematol. 43, pp. 33-56.

Hu, K. *et al.* (2011) Lactoferrin conjugated PEGPLGA nanoparticles for brain delivery: preparation, characterization and efficacy in Parkinson's disease. Int J Pharm. 415, pp. 273-283.

Hu, Q. *et al.* (2013a) Biomaterials peptide for anti-glioma drug delivery, Biomaterials. Elsevier Ltd, 34(4), pp. 1135-1145. doi: 10.1016/j.biomaterials.2012.10.048.

Hu, Q. *et al.* (2013b) F3 peptide-functionalized PEG-PLA nanoparticles co-administrated with tLyp-1 peptide for anti-glioma drug delivery. Biomaterials 34, pp. 1135-1145.

Hu, Q. *et al.* (2013c) Glioma therapy using tumor homing and penetrating peptide-functionalized PEG-PLA nanoparticles loaded with paclitaxel. Biomaterials 34, pp. 5640-5650. doi: 10.1016/j.biomaterials.2013.04.025.

Huang, D. *et al.* (2016) A potential nanofiber membrane device for filling surgical residual cavity to prevent glioma recurrence and improve local neural tissue reconstruction. PLOS ONE 11, e0161435.

Huang, Z. M., Y. Z. Zhang, M. Kotaky & R. S. (2003) A review on polymer nanofibers by electrospinning and their application in nanocomposites. Comps. Sci. Technol. 63, pp. 2223.

Instituto Nacional de Câncer José Alencar Gomes da Silva (2017) Estimativa 2018: Incidência de Câncer no Brasil. Rio de Janeiro. Disponível em: https://www.inca.gov.br/sites/ufu.sti.inca.local/files//media/document//estimativa-incidencia-de-cancer-no-brasil-2018.pdf. Acesso em: 27 de março de 2019.

Irani, M. *et al.* (2017) A novel biocompatible drug delivery system of chitosan/ temozolomide nanoparticles loaded PCL-PU nanofibers for sustained delivery of temozolomide. Int. J. Biol. Macromol. 97, pp. 744–751.

Irani, M. *et al.* (2018) Electrospun biocompatible poly (e-caprolactonediol) based polyurethane core/shell nanofibrous scaffold for controlled release of temozolomide. Int. J. Polym. Mater. Polym. Biomater. 67, pp. 361–366.

Irani, M. *et al.* (2017) The sustained delivery of temozolomide from electrospun PCL-Diol-b-PU/gold nanocomposite nanofibers to treat glioblastoma tumors. Mater. Sci. Eng. C. 75, pp. 165–174.

Jain, N.K., Mishra, V. & Mehra, N.K. (2013) Targeted drug delivery to macrophages, Expert Opin. Drug Deliv. 10, pp. 353–367.

Jiang, X. *et al.* (2014) Nanoparticles of 2-deoxy-D-glucose functionalized poly (ethylene glycol)-co-poly(trimethylene carbonate) for dual-targeted drug delivery in glioma treatment, Biomaterials. 35, pp. 518–529.

Jin, J. *et al.* (2011) In vivo specific delivery of c-Met siRNA to glioblastoma using cationic solid lipid nanoparticles. Bioconjug Chem. 21, pp. 2568-72. doi: 10.1021/bc200406n.

Joh, D.Y. *et al.* (2013) Selective targeting of brain tumors with gold nanoparticle-induced radiosensitization. PLoS One 8, e62425.

Jokerst, J.V. *et al.* (2011) Nanoparticle PEGylation for imaging and therapy. Nanomedicine. 6, pp. 715–728.

Kasai, T. *et al.* (2012) Chlorotoxin Fused to IgG-Fc Inhibits Glioblastoma Cell Motility via Receptor-Mediated Endocytosis. 975763. doi: 10.1155/2012/975763.

Kievit, F.M. *et al.* (2010) Chlorotoxin labeled magnetic nanovectors for targeted gene delivery to glioma, ACS Nano 4, pp. 4587–4594.

Kim, S.S. *et al.* (2014) A nanoparticle carrying the p53 gene targets tumors including cancer stem cells, sensitizes glioblastoma to chemotherapy and improves survival, ACS Nano. 8, pp. 5494-5514. doi: 10.1021/nn5014484.

Kim T. H. *et al.* (2011) Preparation of polylactide-co-glycolide nanoparticles incorporating celecoxib and their antitumor activity against brain tumor cells. Int J Nanomed. 6, pp. 2621-2631.

Kreuter, J*. et al.* (1995) Passage of peptides through the blood-brain barrier with colloidal polymer particles (nanoparticles), Brain Res. 674, pp. 171–174.

Kulkarni, P.V. *et al.* (2010) Quinoline-n-butylcyanoacrylate-based nanoparticles for brain targeting for the diagnosis of Alzheimer's disease. Wiley Interdiscip. Rev. Nanomed. Nanobiotechnol. 2, pp. 35–47.

Kumari, A., Yadav, S.K. & Yadav, S.C. (2010) Biodegradable polymeric nanoparticles based drug delivery systems, Colloids Surf B Biointerfaces. 1, pp. 1-18. doi: 10.1016/j.colsurfb.2009.09.001.

Lamprecht, A. *et al.* (2015) Nanomedicines in gastroenterology and hepatology. Nat. Rev. Gastroenterol. Hepatol. 12, pp. 195–204.

Lapointe, S. *et al* (2018) Primary brain tumours in adults. Lancet. 392, pp. 432-446.

Lee, C. Y. (2017) Strategies of temozolomide in future glioblastoma treatment, OncoTargets and Therapy. 10, pp. 265–270. doi: 10.2147/OTT.S120662.

Lee, J. S. (2004) Role of molecular weight of atactic poly(vinyl alcohol) (PVA) in the structure and properties of PVA nanofabric prepared by electrospinning. Journal of Applied Polymer Science. 93, pp. 1638-1646.

Lei, C. *et al.* (2013) Development of a gene/drug dual delivery system for brain tumor therapy: potent inhibition via RNA interference and synergistic effects. Biomaterials. 34, pp. 7483–7494.

Letchford K. & Burt H. (2007) A review of the formation and classification of amphiphilic block copolymer nanoparticulate structures: micelles, nanospheres, nanocapsules and polymersomes, Eur J Pharm Biopharm. 65, pp. 259-269. doi: 10.1016/j.ejpb.2006.11.009.

Lian, H. & Meng, Z. (2017) Melt electrospinning of daunorubicin hydrochlorideloaded poly (e-caprolactone) fibrous membrane for tumor therapy. Bioactive Mater. 2, pp. 96–100.

Lian, T. *et al.* (2016) Synthesis and characterization of curcumin-functionalized HP-β-CD modified goldmag nanoparticles as drug delivery agents. J Nanosci Nanotechnol. 16, pp. 6258–6264.

Lin, Y. *et al.* (2012) Delivery of large molecules via poly(butyl cyanoacrylate) nanoparticles into the injured rat brain. J Nanotechnol. 23, 165101.

Lio, S. *et al.* (2013) Nek1 kinase associates with ATR–ATRIP and primes ATR for efficient DNA damage signaling. PNAS. 110(6), pp. 2175-2180.

Liu, C. *et al.* (2017) A dual-mediated liposomal drug delivery system targeting the brain: Rational construction, integrity evaluation across the blood–brain barrier, and the transporting mechanism to glioma cells, International Journal of Nanomedicine, 12, pp. 2407–2425. doi: 10.2147/IJN.S131367.

Liu, Z., Yan, H. & Li, H. (2017) Silencing of DNA repair sensitizes pediatric brain tumor cells to γ-irradiation using gold nanoparticles, Environ Toxicol and Pharmacol. Elsevier, 53, pp. 40–45. doi: 10.1016/j.etap.2017.04.017.

Ma, J. *et al.* (2015) Nano-enabled drug delivery systems for brain cancer and Alzheimer's disease: research patterns and opportunities, nanomedicine: nanotechnology. Biol. Med. 11, pp. 1763–1771.

Man, H.B. *et al.* (2014) Synthesis of nanodiamond–daunorubicin conjugates to overcome multidrug chemoresistance in leukemia, nanomedicine: nanotechnology. Biol. Med. 10, pp. 359–369.

Masood, F. (2016) Polymeric nanoparticles for targeted drug delivery system for cancer therapy, Mat Sci and Engin C. Elsevier B.V. 60, pp. 569–578. doi: 10.1016/j.msec.2015.11.067.

Mead, B. P. *et al.* (2016) Targeted gene transfer to the brain via the delivery of brain-penetrating DNA nanoparticles with focused ultrasound. J of Control Release. Elsevier B.V., 223, pp. 109–117. doi: 10.1016/j.jconrel.2015.12.034.

Mehta, A.I. *et al.* (2015) Current status of intratumoral therapy for glioblastoma. J. Neurooncol. 125, pp. 1–7.

Melo-Hanchuk, T.D. *et al.* (2017) NEK1 kinase domain structure and its dynamic protein interactome after exposure to Cisplatin. Sci. Reports. 7, 5445.

Messaoudi, K., Clavreul, A. & Lagarce, F. (2015) Toward an effective strategy in glioblastoma treatment. Part I: resistance mechanisms and strategies to overcome

resistance of glioblastoma to temozolomide, Drug Discov Today. 20, pp. 899-905. doi: 10.1016/j.drudis.2015.02.011.

Misra, A. *et al.* (2003) Drug delivery to the central nervous system: a review, J Pharm Pharm Sci. 6, pp. 252-73.

Mornet, S. *et al.* (2004) Magnetic nanoparticle design for medical diagnosis and therapy, J. Mater Chem. 14, pp. 2161-2175. doi: 10.1039/B402025A.

Mundargi, R.C. *et al.* (2008) Nano/micro technologies for delivering macromolecular therapeutics using poly (D, L-lactide-co-glycolide) and its derivatives, J Control Release. 125, pp. 193–209.

National Comprehensive Cancer Network (2015) Clinical Practice Guidelines in Oncology: Central nervous system cancers. 1. Disponível em: https://www.nccn.org/professionals/physician_gls/pdf/cns.pdf. Acesso em: 27 de março de 2019.

Nel, A. *et al.* (2006) Toxic potential of materials at the nanolevel, Science 311, pp. 622–627.

Ni, S. *et al.* (2014) Biodegradable implants efficiently deliver combination of paclitaxel and temozolomide to glioma C6 cancer cells in vitro. Ann. Biomed. Eng. 42, pp. 214–221.

O'Connell, M. J., Krien, M. J., Hunter, T. (2003) Never say never. The NIMA-related protein kinases in mitotic control. TRENDS in Cell Biology. 13(5), pp. 221-228.

Oh, W.K., Yoon, H. & Jang, J. (2010) Size control of magnetic carbon nanoparticles for drug Delivery, Biomaterials 31, pp. 1342–1348.

Ostrom, Q.T. *et al.* (2015) CBTRuS statistical report: Primary brain and central nervous system tumors diagnosed in the United States in 2008–2012, Neuro-Oncology. 16 (Suppl. 4):iv1–v62. doi: 10.1093/neuonc/nov189.

Pan, L. (2013) Overcoming multidrug resistance of cancer cells by direct intranuclear drug delivery using TAT-conjugated mesoporous silica nanoparticles, Biomaterials 34, pp. 2719–2730.

Papademetriou I.T. & Porter T. (2015) Promising approaches to circumvent the blood-brain barrier: progress, pitfalls and clinical prospects in brain cancer, Ther Deliv. 6, pp. 989-1016. doi: 10.4155/tde.15.48.

Pardridge, W. M. (2005). The Blood-Brain Barrier: Bottleneck in Brain Drug Development, NeuroRx. 2, pp. 3–14. doi: 10.1602/neurorx.2.1.3.

Parsons, D.W. *et al.* (2008) An integrated genomic analysis of human glioblastoma multiforme, Science. 26, pp. 1807-1812. doi: 10.1126/science.1164382.

Patel, T., Zhou, J., Piepmeier, J.M. & Saltzman, W.M. (2012) Polymeric nanoparticles for drug delivery to the central nervous system, Adv Drug Deliv Rev. 15, pp. 701-705. doi: 10.1016/j.addr.2011.12.006.

Peer, D. *et al.* (2007) Nanocarriers as an emerging platform for cancer therapy. Nat. Nanotechnol. 2, 751–760.

Pham, W., U. Sharma & A. G. Mikos. (2006) Electrospinning of Polymeric Nanofibers for Tissue Enginnering Applications: A Review. Tissue Engineering, 12, pp. 1197- 1211.

Piroth, M.D. *et al.* (2007) Postoperative radiotherapy of glioblastoma multiforme: analysis and critical assessment of different treatment strategies and predictive factors, Strahlenther Onkol. 183, pp. 695-702. doi: 10.1007/s00066-007-1739-5.

Polivka, J., Jr. *et al.* (2017) Advances in Experimental Targeted Therapy and Immunotherapy for Patients with Glioblastoma Multiforme. Anticancer Res. 37, pp. 21-33.

Polyzoidis, S. *et al.* (2015) Active dendritic cell immunotherapy for glioblastoma: Current status and challenges, Br J Neurosurg. 29, pp. 197-205. doi: 10.3109/02688697.2014.994473.

Pourgholi, F. *et al.* (2016) Nanoparticles: Novel vehicles in treatment of Glioblastoma, Biomedicine and Pharmacotherapy. 77, pp. 98–107. doi: 10.1016/j.biopha.2015.12.014.

Ramachandran, R. *et al.* (2017) Theranostic 3-Dimensional nano brain-implant for prolonged and localized treatment of recurrent glioma. Sci. Rep. 7, 43271.

Ranganath, S.H. *et al.* (2010) The use of submicron/nanoscale PLGA implants to deliver paclitaxel with enhanced pharmacokinetics and therapeutic efficacy in intracranial glioblastoma in mice. Biomaterials. 31, pp. 5199–5207.

Ranganath, S.H. & Wang, C. (2008) Biodegradable microfiber implants delivering paclitaxel for post-surgical chemotherapy against malignant glioma. Biomaterials. 29, pp. 2996–3003.

Reis, C.P. *et al.* (2006) Nanoencapsulation I. Methods for preparation of drug-loaded polymeric nanoparticles, Nanomedicine. 2, pp. 8-21. doi: 10.1016/j.nano.2005.12.003.

Ren, W.H. *et al.* (2010) Development of transferrin functionalized poly(ethylene glycol)/poly (lactic acid) amphiphilic block copolymeric micelles as a potential delivery system targeting brain glioma. J Mater Sci. 21, pp. 2673–2681.

Ren, Y. *et al.* (2010) Co-delivery of as-miR-21 and 5-Fu by poly(amidoamine) dendrimer attenuates human glioma cell growth in vitro. J Biomater Sci Polym Ed. 21, pp. 303-14. doi: 10.1163/156856209X415828.

Ruan, S. *et al.* (2015) Tumor microenvironment sensitive doxorubicin delivery and release to glioma using angiopep-2 decorated gold nanoparticles. Biomaterials 37, pp. 425–435.

Saucier-Sawyer, J. K. *et al.* (2016) Distribution of polymer nanoparticles by convection-enhanced delivery to brain tumors, J of Control Release. Elsevier B.V., 232, pp. 103–112. doi: 10.1016/j.jconrel.2016.04.006.

Schneider, C. S. *et al.* (2015) Minimizing the non-specific binding of nanoparticles to the brain enables active targeting of Fn14-positive glioblastoma cells, Biomaterials. Elsevier Ltd. 42, pp. 42–51. doi: 10.1016/j.biomaterials.2014.11.054.

Sekerdag, E. *et al.* (2017) A potential non-invasive glioblastoma treatment: Nose-to-brain delivery of farnesylthiosalicylic acid incorporated hybrid nanoparticles, J of Control Release. 261, pp. 187–198. doi: 10.1016/j.jconrel.2017.06.032.

Senter, P.D. & Springer, C.J. (2001) Selective activation of anticancer prodrugs by monoclonal antibody–enzyme conjugates. Adv. Drug Deliv. Rev. 53, pp. 247–264.

Senzer, N. *et al.* (2013). Phase I study of a systemically delivered p53 nanoparticle in advanced solid tumors. Mol. Ther. 21, pp. 1096–1103. doi: 10.1038/mt.2013.32.

She, W. *et al.* (2013) Dendronized heparin−doxorubicin conjugate based nanoparticle as pH-responsive drug delivery system for cancer therapy, Biomaterials. 34, pp. 2252–2264.

Smith, A. *et al.* (2016) Candidate DNA repair susceptibility genes identified by exome sequencing in high-risk pancreatic cancer. Cancer Letters. 370, pp. 302–312.

Sohail, M.F. *et al.* (2016) Folate grafted thiolated chitosan enveloped nanoliposomes with enhanced oral bioavailability and anticancer activity of docetaxel. J Mater Chem. B. 4, pp. 6240–6248.

Sok, J.C. *et al.* (2006) Mutant epidermal growth factor receptor (EGFRvIII) contributes to head and neck cancer growth and resistance to EGFR targeting, Clin Cancer Res. 1, pp. 5064-5073. doi: 10.1158/1078-0432.CCR-06-0913.

Son, S. *et al.* (2011) A brain-targeted rabies virus glycoprotein-disulfide linked PEI nanocarrier for delivery of neurogenic microRNA. Biomaterials. 32, pp. 4968–4975.

Spies, J. *et al.* (2003) Nek1 Regulates Rad54 to Orchestrate Homologous Recombination and Replication Fork Stability. Molecular Cell. 62(6), pp. 903 – 917.

Stupp, R. *et al.* (2005) Radiotherapy plus concomitant and adjuvant temozolomide for glioblastoma, N Engl J Med. 10, pp. 987-996. doi: 10.1056/NEJMoa043330.

Stupp R. *et al.* (2009) Effects of radiotherapy with concomitant and adjuvant temozolomide versus radiotherapy alone on survival in glioblastoma in a randomised phase III study: 5-year analysis of the EORTC-NCIC trial. Lancet Oncol. 10, pp. 459–466.

Subbiah, T. B. *et al.* (2005) Pararneswaran e S. Ramkumar, S. Electrospinning of nanofibers. J. App. Polym. Sci. 96(2), pp. 557-569.

Sun, B. *et al.* (2016) Robust, active tumor-targeting and fast bioresponsive anticancer nanotherapeutics based on natural endogenous materials, Acta Biomater. 45, pp. 223–233.

Sun, C*. et al.* (2008) Tumor-targeted drug delivery and MRI contrast enhancement by chlorotoxin-conjugated iron oxide nanoparticles, Nanomedicine. 3, pp. 495–505.

Sun, T. *et al.* (2014) Engineered nanoparticles for drug delivery in cancer therapy. Angew Chem Int. Ed. 53, pp. 12320–12364.

Suzuki, K. *et al.* (2013) Celecoxib enhances radiosensitivity of hypoxic glioblastoma cells through endoplasmic reticulum stress. Neuro Oncol. 15, pp. 1186-99. doi: 10.1093/neuonc/not062.

Tang, J. *et al.* (2017) Aptamer-conjugated PEGylated quantum dots targeting epidermal growth factor receptor variant III for fluorescence imaging of glioma, Inter. J. of Nanomedicine. 12, pp. 3899–3911. doi: 10.2147/IJN.S133166.

Tavakoli, R. *et al.* (2018) Prolonged drug release using PCL–TMZ nanofibers induce the apoptotic behavior of U87 glioma cells. Int. J. Polym. Mater. Polym. Biomater. 67(15), pp. 873-878.

Taylor, G. (1964) Disintegration of Water Drops in an Electric Field. Proceedings of the Royal Society of London. Series A. Mathematical and Physical Sciences. 280, pp. 383-397.

Thakkar, S. & Misra, M. (2017) European Journal of Pharmaceutical Sciences Electrospun polymeric nanofibers: New horizons in drug delivery, Eur J of Pharm Sci. Elsevier. 107, pp. 148–167. doi: 10.1016/j.ejps.2017.07.001.

Teixeira, M*. et al.* (2005) Development and characterization of PLGA nanospheres and nanocapsules containing xanthone and 3-methoxyxanthone, Eur J Pharm Biopharm. 59, pp. 491-500. doi: 10.1016/j.ejpb.2004.09.002.

Tsiapa, I. *et al.* (2014) (99m)Tc-labeled aminosilane-coated iron oxide nanoparticles for molecular imaging of αvβ3-mediated tumor expression and feasibility for

hyperthermia treatment, J Colloid Interface Sci. 1, pp. 163-175. doi: 10.1016/j.jcis.2014.07.032.

Tseng, Y. *et al.* (2013) Sustainable release of carmustine from biodegradable poly [(d,L)-lactide-co-glycolide] nanofibrous membranes in the cerebral cavity: in vitro and in vivo studies. Expert Opin. Drug Deliv. 10, pp. 879–888.

Tseng, Y.Y. *et al.* (2016) Advanced interstitial chemotherapy combined with targeted treatment of malignant glioma in rats by using drug-loaded nanofibrous membranes. Oncotarget 7, pp. 59902–59916.

Tzeng, S.Y. & Green, J.J. (2013) Subtle changes to polymer structure and degradation mechanism enable highly effective nanoparticles for siRNA and DNA delivery to human brain cancer, Adv Healthc Mater. 2, pp. 468-80. doi: 10.1002/adhm.201200257.

Tzeng, S.Y. & Green, J.J. (2013) Therapeutic nanomedicine for brain cancer, Ther Deliv. 4, pp. 687-704. doi: 10.4155/tde.13.38.

van Linde, M.E. *et al.* (2015) Bevacizumab in combination with radiotherapy and temozolomide for patients with newly diagnosed glioblastoma multiforme, Oncologist. 20, pp. 107-108. doi: 10.1634/theoncologist.2014-0418.

Veiseh, O. *et al.* (2009) Inhibition of tumor-cell invasion with chlorotoxin-bound superparamagnetic nanoparticles, Small. 5, pp. 256–264.

Veiseh, O. *et al.* (2010) Chlorotoxin bound magnetic nanovector tailored for cancer cell targeting, imaging, and siRNA delivery, Biomaterials. 31, pp. 8032–8042.

Verhaak, R.G. *et al.* (2010) Integrated genomic analysis identifies clinically relevant subtypes of glioblastoma characterized by abnormalities in PDGFRA, IDH1, EGFR, and NF1, Cancer Cell. 17, pp. 98-110. doi: 10.1016/j.ccr.2009.12.020.

Verma, J., Lal, S. & Van Noorden, C.J. (2014) Nanoparticles for hyperthermic therapy: synthesis strategies and applications in glioblastoma, Int J Nanomedicine. 10, pp.2863-2877. doi: 10.2147/IJN.S57501.

Vert, M. *et al.* (2012) Terminology for biorelated polymers and applications (IuPAC Recommendations 2012). Pure Appl Chem. 84, pp. 377–410.

Xi, G. *et al.* (2014) Convection-enhanced delivery of nanodiamond drug delivery platforms for intracranial tumor treatment, Nanomedicine: Nanotechnology, Biol Med. 10, pp. 381–391.

Xia, X.X. *et al.* (2014) Hydrophobic drug-triggered self assembly of nanoparticles from silk-elastin-like protein polymers for drug delivery, Biomacromolecules. 15, pp. 908–914.

Xin, H. *et al.* (2012) Anti-glioblastoma efficacy and safety of paclitaxel-loading Angiopep-conjugated dual targeting PEG-PCL nanoparticles, Biomaterials. 33, pp. 8167-76. doi: 10.1016/j.biomaterials.2012.07.046.

Xu, X. *et al.* (2006) BCNU-loaded PEG-PLLA ultrafine fibers and their in vitro antitumor activity against Glioma C6 cells. J. Control. Release. 114, pp. 307–316.

Xue, S. *et al.* (2017) Blocking the PD-1/PD-L1 pathway in glioma: a potential new treatment strategy. J Hematol Oncol, 10, pp. 81.

Wadajkar, A. S. *et al.* (2017) Decreased non-specific adhesivity, receptor targeted (DART) nanoparticles exhibit improved dispersion, cellular uptake, and tumor retention in invasive gliomas, J of Control Release. 267, pp. 144–153. doi: 10.1016/j.jconrel.2017.09.006.

Wang, B. *et al.* (2016) Local in vitro delivery of rapamycin from electrospun PEO/ PDLLA nanofibers for glioblastoma treatment. Biomed. Pharmacother. 83, pp. 1345– 1352.

Wang, H. *et al.* (2015). The Challenges and the Promise of Molecular Targeted Therapy in Malignant Gliomas, Neoplasia. 17, pp. 239–255. doi: 10.1016/j.neo.2015.02.002.

Wang, J. *et al.* (2010) Folate decorated hybrid polymeric nanoparticles for chemically and physically combined paclitaxel loading and targeted delivery. Biomacromolecules. 12, pp. 228–234.

Wang, X. *et al.* (2008) Application of nanotechnology in cancer therapy and imaging. Cancer J. Clin. 58, pp. 97–110.

Wen, P.Y. & Reardon, D.A. (2016) Neuro-oncology in 2015: Progress in glioma diagnosis, classification and treatment, Nat Rev Neurol. 12, pp. 69-70. doi: 10.1038/nrneurol.2015.242.

Weller M, Cloughesy T, Perry JR, Wick W. (2013) Standards of care for treatment of recurrent glioblastoma--are we there yet? Neuro-oncology. 15, pp. 4–27.

Wilczewska, A.Z. *et al.* (2012) Nanoparticles as drug delivery systems, Pharmacol Rep. 64, pp. 1020-37.

Wilhelm, S. *et al.* (2016) Analysis of nanoparticle delivery to tumors. Nat. Rev. Mater. 1, 16014.

Wilson, T.A., Karajannis, M.A. & Harter, D.H. (2014) Glioblastoma multiforme: State of the art and future therapeutics, Surg Neurol Int. 8, pp. 64. doi: 10.4103/2152-7806.132138.

Wohlfart, S. *et al.* (2011) Efficient chemotherapy of rat glioblastoma using doxorubicin loaded PLGA nanoparticles with different stabilizers. PLoS One 6, e19121.

Wolburg, H. *et al.* (2003) Localization of claudin-3 in tight junctions of the blood-brain barrier is selectively lost during experimental autoimmune encephalomyelitis and human glioblastoma multiforme, Acta Neuropathol. 105, pp. 586-592. doi: 10.1007/s00401-003-0688-z.

Wong, H.L. *et al.* (2007) Chemotherapy with anticancer drugs encapsulated in solid lipid nanoparticles, Adv Drug Deliv Rev. 10, pp. 491-504. doi: 10.1016/j.addr.2007.04.008.

Yan, H. *et al.* (2012) Two-order targeted brain tumor imaging by using an optical/paramagnetic nanoprobe across the blood brain barrier, ACS Nano 6, pp. 410–420.

Yang, H. (2010) Nanoparticle-mediated brain-specific drug delivery, imaging, and diagnosis, Pharm Res. 27, pp. 1759-1771. doi: 10.1007/s11095-010-0141-7.

Yang, L. *et al.* (2008) Shape-controlled synthesis of protein-conjugated silver sulfidenanocrystals and study on the inhibition of tumor cell viability, Chem Commun. 26, pp. 2995-2997. doi: 10.1039/b804274h.

Young, R. M., Jamshidi, A., Davis, G., & Sherman, J. H. (2015) Current trends in the surgical management and treatment of adult glioblastoma. Annals of Translational Medicine, 3, pp. 121. doi:10.3978/j.issn.2305-5839.2015.05.10.

Zhang, J. *et al.* (2013) Multifunctional envelope-type mesoporous silica nanoparticles for tumor triggered targeting drug delivery. J Am Chem Soc. 135, pp. 5068–5073.

Zhu, G. *et al.* (2013) Self-assembled, aptamer-tethered DNA nanotrains for targeted transport of molecular drugs in cancer theranostics, Proc Natl Acad Sci. 110, pp. 7998–8003.

Zhu, J. *et al.* (2016) Frequent Nek1 overexpression in human gliomas. Biochem Biophys Res Commun. 476(4), pp. 522-527.

Zhu, X. *et al.* (2015) Anti-neoplastic cytotoxicity of SN-38-loaded PCL/gelatin electrospun composite nanofiber scaffolds against human glioblastoma cells in vitro. J. Pharm. Sci. 104, pp. 4345–4354.

CURRÍCULO LATTES

Luiza Steffens Reinhardt

Endereço para acessar este CV: http://lattes.cnpq.br/0518753445517933
Última atualização do currículo em 21/03/2019

Graduada em Toxicologia Analítica pela Universidade Federal de Ciências da Saúde de Porto Alegre - UFCSPA (2016). Atualmente é mestranda no Programa de Pós-Graduação em Biociências da UFCSPA realizando mestrado sanduíche no Instituto de Tecnologia de Athlone. Tem experiência da área de reparo de DNA, genotoxicidade, mutagenicidade, ensaios in vitro e in vivo, polímeros para aplicações biomédicas e nanotecnologia. **(Texto informado pelo autor)**

Identificação

Nome	Luiza Steffens Reinhardt
Nome em citações bibliográficas	STEFFENS, L.;REINHARDT, LUIZA STEFFENS;Luiza Steffens Reinhardt;Luiza Steffens;STEFFENS, LUIZA;STEFFENS, LUIZA REINHARDT

Endereço

Endereço Profissional	Fundação Universidade Federal de Ciências da Saúde de Porto Alegre, Departamento de Farmacologia e Toxicologia. Rua Sarmento Leite Centro Histórico 90050170 - Porto Alegre, RS - Brasil Telefone: (51) 33038803 URL da Homepage: http://ufcspa.edu.br

Formação acadêmica/titulação

2017	Mestrado em andamento em BIOCIÊNCIAS (Conceito CAPES 4). Fundação Universidade Federal de Ciências da Saúde de Porto Alegre, UFCSPA, Brasil. Orientador: Dinara Jaqueline Moura.
2014 - 2016	Graduação em Toxicologia Analítica. Fundação Universidade Federal de Ciências da Saúde de Porto Alegre, UFCSPA, Brasil.
2010 - 2012	Ensino Médio (2º grau). Colégio Marista Nossa Senhora do Rosário, MARISTA/Rosário, Brasil.

Formação Complementar

2018 - 2018	Communications Module. (Carga horária: 45h). Athlone Institute of Technology, AIT, Irlanda.
2017 - 2017	Minicurso de Quantificação de Imagens. (Carga horária: 3h). Fundação Universidade Federal de Ciências da Saúde de Porto Alegre, UFCSPA, Brasil.
2016 - 2016	Extensão universitária em I Encontro do Programa de Pós-Graduação em Biociências. (Carga horária: 12h). Fundação Universidade Federal de Ciências da Saúde de Porto Alegre, UFCSPA, Brasil.
2016 - 2016	Minicurso em Bioinformática. (Carga horária: 3h). Fundação Universidade Federal de Ciências da Saúde de Porto Alegre, UFCSPA, Brasil.
2015 - 2015	Extensão universitária em V Curso de Inverno - Resposta a danos no DNA: Impl. (Carga horária: 50h). Universidade de São Paulo, USP, Brasil.
2015 - 2015	I Curso de Toxicidade Genética: Causas, Consequências e Ensaio Pré-Clínico. (Carga horária: 50h). Fundação Universidade Federal de Ciências da Saúde de Porto Alegre, UFCSPA, Brasil.

Atuação Profissional

Fundação Universidade Federal de Ciências da Saúde de Porto Alegre, UFCSPA, Brasil.

Vínculo institucional
2017 - Atual Vínculo: Bolsista, Enquadramento Funcional: Mestranda, Carga horária: 40, Regime: Dedicação exclusiva.

Vínculo institucional
2017 - 2017 Vínculo: Bolsista, Enquadramento Funcional: Bolsista de Apoio Técnico, Carga horária: 40, Regime: Dedicação exclusiva.

Outras informações Bolsista de apoio técnico no Laboratório de Genética Toxicológica.

Vínculo institucional
2016 - 2017 Vínculo: Bolsista, Enquadramento Funcional: Iniciação Científica, Carga horária: 20

Vínculo institucional
2016 - 2016 Vínculo: Estagiário, Enquadramento Funcional: Estagiário, Carga horária: 30

Outras informações Estagiário em Genética Toxicológica.

Vínculo institucional
2016 - 2016 Vínculo: Voluntário, Enquadramento Funcional: Monitora, Carga horária: 6

Outras informações Monitora da Disciplina de Bioquímica e Genética Toxicológica

Vínculo institucional
2015 - 2016 Vínculo: Membro de Comissão Interna, Enquadramento Funcional: Membro Efetivo da Comissão Graduação, Carga horária: 1

Outras informações Membro da Comissão de Graduação do Curso de Toxicologia Analítica, como representante discente.

Vínculo institucional
2015 - 2016 Vínculo: Bolsista, Enquadramento Funcional: Iniciação Científica, Carga horária: 20

Outras informações Atuação como IC no projeto de pesquisa "Desenvolvimento de extrato padronizado de Plantago major L. em ácidos triterpênicos e determinação do potencial cicatrizante, anti-inflamatório e da sua segurança toxicológica.

Vínculo institucional
2015 - 2016 Vínculo: Coordenadora Geral de CA, Enquadramento Funcional: Coordenadora Geral do Centro Acadêmico Orfila

Vínculo institucional
2014 - 2015 Vínculo: Bolsista, Enquadramento Funcional: Iniciação Científica, Carga horária: 20, Regime: Dedicação exclusiva.

Outras informações Atuação como IC no projeto de pesquisa "Desenvolvimento de extrato padronizado de Plantago major L. em ácidos triterpênicos e determinação do potencial cicatrizante, anti-inflamatório e da sua segurança toxicológica.

Universidade Federal do Rio Grande do Sul, UFRGS, Brasil.

Vínculo institucional
2016 - 2016 Vínculo: Estagiário, Enquadramento Funcional: Estagiário na área de Toxicologia Analítica, Carga horária: 30

Athlone Institute of Technology, AIT, Irlanda.

Vínculo institucional
2018 - Atual Vínculo: Pesquisador visitante, Enquadramento Funcional: Pesquisador

Vínculo institucional
2018 - 2018 Vínculo: Lab instructor, Enquadramento Funcional: Lab instructor, Carga horária: 20

Projetos de pesquisa

2017 - Atual NIMA-related Kinase 1 e seu papel na resistência tumoral
Descrição: Considerando estes estudos que indicam que Nek1 está relacionada ao processo tumoral, e que a resistência à quimioterapia ainda representa um importante obstáculo clínico e científico, sendo importante buscar novas opções de alvos terapêuticos para propor alternativas metodológicas em tumores que ainda possuem alta taxa de mortalidade, como os gliomas, este projeto visa caracterizar a proteína Nek1 em gliomas, buscando avaliar seu papel no prognóstico e tratamento, assim como na proposição de novas estratégias terapêuticas..
Situação: Em andamento; Natureza: Pesquisa.
Alunos envolvidos: Graduação: (1) / Mestrado acadêmico: (1) / Doutorado: (1) .

Integrantes: Luiza Steffens Reinhardt - Integrante / MORÁS, ANA MOIRA - Integrante / SAFFI, JENIFER - Integrante / MOURA, DINARA JAQUELINE - Coordenador / Elizandra Braganhol - Integrante / Felipe Lopes Schenider - Integrante.

2014 - Atual Estudo de novos parceiros moleculares na resposta a danos no DNA: Avaliação da proteína Nek1 como parceira molecular das proteínas da via de Fanconi

Descrição: Este projeto tem como objetivo determinar uma possível interação entre NEK1 com proteínas da via de Fanconi, mais especificamente as proteínas FANCA, FANCC e FANCD2, na resposta celular a agentes indutores de pontes intercadeias, utilizando linhagens mutantes ou silenciadas nas proteínas Nek1, FANCA, FANCC e/ou FANCD2 expostas a indutores de pontes intercadeia..
Situação: Em andamento; Natureza: Pesquisa.
Alunos envolvidos: Graduação: (1) / Mestrado acadêmico: (1) .

Integrantes: Luiza Steffens Reinhardt - Integrante / Dinara Jaqueline Moura - Coordenador / Helen Taís da Rosa Silva - Integrante / Jenifer Saffi - Integrante / Guido Lenz - Integrante / João Antonio Pegas Henriques - Integrante.

2013 - Atual

Desenvolvimento de um extrato padronizado de Plantago major L. em ácidos triterpênicos e determinação do potencial cicatrizante, anti-inflamatório e da sua segurança toxicológica
Descrição: Este projeto tem como objetivo elaborar um extrato padronizado de P. major, em ácidos triterpênicos, e determinar o potencial cicatrizante e anti-inflamatório deste extrato em modelos in vitro e in vivo. Também serão conduzidos os ensaios biológicos in vitro com células T-helper (TH-1), para avaliação da atividade anti-inflamatória, com células de queratinócitos (HaCaT), para avaliação da atividade cicatrizante. Paralelamente serão realizados ensaios in vitro para determinação do potencial mutagênico. Os ensaios toxicológicos in vivo complementarão os ensaios biológicos e incluirão as avaliações farmacológicas (anti-inflamatória e cicatrizante) e os ensaios de toxicidade aguda, toxicidade de doses repetidas e genotoxicidade utilizando ratos Wistar. Adicionalmente, este projeto prevê a identificação e a caracterização morfoanatômica desta espécie, visando à elaboração de uma descrição detalhada de suas características macroscópicas e microscópicas..
Situação: Em andamento; Natureza: Pesquisa.
Alunos envolvidos: Graduação: (2) / Mestrado acadêmico: (2) .

Integrantes: Luiza Steffens Reinhardt - Integrante / Dinara Jaqueline Moura - Coordenador / Jenifer Saffi - Integrante / Jeferson henn - Integrante / Nathalia Sperotto - Integrante / Valéria Peres - Integrante / Rodrigo Veríssimo - Integrante / Eliane Dallegrave - Integrante.
Financiador(es): Fundação de Amparo à Pesquisa do Estado do Rio Grande do Sul - Auxílio financeiro.

Áreas de atuação

1. Grande área: Ciências Biológicas / Área: Genética / Subárea: Genética Toxicológica.
2. Grande área: Ciências Biológicas / Área: Genética / Subárea: REPARO DE DNA.
3. Grande área: Ciências Biológicas / Área: Genética / Subárea: Bioquímica.
4. Grande área: Ciências Biológicas / Área: Biologia Geral / Subárea: Biologia Celular.
5. Grande área: Ciências Biológicas / Área: Biologia Geral / Subárea: Toxicologia.
6. Grande área: Ciências Biológicas / Área: Biotecnologia.

Idiomas

Português Compreende Bem, Fala Bem, Lê Bem, Escreve Bem.
Inglês Compreende Bem, Fala Bem, Lê Bem, Escreve Bem.

Prêmios e títulos

2019 Melhor resumo Mutagen-Brasil, Mutagen-Brasil.
2017 Menção Honrosa, UFCSPA.
2016 Menção Honrosa, Federação de Sociedades de Biologia Experimental - FeSBE.
2015 Destaque na Categoria Trabalhos Relacionados à Pesquisa, UFCSPA.

Produções

Produção bibliográfica

Artigos completos publicados em periódicos

Ordenar por

Ordem Cronológica

1.

HAUSCHILD, TATIANE CRISTINA ; GUERREIRO, GILIAN ; MESCKA, CAROLINE PAULA ; COELHO, DANIELLA MOURA ; **STEFFENS, LUIZA** ; MOURA, DINARA JAQUELINE ; MANFREDINI, VANUSA ; VARGAS, CARMEN REGLA . DNA damage induced by alloisoleucine and other metabolites in maple syrup urine disease and protective effect of l-carnitine. TOXICOLOGY IN VITRO JCR, v. 57, p. 194-202, 2019.

2. FREESE, LUANA ; ALMEIDA, FELIPE BORGES ; HEIDRICH, NUBIA ; HANSEN, ALANA WITT ; **STEFFENS, LUIZA** ; STEINMETZ, ALINE ; MOURA, DINARA JAQUELINE ; GOMEZ, ROSANE ; BARROS, HELENA MARIA TANNHAUSER . Environmental enrichment reduces cocaine neurotoxicity during cocaine-conditioned place preference in male rats. PHARMACOLOGY BIOCHEMISTRY AND BEHAVIOR JCR, v. 169, p. 10-15, 2018.

3. BOHN, DENISE RAQUEL ; LOBATO, FRANCIELLI OLIVEIRA ; THILL, ALISSON STEFFLI ; **STEFFENS, LUIZA** ; RAABE, MARCO ; DONIDA, BRUNA ; VARGAS, CARMEN REGLA ; MOURA, DINARA J. ; BERNARDI, FABIANO ; POLETTO, FERNANDA . Artificial cerium-based proenzymes confined in lyotropic liquid crystal: Synthetic strategy and *on-demand* activation. Journal of Materials Chemistry B JCR, v. 1, p. 1-9, 2018.

4. DE MOURA SPEROTTO, NATHALIA DENISE ; **STEFFENS, LUIZA** ; VERÍSSIMO, RODRIGO MOISÉS ; HENN, JEFERSON GUSTAVO ; PÉRES, VALÉRIA FLORES ; VIANNA, PRISCILA ; CHIES, JOSÉ ARTUR BOGO ; ROEHE, ADRIANA ; SAFFI, JENIFER ; MOURA, DINARA JAQUELINE . Wound healing and anti-inflammatory activities induced by a Plantago australis hydroethanolic extract standardized in verbascoside. JOURNAL OF ETHNOPHARMACOLOGY JCR, v. 225, p. 178-188, 2018.

5. MARCHETTI, DESIRÈE PADILHA ; **STEFFENS, LUIZA** ; JACQUES, CARLOS E. ; GUERREIRO, GILIAN B. ; MESCKA, CAROLINE P. ; DEON, MARION ; DE COELHO, DANIELLA M. ; MOURA, DINARA J. ; VIARIO, ALICE G. ; POLETTO, FERNANDA ; COITINHO, ADRIANA S. ; JARDIM, LAURA B. ; VARGAS, CARMEN R. . Oxidative Imbalance, Nitrative Stress, and Inflammation in C6 Glial Cells Exposed to Hexacosanoic Acid: Protective Effect of N-acetyl-l-cysteine, Trolox, and Rosuvastatin. CELLULAR AND MOLECULAR NEUROBIOLOGY JCR, v. 1, p. 1-1, 2018.

Citações: SCOPUS 1

6. HENN, JEFERSON GUSTAVO ; **STEFFENS, LUIZA** ; SPEROTTO, NATHALIA DENISE DE MOURA ; DE SOUZA PONCE, BETÂNIA ; VERÍSSIMO, RODRIGO MOISÉS ; BOARETTO, FERNANDA BRIÃO MENEZES ; HASSEMER, GUSTAVO ; PÉRES, VALÉRIA FLORES ; SCHIRMER, HELENA ; PICADA, JAQUELINE NASCIMENTO ; SAFFI, JENIFER ; MOURA, DINARA JAQUELINE . Toxicological evaluation of a standardized hydroethanolic extract from leaves of Plantago australis and its major compound, verbascoside. JOURNAL OF ETHNOPHARMACOLOGY JCR, v. 1, p. 1-1, 2018.

Citações: SCOPUS 3

7. DA SILVA, CLAUDIA B ; GIL, EDUARDA S ; SANTOS, FABIANO DA SILVEIRA ; MORAS, ANA M ; **STEFFENS, LUIZA** ; GONCALVES, PAULO F. B. ; MOURA, DINARA J ; LÜDTKE, DIOGO S. ; RODEMBUSCH, FABIANO SEVERO . Proton-transfer based azides with fluorescence off-on response for detection of hydrogen sulfide. An experimental, theoretical and bioimaging study. JOURNAL OF ORGANIC CHEMISTRY JCR, v. 1, p. acs.joc.8b02489-1, 2018.

8. STEINMETZ, ALINE ; **STEFFENS, LUIZA** ; MORÁS, ANA MOIRA ; PREZZI, FLÁVIA ; BRAGANHOL, ELIZANDRA ; SAFFI, JENIFER ; ORTIZ, RAFAEL SCORSATTO ; BARROS, HELENA M.T. ; MOURA, DINARA JAQUELINE . In vitro model to study cocaine and its contaminants. CHEMICO-BIOLOGICAL INTERACTIONS JCR, v. 285, p. 1-7, 2018.

9. BIANCINI, GIOVANA BRONDANI ; MORÁS, ANA MOIRA ; **REINHARDT, LUIZA STEFFENS** ; BUSATTO, FRANCIELE FACCIO ; DE MOURA SPEROTTO, NATHALIA DENISE ; SAFFI, JENIFER ; MOURA, DINARA JAQUELINE ; GIUGLIANI, ROBERTO ; VARGAS, CARMEN REGLA . Globotriaosylsphingosine induces oxidative DNA damage in cultured kidney cells. NEPHROLOGY JCR, v. 22, p. 490-493, 2017.

10. BORILLE, B. T. ; GONZALEZ, M. ; **STEFFENS, L.** ; ORTIZ, R. S. ; LIMBERGER, R. P. . CANNABIS SATIVA: A SYSTEMATIC REVIEW OF PLANT ANALYSIS. Drug Analytical Research, v. 1, p. http://seer.ufr, 2017.

11. CALETTI, GREICE ; HERRMANN, ANA P. ; PULCINELLI, RIANNE REMUS ; **STEFFENS, LUIZA** ; MORÁS, ANA MOIRA ; VIANNA, PRISCILA ; CHIES, JOSÉ ARTUR BOGO ; MOURA, DINARA JAQUELINE ; BARROS, HELENA MARIA TANHAUSER ; GOMEZ, ROSANE . Taurine counteracts the neurotoxic effects of streptozotocin-induced diabetes in rats. AMINO ACIDS (WIEN. INTERNET) JCR, v. 1, p. 1, 2017.

12. DA COSTA E SILVA, LIANA DANTAS ; PEREIRA, PATRÍCIA ; REGNER, GABRIELA GREGORY ; BOARETTO, FERNANDA BRIÃO MENEZES ; HOFFMANN, CLEONICE ; PFLÜGER, PRICILA ; DA SILVA, LUCAS LIMA ; **STEFFENS, LUIZA REINHARDT** ; MORÁS, ANA MOIRA ; MOURA, DINARA JAQUELINE ; PICADA, JAQUELINE NASCIMENTO . DNA damage and oxidative stress induced by seizures are decreased by anticonvulsant and neuroprotective effects of lobeline, a candidate to treat alcoholism. METABOLIC BRAIN DISEASE JCR, v. 1, p. 1, 2017.

Citações: SCOPUS 1

13. DE SOUZA, VANESSA PEREIRA ; VENDRUSCULO, VINÍCIUS ; MORÁS, ANA M. ; **STEFFENS, LUIZA** ; SANTOS, FABIANO S ; MOURA, DINARA J. ; RODEMBUSCH, FABIANO SEVERO ; RUSSOWSKY, DENNIS . Synthesis and photophysical study of new fluorescent proton transfer dihydropyrimidinone hybrids as potential candidates for molecular probes. NEW JOURNAL OF CHEMISTRY JCR, v. 1, p. 1-1, 2017.

Bancas

Participação em bancas de comissões julgadoras

Outras participações

1. **STEFFENS, L.**. SciFest@College 2018. 2018. Athlone Institute of Technology.
2. **STEFFENS, L.**. III Mostra de Trabalhos de Ensino, Pesquisa e Extensão. 2017. Fundação Universidade Federal de Ciências da Saúde de Porto Alegre.

Eventos

Participação em eventos, congressos, exposições e feiras

1. 26th EORS Annual Meeting. ELECTROSPUN PVA NANOFIBERS FOR BONE DISEASE THERAPY USING MESENCHYMAL STEM CELL. 2018. (Congresso).
2. 43rd Institute of Chemistry of Ireland Congress. Eletrospun PVA-Dacarbazine nanoparticles: a novel drug delivery system for cancer treatment. 2018. (Congresso).
3. ECP4 The European Composites, Plastics and Polymer Processing Platform a. Eletrospun PVA-Dacarbazine nanoparticles: a novel drug delivery system for brain cancer treatment. 2018. (Congresso).
4. Research Presentations & Poster Day.Eletrospun PVA-Dacarbazine nanoparticles: a novel drug delivery system. 2018. (Encontro).
5. Social & Ethical Responsibility of Third Level Colleges towards Community Ey Engagement across the Life Spectrum. 2018. (Congresso).
6. II Encontro do PPG Biociências & Encontro em Fisiologia do RS.O TRATAMENTO COM ÔMEGA-3 PROMOVE A MELHORA DE PARÂMETROS METABÓLICOS E DO ESTRESSE OXIDATIVO E INFLAMAÇÃO INTESTINAL EM MODELO EXPERIMENTAL DE OBESIDADE INDUZIDO POR HIGH FAT DIET. 2017. (Encontro).
7. II Encontro do PPG Biociências & Encontro em Fisiologia do RS.NIMA-RELATED KINASE 1 E SEU PAPEL NA RESISTÊNCIA TUMORAL. 2017. (Encontro).
8. II Encontro do PPG Biociências & Encontro em Fisiologia do RS.ANÁLISE DE PARÂMETROS BIOQUÍMICOS, NO SANGUE E TECIDOS METABÓLICOS, DE FÊMEAS QUE RECE- BERAM DIETA HIPERCALÓRICA OU RESTRITIVA NA GESTAÇÃO E LACTAÇÃO. 2017. (Encontro).
9. I Encontro do Programa de Pós-Graduação em Biociências, XIX Encontro de Geneticistas do Rio Grande do Sul e I Encontro Regional Sul da Sociedade Brasileira de Genética Médica.Estresse oxidativo em linfoblastos de pacientes com Anemia de Fanconi em resposta à cisplatina. 2016. (Encontro).
10. II Mostra de Trabalhos de Ensino, Pesquisa & Extensão da UFCSPA.Extresse Oxidativo em Linfoblastos de Pacientes com Anemia de Fanconi em Resposta à Cisplatina. 2016. (Outra).
11. Toxicologia em Debate: A polêmica dos efeitos da maconha. 2016. (Outra).
12. Toxicologia em Debate: Desastre em Mariana e suas consequências. 2016. (Outra).
13. Toxicologia em Debate: Direção veicular e drogas de abuso, isso combina?. 2016. (Outra).
14. XII Congresso da MutaGen-Brasil. 2016. (Congresso).
15. XXXI Reunião Anual da Federação de Sociedades de Biologia Experimental - FeSBE. Fanconi Anemia: Recent Remarks and Model of Study Using Lymphoblastoid Cells from Patients. 2016. (Congresso).
16. Cellularised Scaffolds, Co-cultures and Bioreactors for Engineering the Vascular Wall: Potential for Tissue Regeneration. 2015. (Outra).
17. Formando Opiniões. 2015. (Outra).
18. GE DAY UFRGS. 2015. (Outra).
19. I Mostra de Trabalhos de Ensino, Pesquisa & Extensão da UFCSPA.Caracterização de linhagens linfoblásticas derivadas de pacientes com Anemia de Fanconi em resposta a agentes quimioterápicos. 2015. (Outra).
20. Soluções para Preparo de Amostras e Separações Cromatográficas. 2015. (Outra).
21. Toxicologia em Debate: Acidentes em Massa. 2015. (Outra).
22. Toxicologia em Debate: Discutindo CSI. 2015. (Outra).
23. X Jornada do Programa de Pós-Gradução em Patologia. 2015. (Outra).
24. III Semana Acadêmica da Universidade Federal de Ciências da Saúde de Porto Alegre. 2014. (Outra).

Organização de eventos, congressos, exposições e feiras

1. MOURA, D. J. ; **STEFFENS, L.** ; BRAGANHOL, E. . II Encontro do PPG Biociências da UFCSPA e Encontro de Pesquisa em Fisiologia do RS. 2017. (Outro).
2. MOURA, D. J. ; **STEFFENS, L.** . Curso Básico de Papiloscopia. 2016. (Outro).
3. **STEFFENS, L.**; MOURA, D. J. . II Jornada Acadêmica da Toxicologia Analítica. 2016. (Outro).
4. MOURA, D. J. ; SAFFI, J. ; MORAS, A. M. ; SILVA, H. T. R. ; **STEFFENS, L.** . I Curso de Toxicidade Genética: Causas, Consequências e Ensaios Pré-clínicos. 2015. (Outro).
5. MOURA, D. J. ; **STEFFENS, L.** . I Jornada Acadêmica do curso de Toxicologia Analítica da UFCSPA. 2015. (Outro).

Orientações

Orientações e supervisões concluídas

Iniciação científica

1. Corentin Labbe. Investigation of the swelling effects of polyvinyl alcohol and polyacrylic acid to mimic the reaction of a human muscle. 2018. Iniciação Científica - Athlone Institute of Technology. Orientador: Luiza Steffens Reinhardt.

Orientações de outra natureza

1. Vinh Nguyen. Conductive Hydrogel. 2019. Orientação de outra natureza - Athlone Institute of Technology. Orientador: Luiza Steffens Reinhardt.

Inovação

Projetos de pesquisa

Educação e Popularização de C & T

Organização de eventos, congressos, exposições e feiras

1. MOURA, D. J. ; SAFFI, J. ; MORAS, A. M. ; SILVA, H. T. R. ; **STEFFENS, L.** . I Curso de Toxicidade Genética: Causas, Consequências e Ensaios Pré-clínicos. 2015. (Outro).
2. MOURA, D. J. ; **STEFFENS, L.** . Curso Básico de Papiloscopia. 2016. (Outro).
3. **STEFFENS, L.**; MOURA, D. J. . II Jornada Acadêmica da Toxicologia Analítica. 2016. (Outro).
4. MOURA, D. J. ; **STEFFENS, L.** ; BRAGANHOL, E. . II Encontro do PPG Biociências da UFCSPA e Encontro de Pesquisa em Fisiologia do RS. 2017. (Outro).
5. MOURA, D. J. ; **STEFFENS, L.** . I Jornada Acadêmica do curso de Toxicologia Analítica da UFCSPA. 2015. (Outro).

Página gerada pelo Sistema Currículo Lattes em 02/04/2019 às 14:44:22

Imprimir currículo